INVESTIGATION OF ALUMINOSILICATE REFRACTORY FOR SOLID OXIDE FUEL CELL APPLICATIONS

by

Paul Steven Gentile

A dissertation submitted in partial fulfillment
of the requirements for the degree

of

Doctor of Philosophy

in

Engineering

MONTANA STATE UNIVERSITY
Bozeman, Montana

November 2010

APPROVAL

of a dissertation submitted by

Paul Steven Gentile

This dissertation has been read by each member of the dissertation committee and has been found to be satisfactory regarding content, English usage, format, citation, bibliographic style, and consistency, and is ready for submission to the Division of Graduate Education.

Dr. Stephen W. Sofie

Approved for the Department of Mechanical Engineering

Dr. Chris Jenkins

Approved for the Division of Graduate Education

Dr. Carl A. Fox

STATEMENT OF PERMISSION TO USE

In presenting this dissertation in partial fulfillment of the requirements for a doctoral degree at Montana State University, I agree that the Library shall make it available to borrowers under rules of the Library. I further agree that copying of this dissertation is allowable only for scholarly purposes, consistent with "fair use" as prescribed in the U.S. Copyright Law. Requests for extensive copying or reproduction of this dissertation should be referred to ProQuest Information and Learning, 300 North Zeeb Road, Ann Arbor, Michigan 48106, to whom I have granted "the exclusive right to reproduce and distribute my dissertation in and from microform along with the non-exclusive right to reproduce and distribute my abstract in any format in whole or in part."

Paul Steven Gentile

November 2010

DEDICATION

For my wife Gina Marie and our daughter Angelina, your infinite love and support were instrumental throughout my academic endeavors.

ACKNOWLEDGEMENTS

I would like to express gratitude to Dr. Stephen Sofie for his extensive guidance and support throughout my research; and Dr. Richard Smith, Dr. Chris Jenkins, Dr. Alan George and Professor Robb Larson for their support as committee members. My gratitude also goes to Camas Key, Paolo Zafred, Cameron Kennedy, Dr. Chih-Long Tsai and Dr. Paul Gannon for their innovative ideas, feedback and assistance. My appreciation extends to Montana State University's Imaging and Chemical Analysis Laboratory and the Department of Mechanical and Industrial Engineering.

Financial support was provided by the United States Department of Energy, National Energy Technology Laboratory, under SECA Cooperative Agreement No. DE-FC26-05NT42613. Any opinions, findings, conclusions, or recommendations expressed herein are those of the authors and do not necessarily reflect the views of the DOE.

TABLE OF CONTENTS

1. INTRODUCTION 1

Problem Overview 1
Reporting of Research Findings 5
Experimental Procedures 7
Aluminosilicate Refractory Material 9
Aluminosilicate Morphology and Chemistry 9
Silicon Volatility and Gas Phase Transport 14
Deposition of Aluminosilicate Vapors on SOFC Materials 17
Silicon Poisoning in SOFCs 18

2. PROGRESS IN UNDERSTANDING SILICA TRANSPORT PROCESS AND EFFECTS IN SOLID OXIDE FUEL CELL PERFORMANCE 20

Contribution of Authors and Co-Authors 20
Manuscript Information Page 21
Abstract 22
Manuscript 23

3. SILICON VOLATILITY FROM ALUMINA AND ALUMINOSILICATES UNDER SOLID OXIDE FUEL CELL OPERATING CONDITIONS 24

Contribution of Authors and Co-Authors 24
Manuscript Information Page 25
Abstract 26
Introduction 26
Experimental Procedure 32
Theoretical Thermodynamic Equilibrium Calculations 32
Dilatometry 33
Thermal Gravimetric and Coupled Mass Spectrometry Analysis 34
Transpiration System utilizing Rutherford Backscattering (RBS) 35
Results 37
Discussion 39
Oxidizing Environments 41
Reducing Environments 45
Conclusions and Recommendations 47
References 50
Acknowledgements 55
Figures 56
Tables 62

TABLE OF CONTENTS - CONTINUED

4. INVESTIGATION OF ALUMINOSILICATE AS A SOLID OXIDE FUEL CELL REFRACTORY 63

Contribution of Authors and Co-Authors 63
Manuscript Information Page 64
Research Highlights 65
Abstract 65
Introduction 65
Experimental Materials and Methods 69
Characterization 71
Electrochemical Performance Test 73
Results & Discussion 74
Aluminosilicate Surface Morphology and Chemistry 74
Aluminum and Silicon Deposition on YSZ 77
SOFC Silicon Poisoning 80
Conclusion 83
Glossary 84
Acknowledgements 84
References 84
Figures 91
Tables 97

5. SUPPLEMENTAL RESULTS & DISCUSSION 98

Alternative Refractory Material Microstructures 98
Aluminosilicate Morphology and Chemistry 99
XPS Curve Decomposition 99
X-ray Diffraction 101
Deposition of Aluminosilicate Vapors on SOFC Materials 102
Silicon Volatility 105
Thermodynamic Equilibrium & Kinetics 105
Thermodynamic Equilibrium Dopant Studies 106
Silicon Poisoning in SOFCs 107

6. CONCLUSION 110

REFERENCES CITED 112

LIST OF TABLES

Table Page

1. Organization of research findings 6
2. Aluminosilicate material properties 9
3. Thermodynamic equilibrium variables 15
4. Thermal gravimetric mass spectrometry summary 62
5. Aluminosilicate thermal expansion coefficient 62
6. Al(2p) and Si(2p) binding energies 97
7. XPS curve fit summary 100
8. Published Si(2p) binding energies 100

LIST OF FIGURES

Figure Page

1. Alumina silica phase diagram 2
2. Silicon poisoning in SOFCs 4
3. Investigation flow diagram 8
4. EDS schematic and aluminosilicate spectra 11
5. EDS penetration 11
6. XPS schematic 13
7. XRD spherical waves 13
8. Deposition experimental setup 17
9. Planar SOFC single cell test fixture 18
10. Electrochemical polarization behavior in Voltage-Current (VI) curves 19
11. Silicon poisoning in tubular SOFCs due to Si volatization from refractory insulation and gas delivery tubing 56
12. Thermodynamic equilibrium partial pressures of Si vapor species or total partial pressure of volatile Si gases from aluminosilicate, high purity alumina, mullite or silica in humidified air 56
13. Thermodynamic equilibrium partial pressures of Si vapor species from aluminosilicate in various SOFC fuel or oxidant gases 57
14. Thermodynamic equilibrium modeled volatility of Si vapor species from 3:2 mullite and high purity alumina in hydrogen 57
15. Thermodynamic equilibrium modeled total volatile Si gas formation in SOFC gases from aluminosilicate, mullite and high purity alumina 58
16. Effect of water vapor on the thermodynamic equilibrium partial pressure of Si gases volatilized from aluminosilicate 58
17. Aluminosilicate thermal gravimetric analysis 59

LIST OF FIGURES - CONTINUED

18. Thermal gravimetric mass spectrometry of refractory insulations in humidified argon 59

19. Dilatometer analysis of aluminosilicate 60

20. Rutherford backscattering transpiration experiments 60

21. RBS comparison of volatility rates 61

22. RBS volatility rates of quartz tubes 61

23. Aluminosilicate electron micrographs with overlaid elemental maps 91

24. Relative elemental concentration of Si in aluminosilicate 91

25. Relative Si/Al concentration ratio in aluminosilicate 92

26. Aluminosilicate Si(2p) and Al(2p) XPS spectra 92

27. Electron micrographs and elemental maps of aluminosilicate vapor deposits on YSZ 93

28. Electron micrographs and elemental lines scans of aluminosilicate vapor deposits on YSZ 93

29. XPS surface scans of the Zr(3d), Y(3d) and Si(2p) peaks from aluminosilicate vapor deposits on YSZ 94

30. Electron micrographs and elemental lines scans of aluminosilicate vapor deposits on nickel 94

31. Electron micrographs and elemental lines scans of aluminosilicate vapor deposits on nickel oxide 95

32. Silicon poisoning SOFC electrochemical performance test 96

33. Electron micrograph and elemental lines scan of SOFC interfaces after Si poisoning 96

34. Micrographs of alternative SOFC refractory materials. 99

35. XPS curve fits 101

36. X-ray diffraction pattern of aluminosilicate powder 102

LIST OF FIGURES - CONTINUED

37. Aluminosilicate cluster on YSZ in direct contact with powder after heat treatment in humidified air at 1000°C for 100 hours. 104

38. Electrochemical performance (1000°C) testing of ESC after in-situ introduction of aluminosilicate powder into the fuel stream at 24 hours..... 108

NOMENCLATURE

DIL - Dilatometry

EBC – Environmental Barrier Coating

ESC – Electrolyte Supported Cell

EDS – Energy Dispersive X-Ray Spectroscopy

ESCA - Electron Spectroscopy for Chemical Analysis

FE-SEM – Field Emission Scanning Electron Microscopy

FWHM – Full Width at Half Maximum

HHV – Higher Heating Value

MS – Mass Spectroscopy

RBS – Rutherford Backscattering Spectroscopy

SOFC – Solid Oxide Fuel Cell

TERRA – Thermodynamic Modeling Software

TGA – Thermal Gravimetric Analysis

TEC – Thermal Expansion Coefficient

TPB – Triple Phase Boundary

VI – Voltage Current

XPS – X-ray Photoelectron Spectroscopy

XRD – X-Ray Diffraction

YSZ – Yttria Stabilized Zirconia

ABSTRACT

Stationary solid oxide fuel cells (SOFCs) have been demonstrated to provide clean and reliable electricity through electro-chemical conversion of various fuel sources (CH_4 and other light hydrocarbons). To become a competitive conversion technology the costs of SOFCs must be reduced to less than $400/kW. Aluminosilicate represents a potential low cost alternative to high purity alumina for SOFC refractory applications. The objectives of this investigation are to: (1) study changes of aluminosilicate chemistry and morphology under SOFC conditions, (2) identify volatile silicon species released by aluminosilicates, (3) identify the mechanisms of aluminosilicate vapor deposition on SOFC materials, and (4) determine the effects of aluminosilicate vapors on SOFC electrochemical performance. It is shown thermodynamically and empirically that low cost aluminosilicate refractory remains chemically and thermally unstable under SOFC operating conditions between 800°C and 1000°C.

Energy dispersive spectroscopy (EDS) and X-ray photoelectron spectroscopy (XPS) of the aluminosilicate bulk and surface identified increased concentrations of silicon at the surface after exposure to SOFC gases at 1000°C for 100 hours. The presence of water vapor accelerated surface diffusion of silicon, creating a more uniform distribution. Thermodynamic equilibrium modeling showed aluminosilicate remains stable in dry air, but the introduction of water vapor indicative of actual SOFC gas streams creates low temperature (<1000°C) silicon instability due to the release of $Si(OH)_4$ and $SiO(OH)_2$. Thermal gravimetric analysis and transpiration studies identified a discrete drop in the rate of silicon volatility before reaching steady state conditions after 100-200 hours. Electron microscopy observed the preferential deposition of vapors released from aluminosilicate on yttria stabilized zirconia (YSZ) over nickel. The adsorbent consisted of alumina rich clusters enclosed in an amorphous siliceous layer. Silicon penetrated the YSZ along grain boundaries, isolating grains in an insulating glassy phase. XPS did not detect spectra shifts or peak broadening associated with formation of new Si-Zr-Y-O phases. SOFC electrochemical performance testing at 800-1000°C attributed rapid degradation (0.1% per hour) of cells exposed to aluminosilicate vapors in the fuel stream predominately to ohmic polarization. EDS identified silicon concentrations above impurity levels at the electrolyte/active anode interface.

INTRODUCTION

Problem Overview

Solid oxide fuel cells (SOFCs) electrochemically convert fuel directly into electricity. The combustion free process is not limited by the Carnot cycle efficiency, permitting higher heating value (HHV) efficiencies for a natural gas SOFC power plant in excess of 60% when thermal energy is recovered in a combined cycle. [1] The thermodynamic efficiency, η_{ideal}, of a reversible fuel cell defines the maximum efficiency obtained when all of Gibbs free energy is converted into electricity without the loss of heat.

$$\eta_{ideal} = \Delta G / \Delta H$$

For example, a cell operating on pure H_2 and O_2 at 25°C where the product H_2O is in liquid form has a change of Gibbs free energy (ΔG) of 237.1 kJ/mole and a change in thermal enthalpy (ΔH) of 285.8 kJ/mole resulting in a thermodynamic efficiency of 83%.

$$H_2 + ½\ O_2 \rightarrow H_2O$$

$$\Delta G^\circ = G^\circ_{H_2} + ½\ G^\circ_{O_2} - G^\circ_{H_20}$$

In order to reach target cost levels where SOFCs are competitive with other lower efficiency standard technologies the overall power block cost must be reduced. High purity alumina refractory is used extensively throughout large stationary fuel cell systems as high temperature insulation and fuel or oxidant delivery tubes. Siemens Energy Inc. has estimated that high purity alumina (Al_2O_3) refractory components embody nearly 1/3 of the overall power block cost in tubular stationary SOFCs.

Aluminosilicate represents a potential alternative to high purity alumina to reduce costs without sacrificing mechanical strength, resistance to thermal shock and creep. Aluminosilicates are alumina (Al_2O_3) based compounds containing silica (SiO_2). The presence of silicon in aluminosilicate reduces the overall cost by eliminating the extensive processing of raw materials required to remove naturally occurring silicon impurities from alumina. The solid solution range of aluminosilicates can be studied in the system's phase diagram (Figure 1). As silica concentration exceeds 20 weight % the regions of liquid phases further expand combined with SiO_2 no longer in solution with alumina. The extent of silicon in solution with alumina affects the stability of silicon due to changes in bonding and hence oxygen coordination.

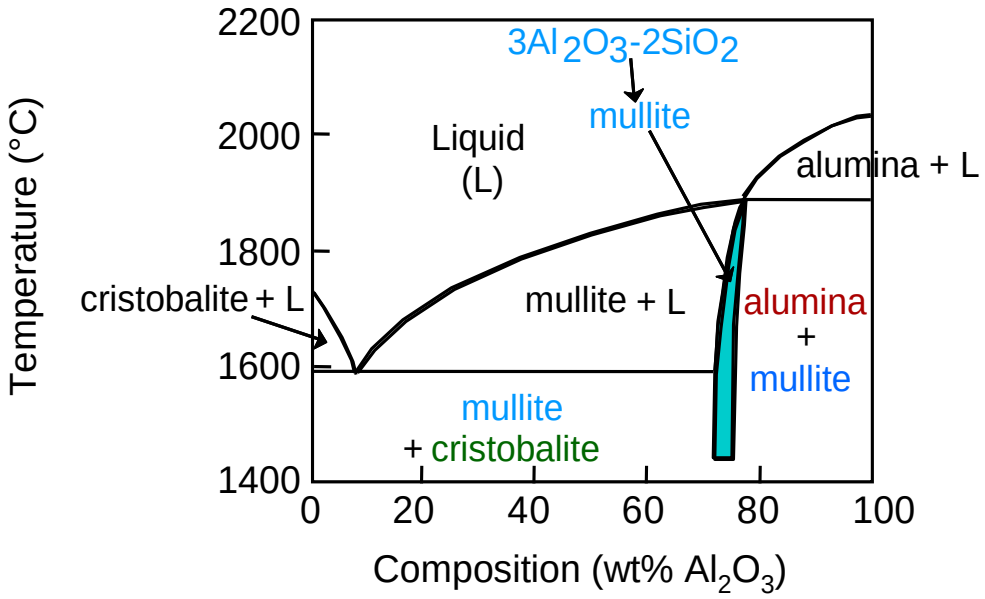

Figure 1: Alumina silica phase diagram

Mullite is an aluminosilicate compound of considerable technical importance as an advanced ceramic material because of its superior mechanical and thermal properties

at high temperatures. It is based on replacement of Al 3^+ ions with Si 4^+ ions. The chemical compositions are represented as:

$$Al_2[Al_{2+2x}Si_{2-2x}]O_{10-x} = Al_{4+2x}Si_{2-2x}O_{10-x}$$

Mullite is a non-stoichiometric compound with x denoting the # of missing oxygen atoms per average unit cell, varying between 0.2 and 0.9 [2] (corresponding to 55-90 mol% Al_2O_3). 3:2 Mullite, $3Al_2O_3 \cdot 2SiO_2$, is produced via solid state reactions during heat treatment of raw materials.

$$x = 0.25, \sim 72 \text{ wt. \% } Al_2O_3$$

2:1 Mullite, $2Al_2O_3 \cdot SiO_2$, is fused-mullite produced by crystallizing aluminosilicate melts.

$$x = 0.40, \sim 78 \text{ wt.\% } Al_2O_3$$

Electro neutrality is obtained by addition of Na^+, K^+ and Ca^{2+} by either doping or natural occurring impurities.

Silicon impurities in YSZ have been shown to detrimentally affect the electrochemical performance of SOFCs by the formation of glassy phases that transport neither electrons, protons nor oxygen ions.[3][4][5] Silicon poisoning due to refractory decomposition has not been previously addressed. The process of silicon poisoning in SOFCs due to aluminosilicate refractory materials can be broken down into a four step process (Figure 2): (1) changes in the aluminosilicate surface exposed to SOFC gas streams, (2) release of silicon vapors into the gas streams, (3) deposition of aluminosilicate vapors on SOFC materials, and (4) degradation of SOFC electrochemical performance.

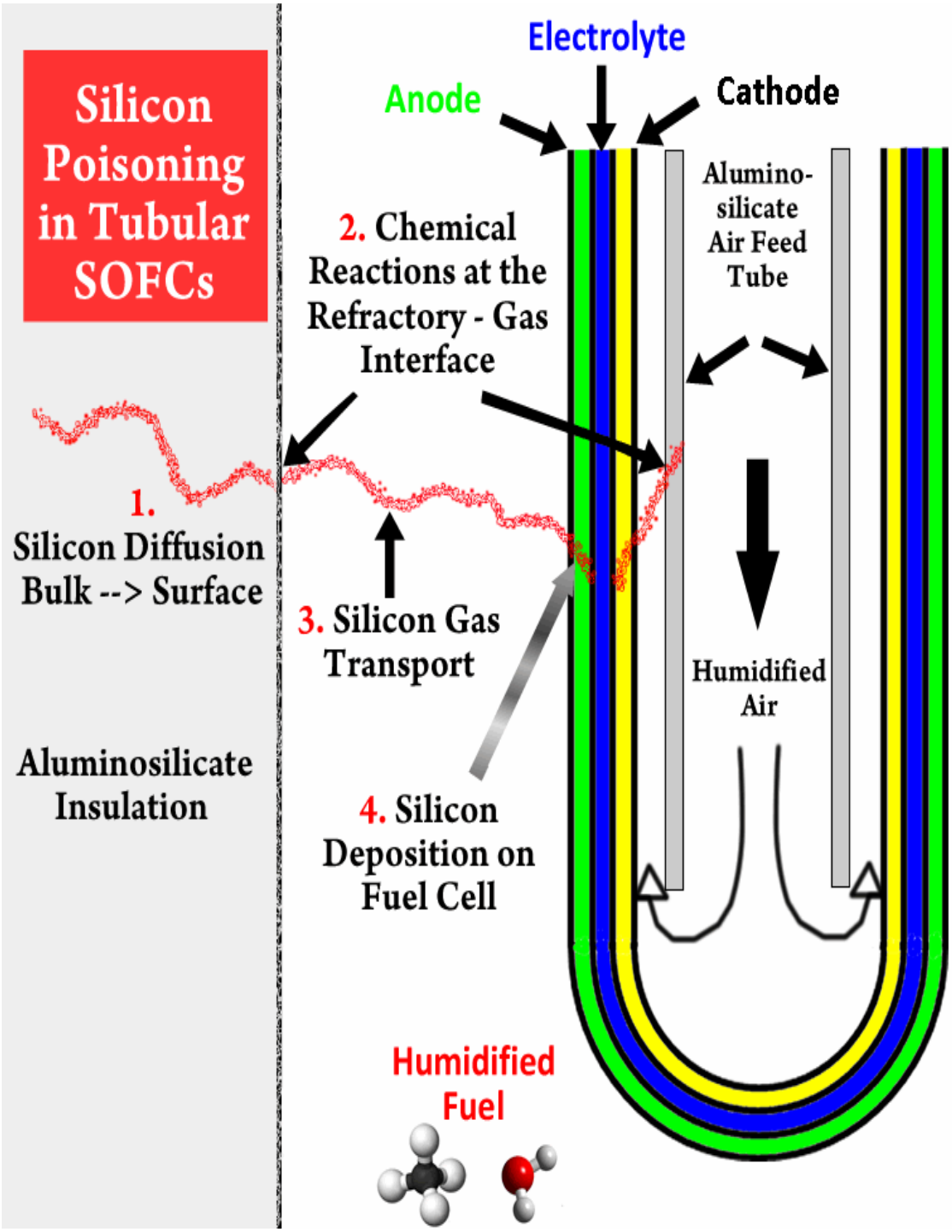

Figure 2: Silicon poisoning in SOFCs

Solid state diffusion of silicon from the aluminosilicate bulk to the surface of refractory insulation boards and gas delivery tubes changes the surface chemistry and morphology of the refractory. Chemical and morphological changes in the aluminosilicate surface subsequently affect the prevalence of chemical reactions leading to volatilization. Silicon vapors volatilized from the aluminosilicate gas-solid interface are then transported in a gaseous phase from the refractory to SOFC components. High temperature condensation/adsorption of silicon vapor species can thus lead to degradation. Silicon related degradation in SOFCs is correlated to a glass phase forming at the electrolyte/electrode interfaces which acts as an electrical insulator, adversely affects O_2 exchange kinetics of electrodes and causes interface delamination.

Reporting of Research Findings

Three independent manuscripts address the aforementioned subject matter. The first manuscript was published in a peer reviewed proceeding publication. The second and third manuscripts have been submitted to peer reviewed journals. Additional content that further supports the manuscripts is included as a chapter in this document titled “Supplemental Results and Discussion”. Table 1 summarizes the subject matter organization in the documents, and lists the experimental techniques used to address the specific problem statements.

Table 1: Organization of research findings

	Publication Title	Research Focus Areas	Experimental Techniques
1	PROGRESS IN UNDERSTANDING SILICA TRANSPORT PROCESS AND EFFECTS IN SOFC PERFORMANCE [6]	VOLATILITY, SI POISON	TERRA, FE-SEM, EDS, EPT
2	SILICON VOLATILITY FROM ALUMINA AND ALUMINOSILICATES UNDER SOFC OPERATING CONDITIONS [7]	VOLATILITY	TERRA, DIL, TGA-MS, RBS*
3	INVESTIGATION OF ALUMINOSILICATE AS A SOFC REFRACTORY [8]	ALUMINO, DEPOSITION, SI POISON	FEM, EDS, XPS, XRD, EPT
4	Dissertation Supplemental Research Discussion	VOLATILITY, SI POISON	TERRA, EPT, FE-SEM

Research Focus Areas
Change in aluminosilicate chemistry and morphology (ALUMINO)
Silicon volatility from aluminosilicate (VOLATILITY)
Silicon deposition on fuel cell components (DEPOSITION)
Silicon poisoning in SOFCs (SI POISON)

Experimental Techniques
Dilatometry (DIL)
Electrochemical Performance Testing (EPT)
Energy Dispersive X-ray Spectroscopy (EDS)
Field Emission Scanning Electron Microscopy (FE-SEM)
Mass Spectroscopy (MS)
Rutherford Backscattering Spectroscopy (RBS) *
Thermal Gravimetric Analysis (TGA)
Thermodynamic Equilibrium Modeling (TERRA)
X-ray Diffraction (XRD)
X-ray Photoelectron Spectroscopy (XPS)

Experimental Procedures

The majority of experimental methods are described in detail throughout the manuscripts. [6][7][8] Experimental methods not described in the manuscripts but related to the supplemental results chapter are presented here. In addition, an overview of the experimental techniques utilized is also provided. The following flow diagram summarizes the progress, planning, and methodology utilized to complete this investigation. It should be noted in some cases this work was an iterative process, such that results further down the line were brought back to an earlier stage for re-analysis or changes in interpretation. Originally FE-SEM/EDS and XRD were conducted to study morphological and chemical changes. After completion of the volatility and gas phase transport analysis, XPS was used to identify the chemical composition of the aluminosilicate in order to correlate volatility reactions with phases present at the gas-solid interfaces. Furthermore, XPS was applied after completion of the silicon poisoning in SOFCs experiment set. XPS was used to determine if new phases were formed between the YSZ and siliceous deposits to further understand the poisoning mechanisms.

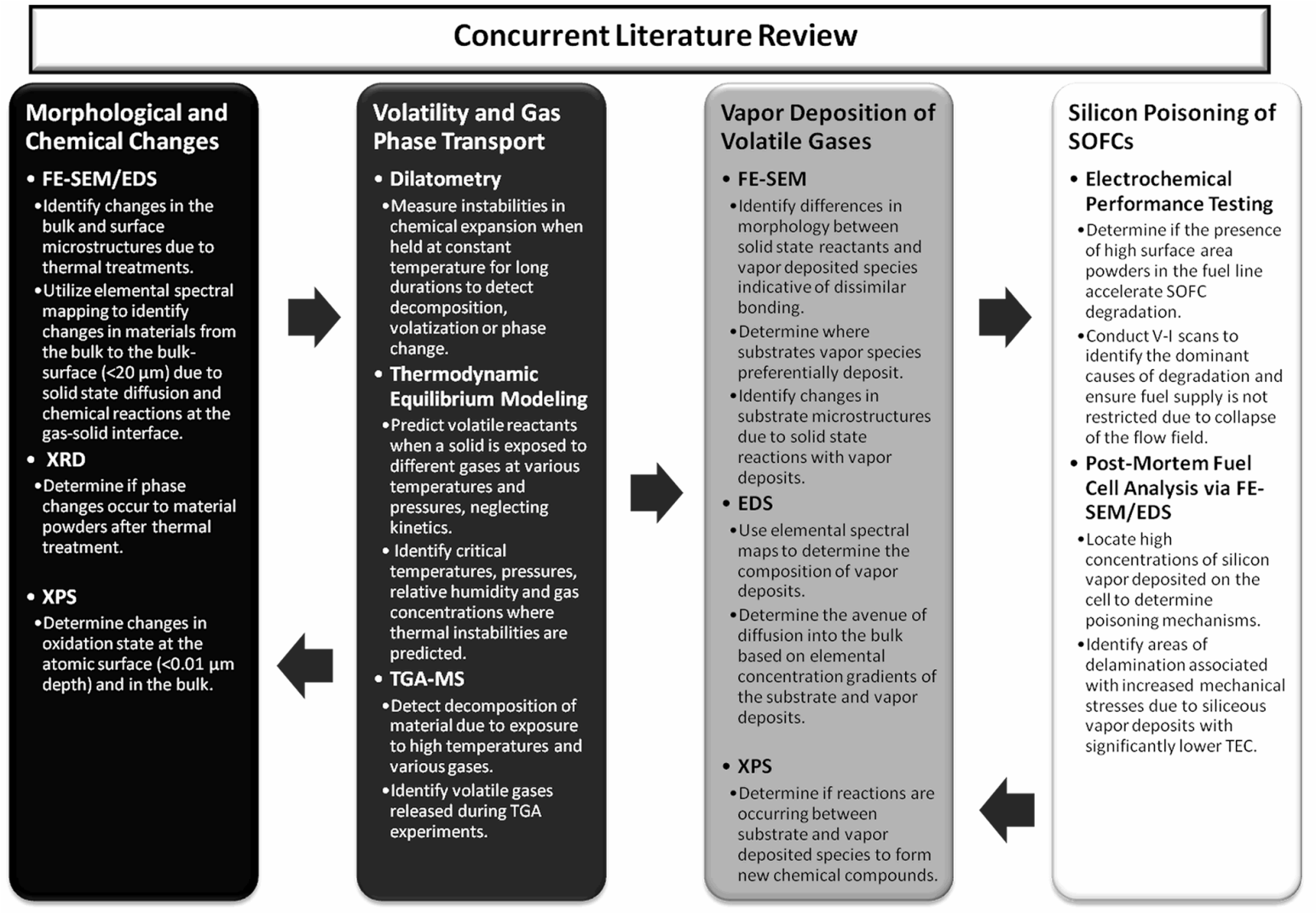

Figure 3: Investigation flow diagram

Aluminosilicate Refractory Material

The primary refractory material investigated as an alternative to high purity alumina is a high density freeze cast aluminosilicate. Chemical analysis performed by Siemens Energy Inc. showed 95.1 wt% Al_2O_3; 4.6 wt % SiO_2. XRD phase analysis results indicate 13.80 wt % $3Al_2O_3 \cdot 2SiO_2$, < 0.2% free silica and the balance Al_2O_3.[9] The aluminosilicate is a thermally stable material (Table 2) that can withstand high temperature fluctuations and gradients common in stationary SOFCs.

Table 2: Aluminosilicate material properties

Mechanical Property			**Thermal Property**		
Theoretical Density	3.9	g/cm^3	Thermal Expansion	7.4	$10^{-6}/°C$
Actual Density	2.74-2.80	g/cm^3	25-1000°C		
Relative Density	70-72	%	Thermal Conductivity		
Flexural Strength, MOR, dry	19-24	MPa	RT	8.6	$W*m^{-1}*K^{-1}$
Flexural Strength, MOR, humid	17-21	MPa	260°C	6.1	$W*m^{-1}*K^{-1}$
Poisson's Ratio, v	0.17		538°C	4.1	$W*m^{-1}*K^{-1}$
Shear Modulus, G	33.23	GPa	815°C	3	$W*m^{-1}*K^{-1}$
Young's Modulus, E	77.53	GPa	1093°C	2.9	$W*m^{-1}*K^{-1}$
Weibull Modulus, m	10.8-11.3				
Fracture Toughness, K_{IC}, dry	1.98-2.00	$MPa/m^{1/2}$			
Fracture Toughness, K_{IC}, humid	1.00-1.57	$MPa/m^{1/2}$			

Source: [9]

Aluminosilicate Morphology and Chemistry

To study changes in the morphology and chemistry of the aluminosilicate refractory due to exposure to SOFC gases at high temperature x-ray photoelectron spectroscopy (XPS), field emission scanning electron microscopy (FE-SEM) coupled with energy dispersive spectroscopy (EDS), x-ray diffraction (XRD) and dilatometry were employed. [8] Prior to selection of the aluminosilicate freeze cast refractory

described previously and studied throughout the manuscripts, the microstructure of high purity (99.8% Al_2O_3) alumina powder (Inframat), various density low purity alumina (97% $A_{l2}O_3$, 3% SiO_2) rigid refractory boards (Zircar ZAL-15AA & ZAL-45AA), and aluminosilicate (43-47% Al_2O_3, 53-57% SiO_2) refractory needled blanket (Unifrax Durablanket S) were studied via FE-SEM. The rigid refractory boards utilize a high purity alumina binder making it well suited to use where silica cannot be tolerated. The density of the refractory boards ZAL-15AA and ZAL-45AA are 0.24 and 0.72 g/cc, respectively. The Durablanket refractory is a completely inorganic flexible blanket spun from cross-linked aluminosilicate ceramic fibers. Each material was separately exposed to unconditioned air at 900°C for 72 hours prior to re-examination of the microstructures.

FE-SEM was utilized to image refractory microstructures at high resolution by exciting low energy secondary electrons with a primary high energy electron beam (up to 20 keV). To produce the image map the detector scans across the surface, measuring secondary electron intensity as a function of position. EDS coupled to FE-SEM utilizes the high energy beam of charged particles bombarding the surface to produce an elemental composition map that can be superimposed over the FE-SEM micrograph. The incident beam excites and ejects an electron from an inner shell, creating an electron hole. In order to minimize energy an electron from an outer higher energy shell fills the hole. The difference in energy between the higher-energy and lower-energy shells is released in the form of an x-ray. (Figure 4)

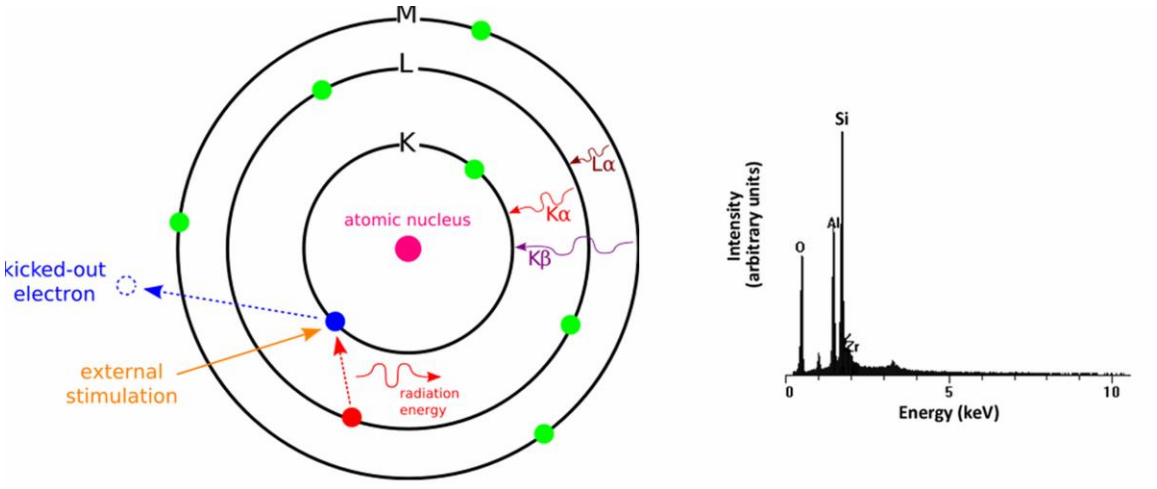

Figure 4: EDS schematic and aluminosilicate spectra

Emitted x-rays can reach the detector from up to 20 µm below the surface (Figure 5), making EDS a bulk-surface sensitive technology compared with XPS which is surface sensitive. EDS is a qualitative chemical analysis measurement that provides only elemental detail.

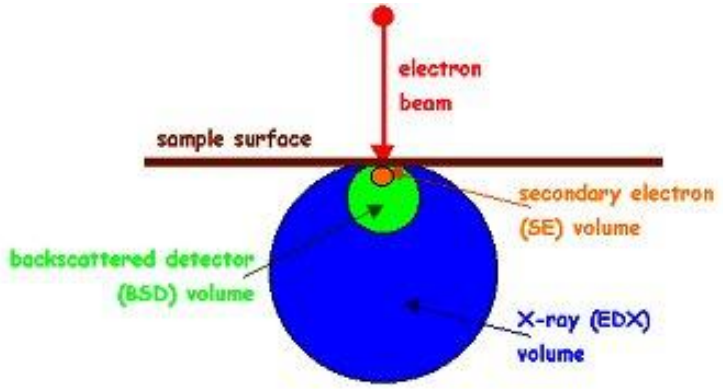

Figure 5: EDS penetration

XPS was used to study changes in chemical compositions and relative concentrations of the constituents in aluminosilicate after high temperature (1000°C) exposure to SOFC gases for 100 hours. XPS measurements are based on the

photoelectric effect. When a material is impacted with low energy x-rays (<1.5 keV) electrons from each orbital are ejected. An electron energy analyzer measures the kinetic energy of the ejected electrons. The kinetic energy, or binding energy, is correlated with electrons released from a specific subshell of an element (Figure 6). Shifts in the spectra are observed due to binding coordination, permitting the identification of chemical compounds and oxidation states of cations. An electron detector counts the electrons released, enabling the correlation of spectra intensity to relative concentration. A relative concentration comparison across a sample set after undergoing several different thermal treatment cycles is useful for detecting significant changes in surface chemistry. XPS is a very surface sensitive technique (<0.01μm) due to the low energy of the impact x-rays and scattering of ejected electrons from below the surface. Space resolved XPS was not available but would have proved useful in identifying oxidation state of vapor deposits, detecting chemical changes in substrate grains versus grain boundaries, and determining the oxidation state of silicon deposits at the SOFC electrolyte/anode interface.

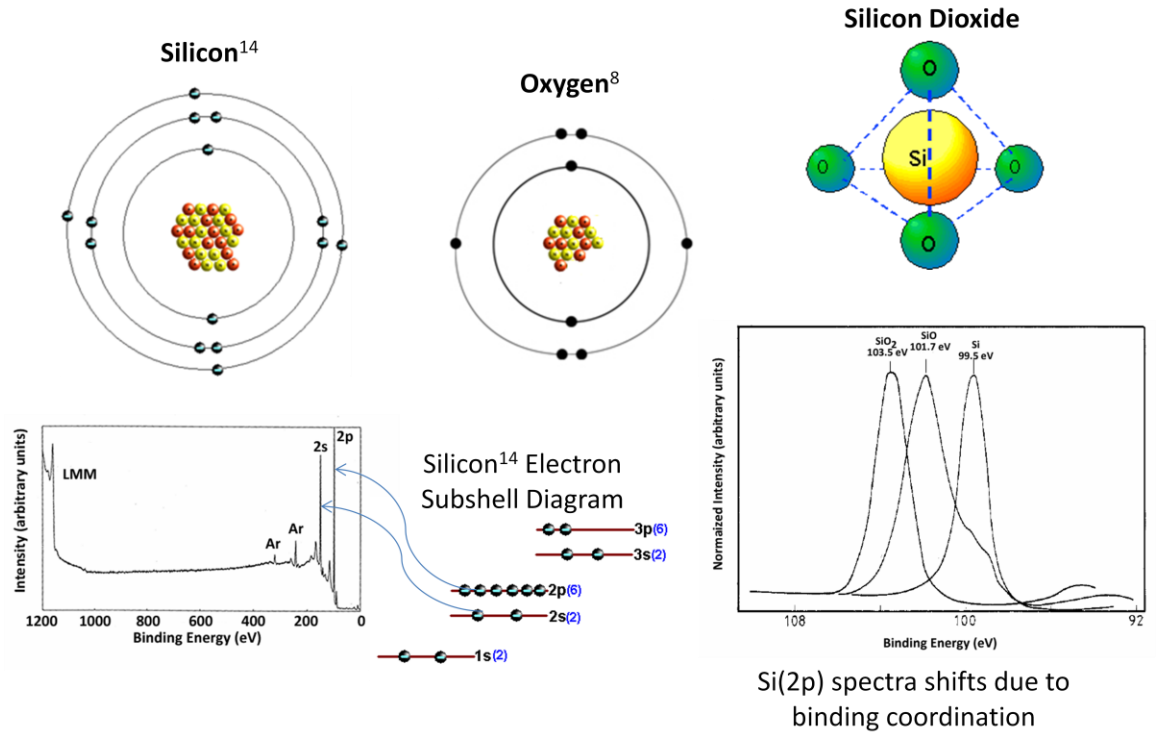

Figure 6: XPS schematic

X-ray diffraction was utilized to detect phase changes in aluminosilicate due to thermal treatment associated with SOFC operation. When high energy x-rays (up to 40kV) impact atoms within a crystal structure they diffract into many specific directions.

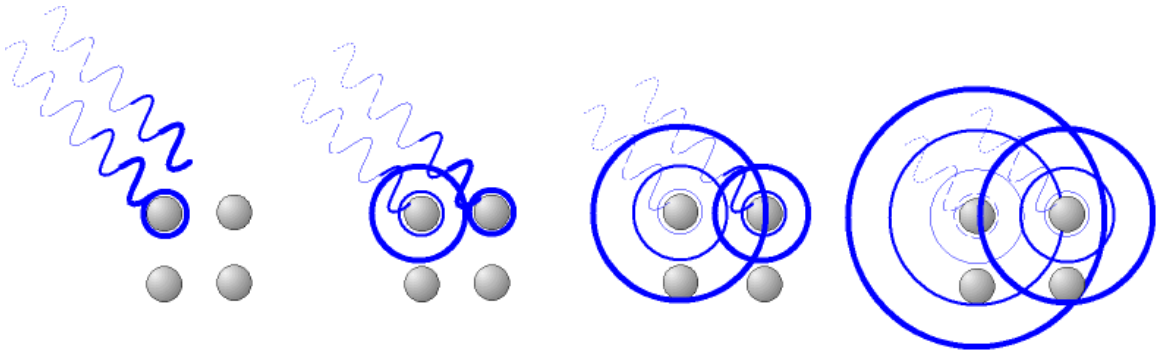

Figure 7: XRD spherical waves

Fundamentally the process involves quantum mechanics processes of absorption and re-emission by the electrons in the lattice planes, which produce spherical waves. (Figure 7) For most angles the re-emitted x-rays interfere destructively with each other, giving off a net signal of zero. However, when theta corresponds with the d-spacing according to Bragg's Law ($\lambda = 2d \cdot \sin\theta$), constructive interference of the x-rays occurs, and a signal is attained. The diffraction pattern obtained reveals detailed information about the chemical composition and crystallographic structure. A powder is used to avoid preferential ordering of the crystals when trying to determine molecular concentrations. Thin-film analysis can be conducted at low angles on a solid to identify the presence of new phases near the surface, but cannot be used for quantitative analysis. In-situ XRD uses a hot-stage and rapid 2θ scanning to correlate temperature with phase changes under a controlled atmosphere. Additionally, in-situ XRD can provide time dependence of phase changes associated with kinetic limitations. In-situ XRD is not presently available at MSU.

Dilatometry was used to measure the change in relative length of aluminosilicate samples due to thermal and chemical expansion when exposed to SOFC gases at 1000°C for 100 hours. A chemical change in sample length when temperature is constant is likely due to decomposition, volatization or phase change. [7]

Silicon Volatility and Gas Phase Transport

The dominant volatile species of silicon vapors released from aluminosilicate, mullite and silica under SOFC operating conditions were predicted utilizing thermodynamic equilibrium modeling software (TERRA).[6][7] The closed

systems are multi-component consisting of gaseous phase, immiscible condensed phase and solid solution components. To predict the partial pressure of all three phases the system's entropy is maximized (in turn minimizing Gibb's Free Energy of Formation) while simultaneously applying conservation of internal energy and mass, and the electroneutrality condition. The normalization conditions for each of the solid solutions are satisfied. [10] Pressure, temperature and composition are the key constraints defined.

$$S = \sum_{i=1}^{k} \left(S_i^{\,0} - R_0 \cdot \ln\left(\frac{R_0 \cdot T n_i}{\nu} \right) \right) \cdot n_i + \sum_{r=1}^{R} \left(S_r^{\,0} \cdot n_r \right) + \sum_{x=1}^{X} \sum_{q=1}^{Q} \left[\left(S_{xq}^{\,0} - R \cdot \ln\left(\frac{n_{xq}}{n_x} \right) \right) \cdot n_{xq} \right]$$

$$-U + \sum_{i=1}^{k} \left(U_i \cdot n_i \right) + \sum_{r=1}^{R} \left(U_r \cdot n_r \right) + \sum_{x=1}^{X} \sum_{q=1}^{Q} \left(U_{xq} \cdot n_{xq} \right) = 0$$

$$b_j = \sum_{i=1}^{k+R+X} \left(a_{ji} \cdot n_i \right) \qquad j = 1, 2 .. m \qquad \sum_{i=1}^{k} \left(a_{ei} \cdot n_i \right) = 0$$

$$\sum_{q=1}^{Q} \left(\frac{n_{qx}}{n_x} - 1 \right) = 0 \qquad n_x \geq 0 \qquad x = 1, 2 .. X$$

Table 3: Thermodynamic equilibrium variables

a_{ei}	Stoichiometric coefficients
a_{ji}	Stoichiometric coefficients
b_j	Mole fraction of the element j in the system
k	# of gas components
n	# of moles
Q_x	# of components in a solid solution x
R	# of single immiscible condense phase components
R	Universal gas constant
S_i^0	Standard entropy of gas phase i at temperature T and pressure 1 atm
S_r^0	Standard entropy of a single condense phase component r [function(T) only]
$S_{xq}^{\,0}$	Standard entropy of component q of the solid solution x

Table 3 Continued

T	Temperature
U	Total internal energy of the system
U_i	Internal energy of gas phase components
U_r	Internal energy of single immiscible components of condense phase
U_{xr}	Internal energy of components of solid solutions
X	# of solid solutions
v	Specific volume of the gaseous phases

Since thermodynamic equilibrium modeling does not account for kinetics and is limited on available thermo-chemical data, thermal gravimetric analysis (TGA) coupled with mass spectrometry (MS) and transpiration techniques were employed. [11] Empirical results provide an estimate of time when a steady state condition relative to thermodynamic equilibrium modeling is reached. TGA measures the change of mass in a small sample under a high temperature controlled atmosphere for extended periods. A TGA is extremely responsive, allowing the detection of milligram weight changes as a result of silicon vaporization. The MS sniffs a small sample of gases exhausted from the sample in the TGA, transporting it to a quadrupole mass spectrometer in a vacuum. The MS measures the mass to charge ratio of ionic compounds and elements. All compounds with an equal mass to charge ratio travel along the same path in the vacuum. When subjected to an electric or magnetic field the compounds will change their path. Knowing the change in position the mass to charge ratio can be calculated to determine compound compositions. Transpiration studies measured the quantity of silicon condensed downstream on a cooled carbon wafer via Rutherford Backscattering Spectrometry (RBS). [12] This work was completed by MSU collaborators and is outside the scope of this dissertation. For more information refer to the manuscript 2. [7]

Thermodynamic equilibrium calculations obtained via TERRA were also utilized to determine the potential for infiltrating the aluminosilicate material with a suitable solution precursor dopant to lock up free silicon and reduce the release rates. These results are reported in the supplemental results section. The following three dopants were evaluated at five weight percent.

1. Calcium Oxide via Calcium Nitrate - $Ca(NO_3)_2$
2. Magnesium Oxide via Magnesium Nitrate - $Mg(NO_3)_2$
3. Titanium Oxide via Titanium Isopropoxide – $Ti[OCH(CH_3)_2]_4$

Deposition of Aluminosilicate Vapors on SOFC Materials

The deposition of vapors released from aluminosilicate on YSZ and nickel pellets at high temperatures under SOFC fuel or oxidant atmospheres (Figure 8) was studied utilizing FE-SEM, EDS and XPS. [8] FE-SEM micrographs of agglomerations are compared with EDS maps to correlate bulk-surface morphology with elemental composition. XPS expands on the EDS elemental maps by providing chemical composition information of the substrate and bonded agglomerations.

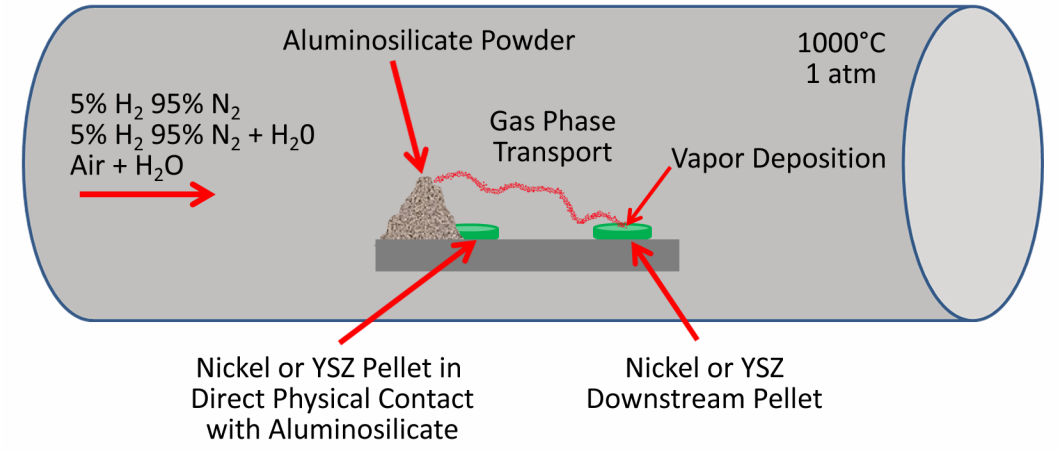

Figure 8: Deposition experimental setup

Silicon Poisoning in SOFCs

Electrochemical performance testing on SOFC electrolyte supported cells (ESC) was conducted to determine the affects of aluminosilicate vapors within the fuel stream. The single cell test fixture, described in detail elsewhere [13][6][8], utilizes a seal free design and permits the studying of planar SOFCs up to 6 cm in diameter. (Figure 9)

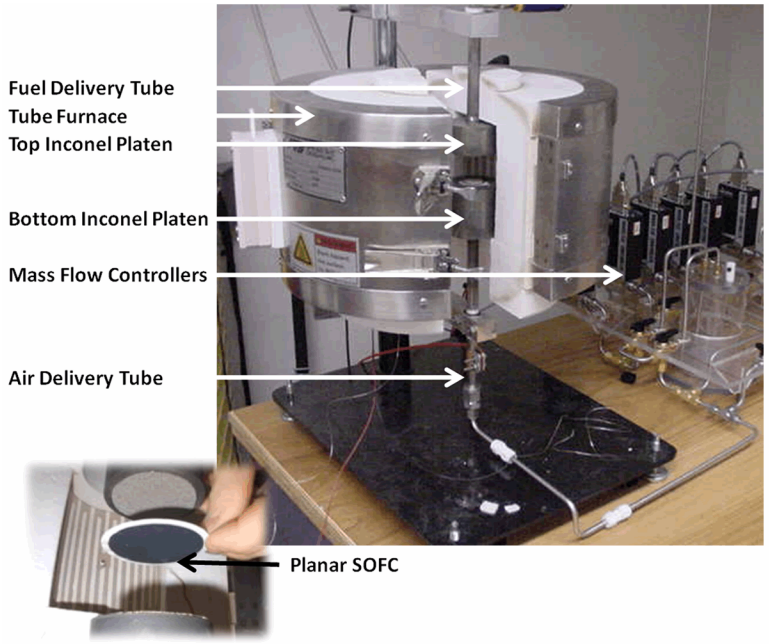

Figure 9: Planar SOFC single cell test fixture

In addition to the results reported in the manuscripts [6][8], electrochemical VI scans characterizing the polarization losses of SOFC unit cells due to exposure to aluminosilicate vapors are presented in the supplemental results. Fuel cells operate below their ideal potential due to activation, ohmic, and concentration polarizations. (Figure 10) Ohmic polarization (η_{ohm}) can be expressed with the following equation:

$$\eta_{ohm} = i*R$$

where i is the current flowing through the cell, and R is the total cell resistance. The total ohmic cell resistance is the culmination of electronic, ionic and contact resistance.

$$R = R_{electronic} + R_{ionic} + R_{contact}$$

The electronic resistance occurs in the electrodes, current collectors and interconnects. Silicon poisoning can be observed as an increase in ohmic polarization due to formation of an ionic and electronically insulating siliceous glass phase at the electrolyte/electrodes interfaces; or as an increase of activation polarization due to the reduction of catalytic activity at nickel sites that are blocked by formation of a siliceous barrier layer. Concentration polarization is due to an inadequate supply of fuel or oxidant reaching the electrochemically active triple phase boundary (TPB).

Deviation from ideal performance due to three polarization effects.

Activation – Kinetic limitations

Ohmic – Electrical and ionic resistance

Concentration – Poor fuel or oxidant delivery to TPB

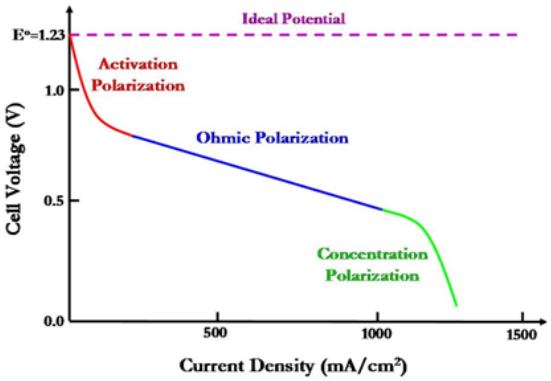

Figure 10: Electrochemical polarization behavior in Voltage-Current (VI) curves

PROGRESS IN UNDERSTANDING SILICA TRANSPORT PROCESS AND EFFECTS IN SOLID OXIDE FUEL CELL PERFORMANCE

Contribution of Authors and Co-Authors

Lead corresponding author: Paolo R. Zafred
Contributions: Drafted introduction based on Siemens prior intellectual work and a MSU literature review detailed in project technical reports. Provided revisions of the article regarding important Siemens intellectual content and continuity. Provided final approval of the manuscript, submitted it to ASME for review and presented the findings at the Eight International Fuel Cell Science, Engineering & Technology Conference.

Co-author: Stephen W. Sofie
Contributions: Collaborated on the conception and design of the study, interpretation of assembled data and drafting of manuscript. Provided critical revisions of the article regarding important intellectual content. Provided final approval of the article.

Co-author: Paul S. Gentile
Contributions: Collaborated on literature review and the conception and design of the study. Collected, assembled, analyzed and interpreted experimental data. Collaborated on the drafting of manuscript. Provided critical revisions of the article regarding important MSU intellectual content.

Manuscript Information Page

- PROGRESS IN UNDERSTANDING SILICA TRANSPORT PROCESS AND EFFECTS IN SOLID OXIDE FUEL CELL PERFORMANCE
- Authors: Paolo R. Zafred, Stephen W. Sofie, Paul S. Gentile
- Journal Name: Proceedings of the ASME Eight International Fuel Cell Science, Engineering & Technology Conference in Brooklyn, New York, USA
- Status of manuscript (check one)

  ☐ Prepared for submission to a peer-reviewed journal

  ☐ Officially submitted to a peer-reviewed journal

  ☐ Accepted by a peer-reviewed journal

  ☒ Published in a peer-reviewed proceedings publication

- Publisher: American Society of Mechanical Engineers
- Published July, 2010

PROGRESS IN UNDERSTANDING SILICA TRANSPORT PROCESS AND EFFECTS IN SOLID OXIDE FUEL CELL PERFORMANCE

Paolo Zafred[a], Stephen W. Sofie[b], Paul S. Gentile[b]

[a] Siemens Energy Inc., Pittsburgh, Pennsylvania, USA
[b] Montana State University, Bozeman, MT, USA

Abstract

One of the enabling technologies required for commercialization of high efficiency solid oxide fuel cell (SOFC) stacks is the development of low cost ceramic refractories capable of withstanding the harsh environment during start-up and steady state operation. Although low density, high purity fibrous alumina materials have been used for more than two decades in manufacturing of SOFC stack components, their low mechanical strength and high cost have precluded their use in the next generation pre-commercial generator modules.

A current trend in SOFC stack design is to use high strength, low purity mullite bonded, cast ceramics which can be produced in large volume at a relatively low cost. Sufficient strength is required to provide structural support of the stack and its upper internals in addition to withstanding the severe thermal gradients in both steady state and transient conditions. To reduce costs while achieving suitable mechanical strength, thermal shock, and creep resistance, certain levels of silica and other impurities are present in the refractory ceramic. Silica, however, has been established to poison SOFC anodes thus degrading cell performance and stack life. Therefore, silica transport within the stack has become a dominant issue in SOFC generator design. As a result, an important design requirement for the stack ceramic materials is to develop a fundamental understanding of the silicon species transport process based on refractory composition and gas atmosphere in effort to minimize silicon species volatilization through the porous material.

The vaporization behavior of the Al-Si-O system has been investigated in numerous studies and verified experimentally. It is well known that when aluminum silicate components are exposed to a reducing atmosphere, the partial pressure of oxygen is low, therefore this causes formation of volatile SiO(g). This SiO(g) gaseous phase is transported by the fuel stream to the anode/electrolyte interface and electrochemically oxidizes back into SiO2 over the triple phase boundaries (TPB) by the oxygen transported via the fuel cell. This re-deposition process of SiO2, known also as Si poisoning, blocks the reaction of fuel oxidation as it takes over the reactive sites, leading to noticeable degradation in cell performance. In this paper, the status of research on formation of volatile silicon species in aluminosilicate SOFC insulation materials is examined. The formation of volatile SiO(g), SiO(OH)(g), and SiO(OH)2(g) are indicated

to facilitate silicon transport in anode fuel streams. Silica deposition is shown to degrade fuel cell anode performance utilizing a novel SOFC silicon poisoning test setup, and silica deposition is only observed on YSZ in the electrochemically active regions of the cell.

Manuscript

SILICON VOLATILITY FROM ALUMINA AND ALUMINOSILICATES UNDER SOLID OXIDE FUEL CELL OPERATING CONDITIONS

Contribution of Authors and Co-Authors

Lead corresponding author: Paul S. Gentile
Contributions: Collaborated on the conception and design of the study. Collected, assembled, analyzed and interpreted thermodynamic equilibrium modeling, thermal gravimetric analysis and dilatometry experimental data. Conducted literature review, led writing efforts on all aforementioned experiments and compiled co-author contributions into a cohesive document. Prepared manuscript, tables and figures for publication. Provided final approval of the manuscript and submitted it to International Journal of Applied Ceramics for review.

Co-author: Stephen W. Sofie
Contributions: Collaborated on the conception and design of the study. Assisted with the interpretation of assembled data. Provided critical revisions of the article regarding important intellectual content. Provided final approval of the article content and journal source.

Co-author: Camas F. Key
Contributions: Collected, assembled, analyzed and interpreted Rutherford Backscattering (RBS) volatility experiments. Contributed discussion regarding the experimental methods and results of RBS experiments.

Co-author: Richard J. Smith
Contributions: Collaborated on the conception and design of the study. Assisted with the interpretation and discussion of RBS results. Reviewed article organization, formatting and technical accuracy.

Manuscript Information Page

- SILICON VOLATILITY FROM ALUMINA AND ALUMINOSILICATES UNDER SOLID OXIDE FUEL CELL OPERATING CONDITIONS
- Authors: Paul S. Gentile, Stephen W. Sofie, Camas F. Key, Richard J. Smith
- Journal Name: International Journal of Applied Ceramic Technology
- Status of manuscript (check one)

  ☐ Prepared for submission to a peer-reviewed journal

  ☒ Officially submitted to a peer-reviewed journal

  ☐ Accepted by a peer-reviewed journal

  ☐ Published in a peer-reviewed journal

- Publisher: Wiley-Blackwell Publishers
- Submitted September 2, 2010

SILICON VOLATILITY FROM ALUMINA AND ALUMINOSILICATES UNDER SOLID OXIDE FUEL CELL OPERATING CONDITIONS

Paul S. Gentile[a], Stephen W. Sofie[a], Camas F. Key[b], Richard J. Smith[b]

[a] Montana State University – Mechanical Engineering – Bozeman, MT, 59717
[b] Montana State University – Physics – Bozeman, MT, 59717

Abstract

Thermodynamic equilibrium modeling indicates the introduction of H_2O in oxidizing environments decreases Si stability due to formation of volatile hydroxide and oxy hydroxides. $3Al_2O_3 \cdot 2SiO_2$ bond offers only a slight improvement on silicon stability over SiO_2 in humidified oxidizing environments. In reducing atmospheres Si stability is improved by the presence of H_2O and Al_2O_3, transitioning from SiO and silane as the dominant volatile species to hydroxides, oxy hydroxides and SiO with increasing water vapor partial pressure. Transpiration, thermal gravimetric and dilatometry studies reveal initial rapid releases of Si from SOFC refractory materials followed by slower solid state diffusion limited release.

1.0 Introduction

Stationary solid oxide fuel cells (SOFCs) have been demonstrated to provide clean, reliable electricity via electro-chemical conversion of various fuel sources. To become a competitive conversion technology for commercial and consumer application, the costs of SOFC systems must be reduced. For large stationary tubular systems a large fraction of the overall generator module costs are from the relatively expensive high purity (>99.8%) alumina (Al_2O_3) refractory boards and fuel or oxidant delivery tubes. The replacement of high purity alumina refractory with aluminosilicate (alumina [Al_2O_3] plus silica) offers promise to drive down system costs. Raw material costs of aluminosilicates are lower than high purity alumina due to the extensive processing required to remove naturally occurring silica impurities from alumina. Mullite ($Al_{4+2x}Si_{2-2x}O_{10-x}$ with x ranging between 0.18 and 0.88 [1]) is an aluminosilicate based on

replacement of Al^{3+} ions with Si^{4+} ions. It is a widely used refractory of considerable technical importance due to its superior mechanical and thermal properties at high temperatures (low thermal expansion coefficient [$5.45*10^{-6}$/°K] [2] and hence excellent thermal shock resistance, beyond that of even high purity alumina [$8.8*10^{-6}$/°K] [3]). However, prior to the implementation of aluminosilicate the thermal stability and hence release of silicon vapors from these materials under humidified reducing and oxidizing environments must be investigated to ensure high temperature SOFC performance and reliability is not sacrificed due to silicon contamination.

Long duration SOFC performance may be limited in part by silicon impurities that form an oxide at the Triple Phase Boundary (TPB). [4][5][6] The silicon oxide does not participate directly in the oxygen exchange reaction, acting as an ionic insulator by blocking active sites supporting oxygen exchange. [7] The silicon oxide also retards water at the TPB which may cause the electrical conduction of the SOFC layers to be much lower. [8] Schmidt et al [9] showed that nickel electrode polarization was increased due to silicon impurities in electrolyte material via impedance spectroscopy.

Acceptable levels of silicon impurities for SOFC operation remain unclear due to the difficulties in quantifying the various sources of silicon. Silicon is second only to oxygen as the most abundant element in the earth's crust and is found throughout SOFC systems, manufacturing plants and laboratories. Silicon sources include oil vapors in laboratory air from vacuum pumps and gas seals [8], bulk powder impurities that diffuse to the surface [10][11] and high temperature processing artifacts from furnace insulation and SiC or $MoSi_2$ heating elements. The source of interest in this investigation is SOFC refractory materials for insulation and gas delivery tubing which constitutes the largest

concentration of potential silicon contamination. Figure 1 illustrates the process of silicon poisoning in tubular SOFCs due to refractory materials including insulation and fuel or oxidant delivery tubes. Silicon migrates via solid state diffusion (1) from the bulk to the surface of the low purity alumina or aluminosilicate refractory insulation and fuel or oxidant delivery tubes. At the gas-solid interface chemical reactions driven by thermodynamics and kinetics occur between silicon and the humidified fuel or oxidant gas streams (2). The volatile silicon species are then transported in gas phase to the SOFC (3). Finally, the silicon diffuses through the electrodes to the triple phase boundary (4) where it acts as an electrical insulator and adversely affects O_2 exchange kinetics.

The volatility of vapor species from silica (SiO_2) has been studied extensively. [12][13][14][15][16][17][18][19][20][21][22][23] It was found that in dry oxygen, SiO_2 is remarkably durable at 1000 °C. [24] However, literature findings [17][19][20][23] suggest silicon hydroxides and –oxy hydroxides play an important role in the volatility of Si from silica in the presence of water vapor (Eqns. 1-4), which is ubiquitous in fuel cell gas streams. The decomposition of the $Al_6Si_2O_{13}$ phase on the bulk surface of mullite into alumina through removal of the silica component as silicon hydroxide has been reported in air at 1500 °C with 30 wt% water vapor [25] (Eqn. 5). The silicon oxy hydroxide gases may be electrochemically reduced to silicon monoxide and deposited on the solid oxide fuel cell (Eqn. 6). Furthermore, hydrocarbon fuel reformation in the SOFC consumes water leading to a lower partial pressure of water vapor on the fuel anode side (Eqn. 7) and could cause silica deposition from silicon hydroxide (reverse of Eqn. 1).

The reformation process also releases carbon monoxide which has been shown to react with silica and mullite to form volatile silicon monoxide (SiO) (Eqns. 8-9). [26][27]

1 $\mathbf{SiO_2}(s) + \mathbf{2H_2O}(g) \rightarrow \mathbf{Si(OH)_4}(g)$

2 $\mathbf{2SiO_2}(s) + \mathbf{H_2O}(g) \rightarrow \mathbf{2SiO(OH)}(g) + \mathbf{½O_2}(g)$

3 $\mathbf{SiO_2}(s) + \mathbf{H_2O}(g) \rightarrow \mathbf{SiO(OH)_2}(g)$

4 $\mathbf{2SiO_2}(s) + \mathbf{3H_2O}(s) \rightarrow \mathbf{Si_2O(OH)_6}(g)$

5 $\mathbf{Al_6Si_2O_{13}}(s) + \mathbf{4H_2O}(g) \rightarrow \mathbf{3Al_2O_3} + \mathbf{2Si(OH)_4}(g)$

6 $\mathbf{SiO(OH)}(g) + \mathbf{O_2^-}(g) \rightarrow \mathbf{SiO}(s) + \mathbf{H_2O}(g) + \mathbf{2e^-}$

7 $\mathbf{CH_4} + \mathbf{H_2O} \rightarrow \mathbf{CO} + \mathbf{3H_2}$

8 $\mathbf{2SiO_2}(s) + \mathbf{H_2}(g) + \mathbf{CO}(g) \rightarrow \mathbf{2SiO}(g) + \mathbf{H_2O}(g) + \mathbf{CO_2}(g)$

9 $\mathbf{Al_6Si_2O_{13}}(s) + \mathbf{2CO}(g) \rightarrow \mathbf{3Al_2O_3}(s) + \mathbf{2SiO}(g) + \mathbf{2CO_2}(g)$

SiO can volatize at high temperatures as a result of the interaction between solid state silica and Si (Eqn. 10). [28] In a reducing H_2 atmosphere at high temperature silicon dioxide will break down to form silicon monoxide due to the low partial pressure of oxygen (Eqn. 12) even in the presence of water vapor. [29] Similarly, the reduction of mullite by hydrogen gas to form volatile SiO has been reported (Eqn. 13). [30] Since SiO condenses easily to amorphous monoxide on cooler surfaces [31] it is likely to form a glassy layer on the SOFC surface in a reducing atmosphere. Condensed SiO can readily accept available oxygen at SOFC temperatures to form silicon dioxide (Eqn. 14). Furthermore, condensed SiO(s) undergoes a phase transformation (decomposition) to the more stable mixture of SiO_2(s) + Si(s) over the wide temperature range of 27-1450 °C (Eqn. 15). [31]

10 $\mathbf{SiO_2}(s) + \mathbf{Si}(s) \rightarrow \mathbf{2SiO}(g)$

11 $\mathbf{SiO_2}(s) + \mathbf{H_2}(g) \rightarrow \mathbf{SiO}(g) + \mathbf{H_2O}(g)$

12 $\mathbf{SiO_2}(s) \rightarrow \mathbf{SiO}(g) + \mathbf{½O_2}(g)$

13 $\mathbf{Al_6Si_2O_{13}}(s) + \mathbf{2H_2}(g) \rightarrow \mathbf{3Al_2O_3}(s) + \mathbf{2SiO}(g) + \mathbf{2H_2O}(g)$

14 $\mathbf{2SiO}(s) + \mathbf{O_2}(g) \rightarrow \mathbf{2SiO_2}(s)$

15 $\mathbf{2SiO}(s) \rightarrow \mathbf{SiO_2}(s) + \mathbf{Si}(s)$

Volatile silane gases (SiH_x, where x=1,2,4) have the potential to form as a result of interaction of silica with water vapor (Eqns. 16-17) or hydrogen (Eqns. 18-20) in reducing atmospheres due to the low partial pressure of oxygen. The silane gases then may deposit as silica when exposed to oxygen at the triple phase boundary (TPB). Mullite heat treated in a CO environment at temperatures between 1000 and 1600 °C was shown to decompose into corundum (Al_2O_3) and SiO (Eqn. 21). [27] During tests conducted by Kronert and Buhl an increase in the quantity of corundum was observed as a function of reduction temperature and time, where results suggest the rate the reaction proceeds is governed by gas diffusion and not the reaction at the phase boundary.

16 $\mathbf{2SiO_2}(s) + \mathbf{2H_2O}(g) \rightarrow \mathbf{2SiH_2}(g) + \mathbf{3O_2}(g)$

17 $\mathbf{SiO_2}(s) + \mathbf{2H_2O}(g) \rightarrow \mathbf{SiH_4}(g) + \mathbf{2O_2}(g)$

18 $\mathbf{2SiO_2}(s) + \mathbf{H_2}(g) \rightarrow \mathbf{2SiH}(g) + \mathbf{2O_2}(g)$

19 $\mathbf{SiO_2}(s) + \mathbf{H_2}(g) \rightarrow \mathbf{SiH_2}(g) + \mathbf{O_2}(g)$

20 $\mathbf{SiO_2}(s) + \mathbf{2H_2}(g) \rightarrow \mathbf{SiH_4}(g) + \mathbf{O_2}(g)$

21 $\mathbf{Al_6Si_2O_{13}}(s) + \mathbf{2CO}(g) \rightarrow \mathbf{3Al_2O_3}(s) + \mathbf{2SiO}(g) + \mathbf{2CO_2}(g)$

Brady [17] calculated the likely volatile silicon-containing molecular species from silica in humidified air based on: (1) experimental results reported in the literature [13][14][15][32] regarding the concentration of silica in the vapor phase when steam is equilibrated with siliceous molecules, and (2) Newton's [33] calculated ratio of fugacity to pressure for gases which obey the van der Waals equation of state in reduced form. It was concluded that $Si(OH)_4$ and $Si_2O(OH)_6$ were the likely volatile silicon species at low temperatures (205-260°C), with the former predominating at pressures from approximately 400-2000 atm and the latter dominating at lower pressures from 33-400 atm. Based on findings [18] [20][21] analyzed and verified by Jacobson[20] it appears that silicon hydroxide ($Si(OH)_4$) is the dominant vapor species from silica at temperatures from approximately 900-1100 °C with $x(H_2O)$=0.37 atm and P(total)=1 atm, whereas above 1100 °C silicon oxy hydroxide ($SiO(OH)_2$) release may also be important. Opila's [23] discussion of the findings of Hashimoto [18] and Krikorian [21] indicates that in an oxidizing environment from 1100-1500 °C with a partial pressure of water vapor ranging from 0.1-1.0 atm $Si(OH)_4$ and $SiO(OH)_2$ remain the dominant volatile species, where at $x(H_2O)$=0.1 atm $SiO(OH)_2$ dominates and at $x(H_2O)$=1.0 atm contributions from both $Si(OH)_4$ and $SiO(OH)_2$ are significant.

The volatile silicon gases represent a potential problem since humidified oxidant and hydrogen fuel streams in SOFCs are in direct contact with the refractory materials at temperatures from 800-1000°C. Therefore the stability of silicon phases in aluminosilicates represents a potential roadblock to their implementation in SOFCs, particularly systems designed for long operational cycles. Despite great efforts made in understanding Si volatility from silica compounds, little efforts have been made to

understand the release of Si from aluminosilicates including 3:2 mullite under SOFC operating conditions. The objectives of this investigation are to: (1) identify the volatile silicon species that can be released by alumina or aluminosilicate refractory compounds under SOFC operating conditions, (2) identify potential mechanism(s) of volatilization and (3) quantify the overall rate of release.

2.0 Experimental Procedure

All molecular compositions reported throughout this paper are stated in molar concentration unless otherwise noted. A custom formulated aluminosilicate refractory compound developed for SOFC applications (MSU1) was thermodynamically modeled and experimentally studied via thermal gravimetric analysis (TGA), dilatometry and Rutherford Backscattering (RBS) techniques. MSU1 refractory represents a lower cost alternative than both high purity alumina and pure mullite, with sufficient silicon content for experimental study. MSU1 was prepared by freeze casting and sintering to obtain a relatively high theoretical density (~70%) and low porosity (20-23%) refractory with molar concentrations calculated via x-ray diffraction of approximately 96.31% alumina (Al_2O_3) and 3.69% mullite ($Al_6Si_2O_{13}$). The molar concentration of free silica and impurities present in MSU1 was below the XRD phase detection limit of 0.4%.

2.1 Theoretical Thermodynamic Equilibrium Calculations

Thermodynamic modeling software (TERRA) models the equilibrium states in isolated multi component systems containing gaseous phase, immiscible condensed phase and solid solutions components. TERRA software is described in detail elsewhere [34] therefore only a brief discussion is included here. TERRA is a version of the ASTRA code which utilizes the universal method and calculation algorithm based on the

fundamental principles of chemical thermodynamics. In compliance with the second law of thermodynamics the system's entropy is maximized. Simultaneously conservation of energy and mass for the isolated system and the electro neutrality condition are applied to obtain all phase equilibrium parameters. TERRA interfaces with a large thermochemical database containing amongst others silica, alumina and aluminosilicates (including mullite) refractory compounds, as well as aluminum and silicon based compounds in the gaseous phase compatible with JANAF-NIST and SGTE. [35] [36] [37] The database was further expanded for this study to contain the expected volatile silicon gases including $Si(OH)_2$, $Si(OH)_4$, $SiO(OH)$, $SiO(OH)_2$ and H_2SiO based on data published by Sandia National Laboratory. [38] Thermodynamic equilibrium modeling simulated the previously mentioned MSU1 aluminosilicate material (Al_2O_3 96.31%, $Al_6Si_2O_{13}$ 3.69%), high purity alumina (Al_2O_3 99.96%, SiO_2 0.04%), pure 3:2 mullite ($Al_6Si_2O_{13}$ or alternatively written as $3Al_2O_3{\cdot}2SiO_2$), and quartz (SiO_2). All modeling experiments were conducted throughout a temperature range of 600-1400°C and the pressure was set at atmospheric (0.1 MPa) since fuel and oxidant streams in SOFCs are not typically pressurized. Thermodynamic modeling environments simulated include dry air (Ar 0.933%, CO_2 0.030%, N_2 78.088%, O_2 20.949%), high humidity air (Ar 0.589%, CO_2 0.019%, N_2 49.267%, O_2 13.217%, H_2O 36.909%), low humidity air (Ar 0.911%, CO_2 0.029%, N_2 76.243%, O_2 20.454%, H_2O 2.363%), hydrogen (H_2), humidified hydrogen (H_2 97.69%, H_2O 2.31%), simulated reformate gas (CO 5.1%, CO_2 23.8%, H_2 11.9%, CH_4 15.4%, H_2O 43.4%, N_2 0.4%), syngas (CO 2.1%, CO_2 8.6%, H_2 84.5%, CH_4 3.0%, N_2 1.8%) and humidified argon (Ar 64.3%, H_2O 35.7%).

2.2 Dilatometry

Dilatometry studies were completed using an upright dilatometer (Linseis L75), force controller box (Linseis L75/N2), alumina push rod and type S thermocouple. A preloading force of 300 mN was applied to the samples. Dilatometer measurements were completed on solid (7 x 7 x 2 mm) blocks cut with a diamond saw from a large freeze cast block of the MSU1 aluminosilicate material. The tests were separately run on new samples for 100 hours at 1000°C in humidified air, hydrogen forming gas (5.2% H_2, Balance N_2) and humidified hydrogen forming gas. A compressed gas cylinder provided the hydrogen forming gas while the ultra-high purity (UHP) hydrocarbon free compressed air was provided with a zero air generator (Packard 2500). Gases were fed to a gas control box (Linseis L40/2054) where flow rates were controlled at 1.5 liters per hour at P(total)=0.10 MPa. For humidification the compressed gases leaving the flow controller box were introduced into the bottom of a bubbler cylinder of deionized water at ambient temperature. Complete saturation is assumed based on the gas path length through the water resulting in the partial pressure of water vapor during humidified experiments of $x(H_2O)$=0.027 atm in air and $x(H_2O)$=0.023 atm in the reducing hydrogen forming gas. Gases were then introduced into the bottom of the airtight dilatometer high purity alumina furnace chamber starting 2 hours prior to the heating cycle, passed over the sample and evacuated through the top. Dilatometer baseline measurements were collected separately under each atmosphere and subtracted from sample runs to compensate for equipment thermal expansions which vary in the different gases. All experiments were ramped from ambient to 1000°C at a rate of 5°C per minute and held at temperature for 100 hours.

2.3 Thermal Gravimetric and Coupled Mass Spectrometry Analysis

TGA was conducted on an upright system (Linseis Thermowaage L81). An MSU1 freeze cast block was crushed into a powder utilizing a mortar and pestle (Diamonite^{TM}) manufactured from finely powdered synthetic sapphire. Particle size analysis on the powder was conducted using a standard light optical microscope. Results indicate an average particulate size of 477 μm, ranging from 66 to 1765 μm with a standard deviation of 361 μm. Sample sizes were approximately 1850 mg, where results are normalized and presented as relative weight change (%). TGA experiments on MSU1 were run in humidified air, hydrogen forming gas (5.2% H_2, Balance N_2) and humidified hydrogen forming gas to study the change in weight at 1000 °C over 250 hours, after the initial heating cycle from ambient to 1000°C at a rate of 5°C per minute. Gases were supplied and controlled identical to the methods described for the dilatometer experiments.

TGA coupled with evolved gas analysis via mass spectrometry the volatility of 3:2 mullite ($Al_6Si_2O_{13}$), low purity alumina (Al_2O_3 96% SiO_2 4%) and high purity alumina (Al_2O_3 99.9% SiO_2 0.1%) held at 850°C in argon (99.999% pure) plus 20 weight percent H_2O for up to 50 hours according to the techniques described in detail elsewhere. [39] Gases flowing at a constant rate of 30 liters per hour and steam were introduced through a water flask heated to give the desired water vapor partial pressure. TGA coupled with evolved gas analysis was conducted using a thermobalance (sensitivity of 10^{-7} g) of symmetrical thermoanalyser (SETARAM-TAG 160model). Volatile silicon species were identified utilizing a Quadrupole Mass Spectrometer (PFEIFFER VACUUM Instruments QMS 422) located inside the oxidation system. Respective backgrounds were subtracted from all mass spectrometry results.

2.4 Transpiration System utilizing Rutherford Backscattering (RBS)

A simple transpiration experiment for evaluating volatile impurities in SOFCs systems was developed as described by Collins. [40] The transpiration apparatus consisted of a 33 cm long tube furnace with a 35 mm diameter heating zone used to heat low purity alumina, mullite and quartz tubes as well as MSU1 refractory cubes to a max temperature of 800°C in the furnace's central heating zone. Volatility measurements were carried out on each tube by fitting a bubbler to one end of the tube, thus providing humidification to the incoming gas stream. On the exiting end of the tube, a 27 mm diameter water cooled copper heat-sink, fitting snugly within the tube, condensed volatile elements from the outpouring gas stream. The primary focus of this study was to measure raw Si release rates from tubes and refractory materials.

To facilitate RBS analysis, a thin glassy carbon wafer was well adhered to the copper heat-sink using carbon tape. Wafers were swapped out with new ones every 48 hours to measure the amount of Si condensed on their surface. In the RBS measurements a clean peak in the spectrum, quantifying the amount of Si collected, was obtained because the carbon substrate has a lower atomic mass than Si on its surface. Therefore backscattered ions from Si registered at a higher energy in the backscattering spectrum than backscattered ions from C. By calculating a yield of backscattered ions from Si, a quantitative computation for total μg of Si collected per 48 hour investigation was obtained. Uniform Si collection over the entire area of the condensing surface was confirmed with multiple measurements at several locations on the C wafer.

Three different tubes were used in this study: a low purity alumina tube (Al_2O_3 95.5%, SiO_2 2.90%, MgO 1.10%, CaO 0.28%, Na_2O 0.09%, Fe_2O_3 0.11%), a 3:2 mullite

tube ($Al_6Si_2O_{13}$ 78.3%, Al_2O_3 13%, MgO 0.8%, CaO 0.4%, Na_2O 0.8%, Fe_2O_3 2.1%, K_2O 2.5%, TiO_2 2.1%), and a clear fused quartz (SiO_2 100%) glass tube. Additionally, the aforementioned MSU1 (Al_2O_3 96.31%, $Al_6Si_2O_{13}$ 3.69%) refractory freeze cast blocks were cut into 2 cm^3 cubes and placed in the 800°C zone of the furnace inside a quartz tube. The quartz tube was utilized based on the highest consistency of silicon release as a background. Measurements were carried out to observe any additional Si release above the baseline obtained for the quartz tube alone. Quartz, low purity alumina and mullite tubes, and the MSU1 refractory blocks were tested in humidified air with $x(H_2O)$=0.60 atm at a flow rate of 0.8 liters per minute. Additionally, quartz tubes were tested in humidified air with $x(H_2O)$=0.023 atm, and in humidified forming gas (5% H_2, balance N_2) with $x(H_2O)$=0.58 atm.

3.0 Results

Thermodynamic equilibrium modeling via TERRA software identified numerous volatile silicon species for high purity alumina, mullite, MSU1 and silica materials under the previously described high temperature SOFC environments. All plots list only Si compounds in gaseous form, neglecting all condensed compounds and non-silicon containing gases. However the non-silicon containing gases were not excluded from equilibrium calculations. A comparison of the dominant volatile Si gases released from MSU1 versus high purity alumina, mullite and silica in humidified air ($x(H_2O)$=0.37atm) is presented in Figure 2 and illustrates that $Si(OH)_4$ is the dominant species. Figure 3 shows the contrast in Si gas species volatized from MSU1 when exposed to different SOFC environments. Silicon in MSU1, mullite and high purity alumina is thermodynamically predicted to behave nearly identical in all SOFC gases with the

exception of pure hydrogen. Figure 4 shows the significant differences in volatile silicon species from mullite and high purity alumina in H_2 for comparison with MSU1 in Figure 3. The mullite figure includes a series of modeling artifact peaks at 800°C due to a discontinuity in the thermodynamic database. The total equilibrium partial pressure of volatile Si gases in the various SOFC environments can be contrasted in Figure 5 for MSU1, pure mullite and the current industry standard high purity alumina. The effect of water vapor partial pressure on total silicon vapor release from MSU1 as predicted by thermodynamic equilibrium modeling is shown in Figure 6.

TGA results of the MSU1 powder in humidified air, hydrogen forming gas and humidified hydrogen forming gas at 1000°C for 250 hours are shown in Figure 7. TGA coupled mass spectrometry results of the high purity alumina, low purity alumina and 3:2 mullite in humidified argon are presented in Figure 8 and Table 1. The mass spectrometer indicated the presence of SiO (g) for the mullite sample and silicon oxy hydroxide ($Si_2O(OH)_6$) for the low purity alumina. Dilatometer normalized results are presented in Figure 8 as relative length change. The variations of thermal expansion coefficient (TEC) in the MSU1 aluminosilicate material under humidified UHP air and humidified hydrogen forming gas at 1000°C throughout 100 hours are presented in Table 2.

The RBS results of silicon transport rates from quartz, low purity alumina and mullite tubes are presented in Figure 10. Humidified air ($x(H_2O)$=0.60 atm) was passed through the tubes at a flow rate of 0.8 liters per minute for the experimental data shown in Figure 10. Volatility measurements using three MSU1 cubes inside a quartz tube can be seen in Figure 11 and are compared with baseline measurements from the empty quartz

tube. Measurements indicated volatilization of Th, Ru, Zn, Cr and Ca from the MSU1 cube. Th, Ru, Zn, Cr and Ca had also been detected in the RBS data from alumina and mullite tubes during early stages of heating. Figure 12 compares the Si released from experiments performed with humidified air ($x(H_2O)$=0.60 atm & $x(H_2O)$=0.023 atm) using identical quartz tubes. Figure 12 also shows data where humidified hydrogen forming gas (5% H_2, balance N_2) was passed through an empty quartz tube at flow rates of 0.80 liters per minute with $x(H_2O)$=0.60 atm. The atmosphere conditions for each RBS experiment at 800 °C and 1 atm were thermodynamically modeled and all simulations indicate $Si(OH)_4$ will dominate at an equilibrium partial pressure ranging between

10^{-9} and 10^{-10} atm. All other Si gaseous species volatilized were negligible.

4.0 Discussion

As silica concentrations in aluminosilicates exceed 30 wt % (42 mol %) the regions of liquid phases expand and SiO_2 is no longer found in solution with alumina. Solid solutions of SiO_2 in aluminosilicates exist due to the differences in diffusion coefficients of the aluminum and silicon cations. [41] The extent of silicon in solution with alumina affects the stability of Si due to changes in bonding and hence oxygen coordination. Intermediate forms between silicon dioxide to elemental silicon exist due to silicon's electronic structure $3s^2p^2$ which can have four different degrees of oxidation (1^+ ($3s^2p^1$), 2^+ ($3s^2$), 3^+ ($3s^1$), 4^+ ($2s^2p^6$)). [26] Thermodynamic equilibrium modeling has shown Si can volatize from alumina and aluminosilicate refractory materials and be transported in the gas phase under high temperature SOFC conditions as silicon monoxide SiO, silicon hydroxide $Si(OH)_x$, silicon oxy hydroxides $(SiO_x(OH)_{4-2x})_n$ and

silicon hydrides (Si_nH_{2n+2}). The thermodynamic simulations are based on Gibb's Free Energy of Formation utilizing the governing equation: $\Delta G_{rx}=\Delta H_{rx}-T(\Delta S_{rx})$. It is important to note that these simulations do not account for reaction rates and other kinetic barriers for interaction but are intended to provide a basis for experimental work and theoretical understanding of volatile species present in the system. The thermodynamic simulation is limited by bulk volatilization as opposed to volatilization from high surface area (large positive curvature) yielding variation from equilibrium to empirical characterization.

Sources of Si in MSU1 (Al_2O_3 96.31%, $Al_6Si_2O_{13}$ 3.69%) and pure mullite ($Al_6Si_2O_{13}$) are modeled identically as 3:2 mullite ($3Al_2O_3$:$2SiO_2$ represented as $Al_6Si_2O_{13}$) such that the only difference is the presence of Al_2O_3 in MSU1. Correspondingly, the sources of Si in the high purity alumina (Al_2O_3 99.96%, SiO_2 0.04%) and silica (SiO_2) are modeled as silicon dioxide (SiO_2) such that the only difference is the high purity alumina also contains Al_2O_3. The different entropies of formation for each solid combined with the imposed thermodynamic restrictions to conserve energy and mass of the isolated systems and obey the electro neutrality condition can result in varying equilibrium partial pressures of Si gases despite no change in the solid state Si compounds. Thermodynamic equilibrium models estimate the stability of Si in each material and are not normalized based on the total amount of material required. For example, although the stability of Si chemically bonded as $Al_6Si_2O_{13}$ in the MSU1 and mullite models is equivalent under the simulated humidified air ($x(H_2O)$=0.023 atm) at ambient pressure, this cannot be interpreted as the same amount of Si gases will be introduced into the SOFC because the mass of Si present in

MSU1 (Al_2O_3 96.31%, $Al_6Si_2O_{13}$ 3.69%) is significantly lower than in the mullite (100% $Al_6Si_2O_{13}$). Normalization is not conducted here because the same mass of one refractory would not necessarily provide an equivalent R-value or structural support for a different refractory due to varying properties such as thermal conductivity, density, fracture toughness and yield stress. RBS tests establish a means to quantitatively analyze Si release rates by first acquiring long term baseline data on a variety of tubes while simultaneously providing insight to the cost/performance ratio of gas-feed tube materials. The baseline analysis performed provided a way of evaluating SOFC refractory materials in reducing and oxidizing environments.

Alumina is known to volatize at high temperatures in the presence of water vapor; however the volatility is not an issue for SOFCs despite long lifetimes (>100,000 hours) since the operating temperatures are well below 1300 °C where alumina volatility by $Al(OH)_3(g)$ becomes an issue. [29] Furthermore, no reports to date have indicated alumina poses a threat to long term operation of SOFCs despite its adoption of use as the industry standard SOFC refractory material. Thermodynamic modeling did not exclude volatile alumina or other impurity species from equilibrium calculations; however they are absent from all equilibrium graphs for clarity and simplicity. Considerations of their effects on results are only presented when necessary to stay within the scope of this paper.

4.1 Oxidizing Environments

All thermodynamic simulations of high purity alumina, MSU1, mullite and silica in dry air suggest silicon remains sufficiently stable throughout SOFC operating temperatures corresponding to what has been reported in the literature. [24] However,

the addition of steam to air in the thermodynamic model mimicry of actual SOFC oxidant streams results in significant volatility of silicon hydroxide ($Si(OH)_4$) and -oxy hydroxide $SiO(OH)_2$ from MSU1, mullite and silica as seen in Figure 2. Silicon vapor species in SOFC humid atmospheres most likely contain water vapor bonded to SiO_2 molecules since SiO_2 has a very low vapor pressure at temperatures between 800-1000 °C. $Si(OH)_4$ was previously shown to be the dominant species from 900°C to 1150°C in the presence of water vapor with $x(H_2O) = 0.37$ and P(total) = 0.1 MPa. [19] At moderate steam partial pressures and temperatures above 925°C, SiO(OH) & $SiO(OH)_2$ have been designated as important contributors; while at steam pressures above 10 MPa and temperatures up to 1525°C, $Si_2O(OH)_6$ has also been designated an important contributor. [19][20] Equations 1 and 3 describe the likely breakdown of the SiO_2 when exposed to water vapor in an oxidizing environment, volatilizing the silicon and oxygen completely. Thermodynamically the formation of silicon hydroxide ($Si(OH)_4$) is favored, however since equation 1 requires the interaction of two H_2O molecules with one molecule of SiO_2 it may be kinetically limited. Equation 5 shows the breakdown of mullite to form silicon hydroxide ($Si(OH)_4$), yielding Al_2O_3. The stability of silica at SOFC operating temperatures in humidified air ($x(H_2O)$=0.37 atm) at ambient pressure, Figure 2, suggests that the SiO_2 bond is less stable than the $Al_6Si_2O_{13}$ bond. However, $Al_6Si_2O_{13}$ likely offers only a slight improvement in silicon volatility in oxidizing atmospheres containing water vapor, Figure 2, due to its high silica activity (0.3-0.4). [42]

As the steam partial pressure increases the stability of Si in MSU1 decreases (Figure 6), where the effect is more enhanced at low temperatures (600-800°C) than above SOFC operating temperatures (1000-1400°C). RBS data (Figure 12) used to

validate the formation and volatization of silicon species confirms the silicon volatilization process strongly depends on moisture content. However this data does not necessarily correlate directly to fuel cell degradation since at high temperatures the volatile phase may not readily condense in the SOFC unless the formation of stable Si solids is stimulated by an external element such as catalysis or electrochemical oxygen transport. RBS Si volatility measurements of the quartz, low purity alumina and mullite tubes in humidified air generated a few unexpected results. The fused quartz (pure amorphous SiO_2) tube consistently registered the fewest μg of Si collected per 48 hours, contrary to what is predicted via equilibrium modeling. Both the low purity alumina and mullite tubes released large amounts of Si during the first 100-200 hours of heating (Figure 10). These results could indicate free Si and silica residing on the low purity alumina and mullite tubes' surface due to the sintering or manufacturing process, and suggest that free silica is less stable than the bulk refractory. Further, the extremely smooth surface morphology of the quartz tube can kinetically limit the volatization of Si compounds. It is interesting to note that mullite tubes *consistently* produced the highest volatility over 600 plus hours of testing (Figure 10). If 3:2 mullite and free silica are the primary impurities in the 96% pure alumina tube, as suggested by manufacturer specifications and chemical analysis of other aluminosilicate materials, the principle source for long term (greater than 700 hours) Si release could be accounted for in low purity alumina tubes. A large amount of Si was also initially released from the MSU1 cube samples (Figure 11) providing further evidence for observations made on the mullite and low purity alumina tubes. Based on equilibrium modeling it is believed that all RBS experiments in humidified oxidizing environments were dominated by the release of Si as

$Si(OH)_4$ and then condensed as SiO_2 on the carbon substrate according to equation 1. The TGA results of MSU1 (Figure 7) showing a more rapid weight loss during hours 0-85 than hours 86-250 at 1000°C in a humidified oxidizing atmosphere suggests that the decomposition of MSU1 is slowed due to solid state diffusion limitations as represented by a discrete change in slope at 85 hours. This initial release of Si may still be detrimental to the SOFC, requiring initial thermal pre-treatment or chemical surface treatments to lock up free/high surface area silica and aluminosilicate compounds. Furthermore, the volatilization of Zn and Ca from the MSU1 cube, low purity alumina and mullite tubes also supports that impurities from the manufacturing process reside on the surface of the refractory materials. While Zn and Ca are common impurities in refractory materials, evidence of Ru and Th is unusual. A metal bonded diamond saw blade was used to cut MSU1 into smaller cubes which could have deposited impurities on the surface of the refractory specimen yielding a potential source for some of the elements.

The decline in TEC measured via a dilatometer of MSU1 in humidified UHP air and humidified H_2 forming gas during the first 85 hours at 1000°C (Table 1) indicates a transport limited process in which an oxygen gradient exists in the refractory specimen even though the material has substantial open porosity. The slow diffusion of oxygen into the bulk may be an additional contributing factor to the initial rapid release of Si observed via TGA and RBS. Upon reduction, many ionic oxides yield increases in thermal expansion as the oxide transitions to a more metallic state. In this case, reduced oxygen stoichiometry causes the cation(s) to increase in electron density, thus expanding the ionic radii. These results indicate a continued drop in thermal expansion thus

suggesting phase changes (specifically the silicon impurity phase) associated with changes in oxygen stoichiometry. All dilatometer results of MSU1 (Figure 8) include the presence of an 8 hour cyclic pattern in relative length change for which the inclusion of H_2O enhances this effect. The experiments were started at random times of the week yet cycle times coincide. Furthermore, experiments on different materials and calibration tests do not indicate these cyclic patterns reducing the likelihood that building pressure fluctuations, laboratory activities or system noise is the cause. It is speculated that surface reactions may be causing a phenomenon similar to spallation where new surface exposed is volatized or transformed into different phases; however further investigation into this phenomenon is required before any conclusions can be drawn.

4.2 Reducing Environments

The thermodynamic modeling results of MSU1 in a dry hydrogen reducing environment (Figure 3) predict silicon monoxide and silane gases dominate the release of Si at SOFC operating temperatures. In the dry reducing H_2 atmosphere from 600-1350 °C the presence of alumina in MSU1 (Al_2O_3 96.31%, $Al_6Si_2O_{13}$ 3.69%) significantly increased the thermodynamic equilibrium stability of Si locked up in the $Al_6Si_2O_{13}$ structure compared to the pure mullite ($Al_6Si_2O_{13}$). The presence of alumina in MSU1 has also been shown empirically to stabilize the SiO_2 reaction with H_2 gas, where the rate limiting step is bulk diffusion. [43] A driving force for Si degradation in the dry reducing atmosphere is the minimization of the system's entropy by increasing the oxygen partial pressure. In MSU1 the Al_2O_3 and $Al_6Si_2O_{13}$ are both sources of oxygen, whereas in pure mullite only the $Al_6Si_2O_{13}$ bonds can be broken down to release oxygen. Despite the greater stability of the alumina, since MSU1 is 96.31% Al_2O_3 oxygen will still be

harvested at a significant rate from the alumina, reducing the breakdown rate of Si bonds to minimize the system's entropy. In the TGA experiment of MSU1 in dry hydrogen forming gas (Figure 7), the initial rapid weight loss observed is attributed to both the release of oxygen due to low partial pressure and silicon volatilization as silane and SiO.

The presence of H_2O in a hydrogen reducing environment results in greater Si thermodynamic equilibrium stability in MSU1 from 600-800 °C (Figure 5), however to the contrary Si is more volatile from 800-1600 °C. This same trend is predicted for the SiO_2 impurity in alumina (Figure 5), except that the lower temperature region is extended up to 980 °C. Silicon remains more stable when exposed to humidity in a reduced atmosphere from 600-1400 °C because oxygen is harvested not only from $Al_6Si_2O_{13}$, SiO_2 and Al_2O_3 but is also released during the breakdown of H_2O. Therefore the presence of steam in the reducing atmosphere decreases the likelihood of forming silane and SiO while increasing formation of silicon hydroxide ($Si(OH)_4$) and –oxy hydroxide ($SiO(OH)_2$). In the RBS experiment at a water vapor pressure of 0.60 atm there was no noticeable difference in Si volatility rates from quartz between the reducing and oxidizing carrier gases (Figure 12), similar to what is predicted via equilibrium modeling (Figure 5). RBS measurements in the reducing gases were not carried out beyond 100 hours, because it was assumed that the quartz tube was volatilizing Si at a constant rate. As expected the TGA-MS results showed the greatest weight loss for mullite in the humidified argon reducing atmosphere; and the low purity alumina lost more weight compared to the high purity alumina (Figure 8). This indicates that despite approximately equal equilibrium stability of Si, the atomic concentration of silicon is the leading factor in determining the quantity of Si released into the system. Mass

spectrometry showed the volatilization from 3:2 mullite and low purity Al_2O_3 under humidified reducing argon gas at 850°C to be SiO and $Si_2O(OH)_6$, respectively. The presence of volatile SiO gas suggests decomposition of mullite due to the low partial pressure of oxygen despite the presence of water vapor. [30] $Si_2O(OH)_6$ suggests SiO_2 impurities in the low purity alumina reacted with water vapor (Eqn. 4) as suggested by Brady's calculations [17] at lower temperatures (205-260 °C) and higher pressures (33-400 atm). Thermodynamic modeling predicted under the TGA-MS experimental conditions that the Si in the mullite as $Al_6Si_2O_{13}$ and in the alumina as SiO_2 would preferentially volatilize as $Si(OH)_4$ yet the lack of observation of silicon hydroxide via mass spectroscopy may be due to surface adsorption, bulk absorption or the following gas phase reaction:

22 $\mathbf{2Si(OH)_4}(g) \rightarrow \mathbf{Si_2O(OH)_6}(g) + \mathbf{H_2O}(g)$

5.0 Conclusions and Recommendations

Results show the influence of material composition, atmosphere and temperature on chemical stability of Si in aluminosilicate, alumina and silica. Thermodynamic modeling illustrates the strong dependence of operating temperature on silicon release. Low temperature SOFC operating conditions (< 800°C) demonstrate the high Si stability required due to thermodynamic limitations on the reaction rates. Si remains stable in aluminosilicates, silica and alumina in a dry oxidizing environment for high temperature SOFCs. However, increasing H_2O partial pressure significantly reduces stability of Si in alumina and aluminosilicates in an oxidizing atmosphere, with the effects more enhanced at low SOFC temperatures. Thermodynamic modeling, mass spectrometry results and

literature findings demonstrate that steam at SOFC temperatures results primarily in the formation of volatile silicon hydroxide $Si(OH)_4$, with silicon oxy hydroxide $SiO(OH)_2$ becoming more significant with increases in temperature. In humid oxidizing environments the $Al_6Si_2O_{13}$ bond offers only a slight improvement on the stability of Si over SiO_2. Therefore the driving factor in material selection for SOFCs exposed to moist oxidizing environments should be the total quantity of silicon by mass.

Si stability of mullite in a dry reducing atmosphere at SOFC temperatures is poor due to the driving force to minimize the system's free energy by increasing the partial pressure of oxygen. The primary Si volatile gases in the dry reducing atmosphere are SiO and silane. The presence of alumina in aluminosilicate and high purity alumina significantly improves the stability of the Si solid phases. Contrary to the oxidizing environment, the addition of water vapor to the reducing atmosphere improves the low temperature stability of Si in mullite by equilibrating the oxygen partial pressure through decomposition of H_2O. The increased release of silicon hydroxide and oxy hydroxide in the humidified reducing environment is overshadowed by the greater decrease in SiO and silane volatility.

An initial rapid release of Si was observed in the TGA and RBS experiments during approximately the first 100 hours at temperature, after which the rate was decreased indicating that the process is limited by solid state diffusion. Dilatometer results also suggest oxygen diffusion into the bulk is slow and non-uniformities in the MSU1 refractory are subject to decomposition, volatization, or phase change. It is believed that non-uniformities of Si and SiO_2 on the surface combined with the slow

diffusion rates of oxygen into the bulk are the causes for the initial accelerated release rates.

SOFC developers investigating the replacement of expensive high purity alumina with low purity alumina or aluminosilicates including 3:2 mullite are recommended to consider a pre-installation thermal treatment, surface treatments and other manufacturing processes to lock up the Si in the bulk. Results demonstrating that low purity alumina released a significant quantity of silicon oxy hydroxides at 850°C should lead SOFC developers to use caution when selecting refractory materials containing significant quantities of Si. Alumina has been shown to successfully act as a protective layer against various corrosive compounds including water vapor for silicon based ceramics and should be considered as a potential environmental barrier coating for aluminosilicate refractory materials utilized in SOFCs. [44] Several silicate environmental barrier coatings (EBCs) such as barium strontium aluminosilicate (BSAS) [45] and rare earth (RE) silicates of the $RESi_2O_5$ [46] structure have been developed to limit volatility of silica-forming ceramics used in high temperature environments where high partial pressures of water vapor are present, such as in power or propulsion applications. The presence of CaO in aluminosilicate has been shown to reduce the activation energy, suggesting a potential dopant to lock up the silicon. [43]

References

[1] R. X. Fishcer, H. Schneider and D. Voll, "Formation of Aluminum Rich 9:1 Mullite and its Transformation to Low Alumina Mullite upon Heating," *J. Eur. Ceram. Soc.*, 16 109-113 (1996).

[2] G. Brunauer, F. Frey, H. Boysen and H. Schneider, "High tmperature thermal expansion of mullite: an in situ neutron diffraction study up to 1600 C," *J. Eur. Ceram. Soc.*, 21 [14] 2563-2567 (2001).

[3] C. R. He and W. G. Wang, "Alumina Doped Ni/YSZ Anode Materials for Solid Oxide Fuel Cells," *Fuel Cells*, 9 [5] 630-635 (July 2009).

[4] M. Aoki et al., "Solute segregation and grain-boundary impedance in high-purity stabilized," *J. Am. Ceram. Soc.*, 79 1169-1180 (1996).

[5] S.P. S. Badwal, J. Drennan, A. E. Hughes and B.A. A. Sexton, "A study of impurity phase segragation in fully stabilized yttria-zirconia," *Mater. Sci. Forum*, 34-36 195-199 (1988).

[6] G. M. Ingo and G. Padeletti, *Surf. Interface Anal.* p. 21 (1994).

[7] Joshua L. Hertz, Avner Rothschild and Harry L. Tuller, "Highly enhanced electrochemical performance of silicon-free platinum–yttria stabilized zirconia interfaces," *J. Electroceram.* (September 2007).

[8] M. Mogensen, K. V. Jensen, M. J. Jorgensen and S. Primdahl, "Progress in understanding SOFC electrodes," *Solid State Ionics*, 150 123-129 (2002).

[9] M. S. Schmidt, K. V. Hansen, K. Norman and M. Mogensen, "Effects of trace

elements at the Ni/ScYSZ interface in a model solid oxide fuel cell anode," *Solid State Ionics*, 179 1436-1441 (2008).

[10] M. Backhaus-Ricoult and M. F. Tichet, "Interfacial chemistry at metal electrode–oxide electrolyte contacts," *Solid State Ionics*, 150 143-156 (2002).

[11] A. Bernasik, K. Kowalski and A. Sadowski, "Surface segregation in yttria-stabilized zirconia by means of angle resolved X-ray photoelectron spectroscopy," *J. Phys. Chem. Solids*, 63 [2] 233-239 (2002).

[12] C. J. van Nieuwenburg and P. M. van Zon, "Semi-quantitative measurements of the solubility of quartz in supercritical steam," *Recl. Trav. Chim. Pays-Bas*, 54 p. 129 (1935).

[13] F. G. Straub, "Silica deposition in steam turbines," *University of Illinois Engineering Experiment Station Bull.*, 67 p. 309 (1945).

[14] G. W. Morey and J. M. Hesslegesser, "Solubility of quartz and some other substances in superheated steam at high pressures," *Trans. ASME*, 73 865-875 (1951).

[15] G. C. Kennedy, "A portion of the system silica-water," *Econ. Geol.*, 46 p. 821 (1951).

[16] M. D. Allendorf, C. F. Melius, P. Ho and M. R. Zachariah, "Theoretical study of the thermochemistry of molecules in the Si-O-H system," *J. Phys. Chem.*, 99 15284-15293 (1999).

[17] E. L. Brady, "Chemical Nature of Silica Carried by Steam," *J. Phys. Chem.*, 57 706-

710 (1953).

[18] A. Hashimoto, "The effect of H2O gas on volatilities of planet-forming major elements: I. Experimental determination of thermodynamic properties of Ca-, Al-, and Si-hydroxide gas molecules and its application to the solar nebula, Geochim.," *Geochim. Cosmochim. Acta*, 56 511-532 (1992).

[19] D. L. Hildenbrand and K. H. Lau, "Thermochemistry of gaseous SiO(OH), SiO(OH)2, and SiO2," *J. Chem. Phys.*, 101 [7] 6076-6079 (1994).

[20] N. Jacobson, M. Dwight, E. Opila and E. Copland, "Interactions of water vapor with oxides at elevated temperatures," *J. Phys. Chem. Solids*, 66 471-478 (2005).

[21] O. H. Krikorian, "Predictive calculations of volatilities of metals and oxides in steam-containing environments.," *High Temp. - High Pressures*, 14 387-397 (1982).

[22] O H Krikorian, "Thermodynamics of the Silica-Steam System," in *Symposium on Engineering with Nuclear Explosives*, vol. 1, Las Vegas, NV, January 14-16, 1970.

[23] E. J. Opila, D. S. Fox and N. S. Jacobson, "Mass Spectrometric Identification of Si-O-H(g) Species from the Reaction of Silic with Water Vapor at Atmospheric Pressure," *J. Am. Ceram. Soc.*, 80 1009-1012 (1997).

[24] Nathan S. Jacobson, "Corrosion of Silicon-Based Ceramics in Combustion Environments," *J. Am. Ceram. Soc.*, 76 3-28 (1993).

[25] S. Ueno, T. Ohju and H. -T. Lin, "Corrosion and recession of mullite in water vapor environment," *J. Eur. Ceram. Soc.*, 28 431-435 (2008).

[26] V. E. Roshin, A. V. Roshin, A. A. Berdnikov and Yu N. Goikhenberg, "Formation

and Sublimation of the Intermediate Products of the Reduction of Silicon from its Dioxide," *Russ. Metall. (Engl. Transl.),* 4 281-285 (2008).

[27] W. Kronert and H. Buhl, "The influence of various gaseous atmospheres on refractories of the system Al2O3-SiO2 (Part II)," *Interceram*, 2 140-146 (1978).

[28] H. N. Potter, "Silicon Monoxide," *Trans Am. Electrochem. Soc.* (1907).

[29] E. J. Opila, N. S. Jacobson, D. L. Myers and E. H. Copland, "Predicting Oxide Stability in High-Temperature Water Vapor," Glenn Research Center, NASA, Cleveland, OH, Research Summary 2006.

[30] T. P. Herbell, D. Hull and G. W. Hallum, "Effect of high temperature hydrogen exposure on the strength and microstructure of mullite," in *Conference on Environmental Effects on Advanced Materials,* 1990, pp. 351-359.

[31] S. M. Schnurre, J. Grobner and R. Schmid-Fetzer, "Thermodynamics and pahse stability in the Si-O system," *J. Non-Cryst. Solids,* 336 1-25 (2004).

[32] C. Jacklin and S. R. Browar, "Correlation of silica carry-over and solubility studies," , Nov. 25-30, 1951, p. 27.

[33] R. H. Newton, "Activity coefficients of gases," *Ind. Eng. Chem.*, 27 302-306 (1935).

[34] V. Gorokhovsky et al., "Tribological performance of hybrid filtered arc-magnetron coatings Part I: Coating deposition process and basic coating properties characterization," *Surf. Coat. Technol.*, 206 [6] 3732-3747 (December 2006).

[35] National Institute of Standards and Technology, Forente stater Department of Commerce, *NIST-JANAF thermochemical tables*, M.W. Jr. Chase, Ed.: Springer-

Verlag New York, LLC, 1998

[36] L. V. Gurvich et al., *Thermodynamic Properties of Individual Substances*, Vol. 2, Fourth Edition. Moscow, Russia: Hemisphere Publishing Corporation, 1991

[37] P. J. Spencer and H. Holleck, "Application of a thermochemieal data bank system to the calculation of metastable phase formation during PVD of carbide, nitride, and boride coatings," *High Temp. Sci.*, 27 p. 295 (1990).

[38] Mark D. Allendorf. (2009, October) Sandia National Laboratories Thermochemistry Database for High-Temp Materials Synthesis. [Online]. http://www.sandia.gov/HiTempThermo/

[39] F. J. Perez-Trujillo and S. I. Castaneda, "Study by Means of the Mass Spectrometry of Volatile Species in the Oxidation of Cr, Cr2O3, Al, Al2O3, Si, SiO2, Fe and Ferritic/Martensitic Steel Samples at 923 K ub Ar+(10 to 80%) H2O Vapor Atmospheres for New-Materials Design," *Oxid. Met.*, 66 231-251 (2006).

[40] C. Collins et al., "Chromium volatility of coated and uncoated steel interconnects for SOFCs," *Surf. Coat. Technol.*, 201 4467-4470 (2006).

[41] A V Belyakov and A. V. Belyakov, "Solid solutions of silicon oxide in mullites," *Glass Ceram.*, 60 402-405 (2003).

[42] K. N. Lee and R. A. Miller, "Development and environmental durability of mullite and mullite/YSZ dual layer coatings for SiC and Si3N4 ceramics," *Surf. Coat. Technol.*, 86-87 142-148 (1996).

[43] Stephen T. Tso and Joseph A. Pask, "Reaction of Silicate Glasses and Mullite with

Hydrogen Gas," *J. Am. Ceram. Soc.*, 65 [8] 383-387 (1982).

[44] M. G. Lawson, F. S. Pettit and J. R. Blachere, "Hot corrosion of alumina," *J. Mater. Res.*, 8 1964-1971 (Aug 1993).

[45] K. N. Lee et al., "Upper Temperature Limite of Environmental Barrier Coatings Based on Mullite and BSAS," Glenn Research Center, Cleveland State University, Cleveland, OH, Technical Memorandum 2002.

[46] K. N. Lee, D. S. Fox and N. P. Bansal, "Rare earth silicate evironmental barrier coatings for SiC/SiC composites and Si3N4 ceramics," *J. Eur. Ceram. Soc.*, 25 1705-1715 (2005).

Acknowledgements

The authors gratefully acknowledge Dr. Paul Gannon and Professor Boris G. Trusov for their assistance with thermodynamic calculations, and Dr. Javier Pérez Trujillo for completion of the mass spectrometer experiments.

Figures

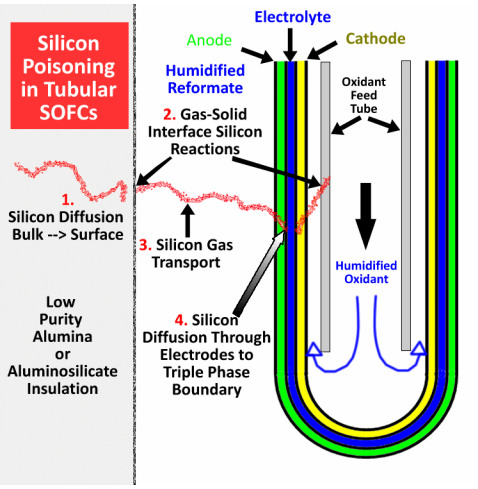

Figure 1: Silicon poisoning in tubular SOFCs due to Si volatization from refractory insulation and gas delivery tubing.

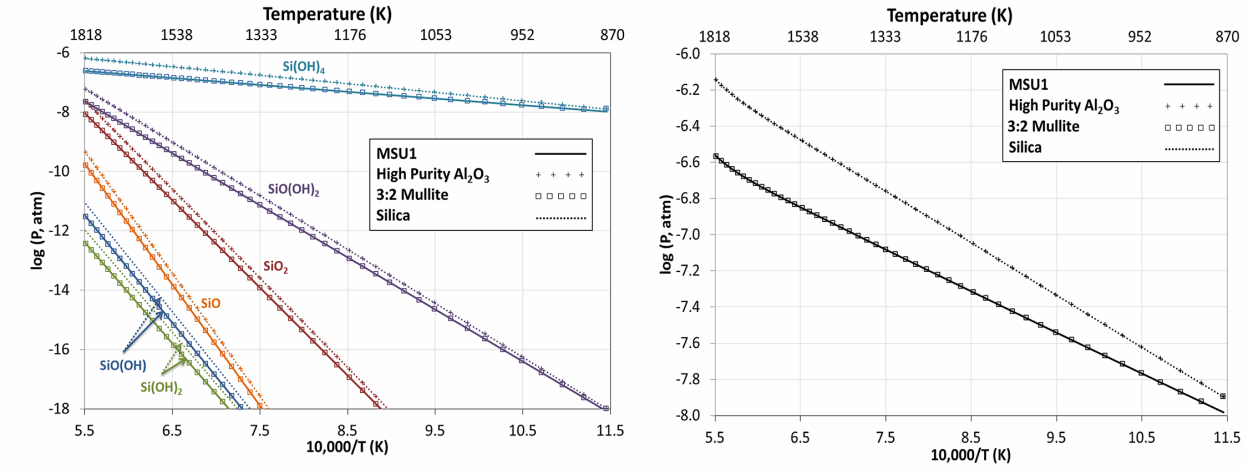

Figure 2: Thermodynamic equilibrium partial pressures of Si vapor species (left) or total partial pressure of volatile Si gases (right) from MSU1 ($Al_6Si_2O_{13}$ 3.69% Al_2O_3 96.31%), high purity alumina (Al_2O_3 99.96% SiO_2 0.04%), mullite ($Al_6Si_2O_{13}$) or silica (SiO_2) in humidified air (O_2 – 13.217%, H_2O – 36.909%, Ar – 0.589%, CO_2 – 0.019%, N_2 – 49.267%). P (total) = 1 atm

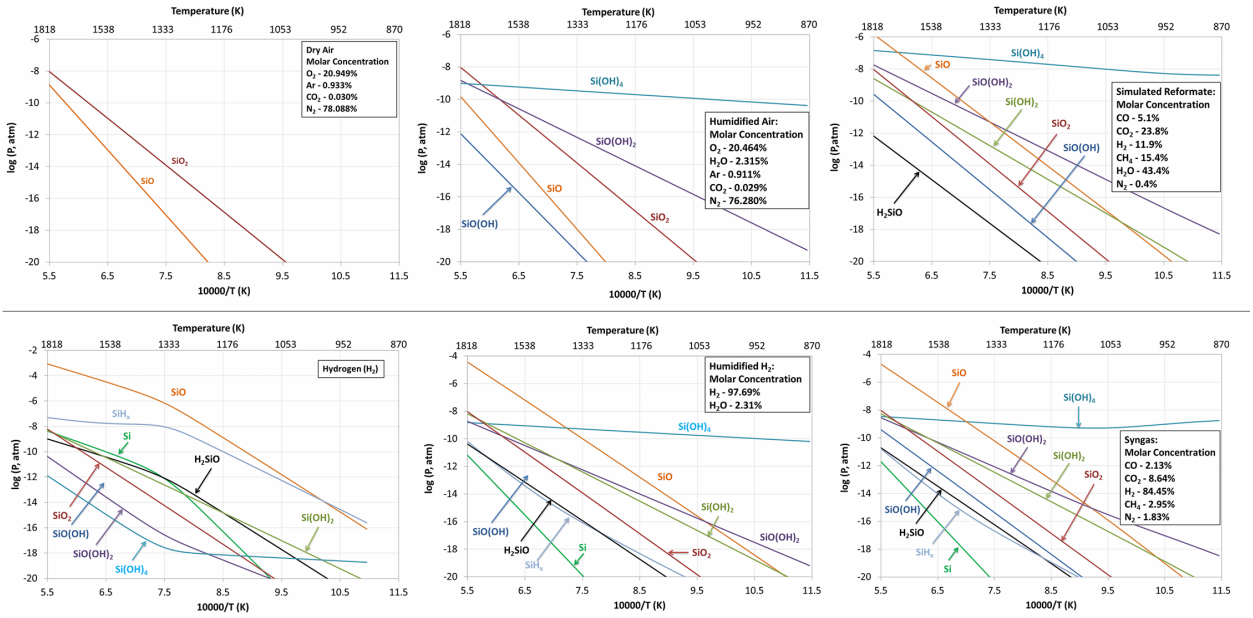

Figure 3: Thermodynamic equilibrium partial pressures of Si vapor species from MSU1 ($Al_6Si_2O_{13}$ 3.69% Al_2O_3 96.31%) in various SOFC fuel or oxidant gases. P (total) = 1 atm

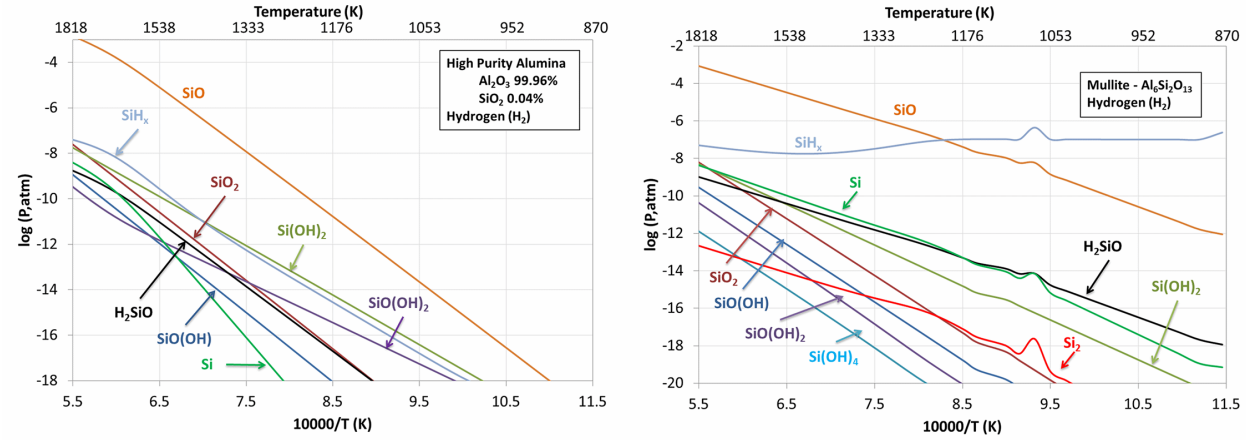

Figure 4: Thermodynamic equilibrium modeled volatility of Si vapor species from 3:2 mullite and high purity alumina in hydrogen. P (total) = 1 atm

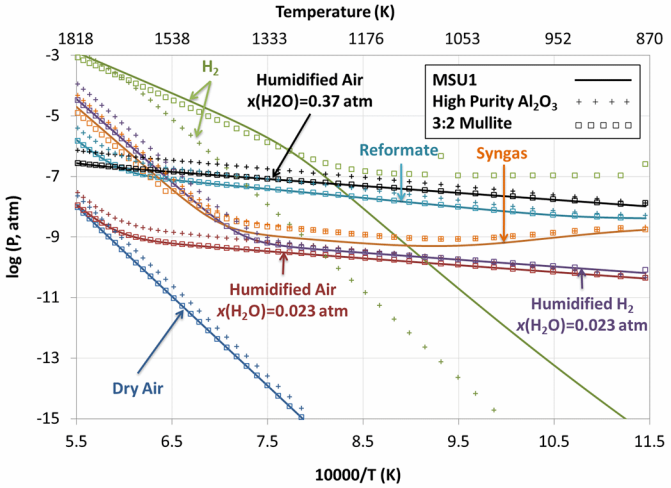

Figure 5: Thermodynamic equilibrium modeled total volatile Si gas formation in SOFC gases from MSU1 refractory material ($Al_6Si_2O_{13}$ 3.69% Al_2O_3 96.31%), mullite ($Al_6Si_2O_{13}$) and the current SOFC industry standard high purity alumina fuel/oxidant delivery tube (Al_2O_3 99.96% SiO_2 0.04%). P (total) = 1 atm

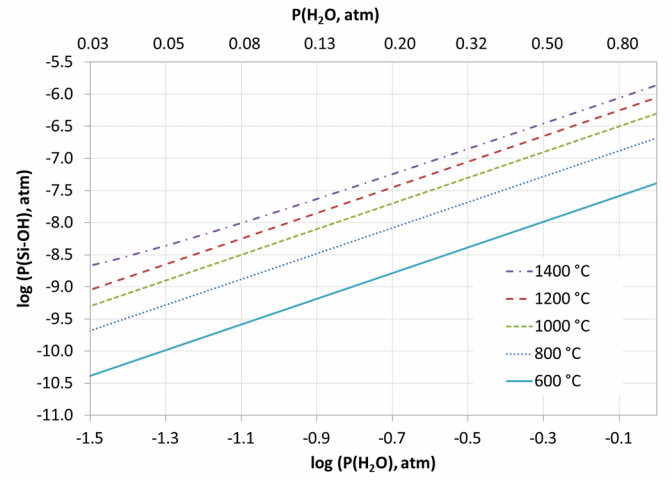

Figure 6: Effect of water vapor on the thermodynamic equilibrium partial pressure of Si gases volatilized from MSU1 ($Al_6Si_2O_{13}$ 3.69% + Al_2O_3 96.31%).

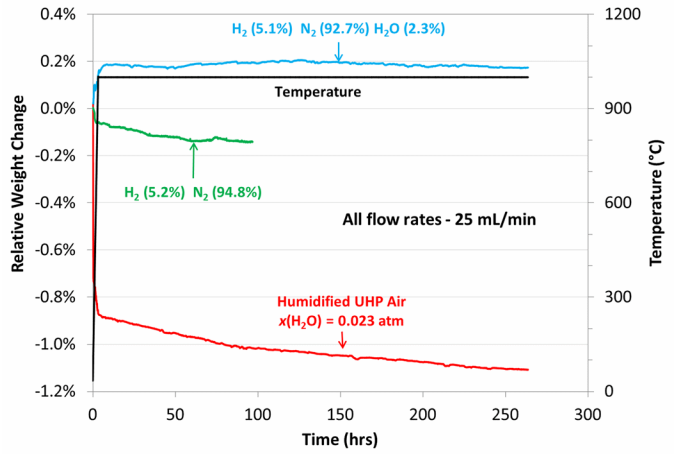

Figure 7: MSU1 (Al_2O_3 96.31%, $Al_6Si_2O_{13}$ 3.69%) thermal gravimetric analysis for 250 hours at 1000°C.

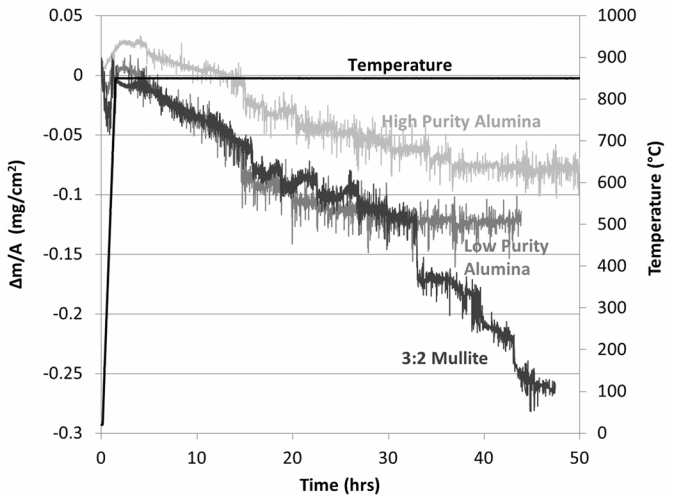

Figure 8: TGA-MS data for refractory insulations in Ar + 20% H_2O up to 50 hours at 850 °C.

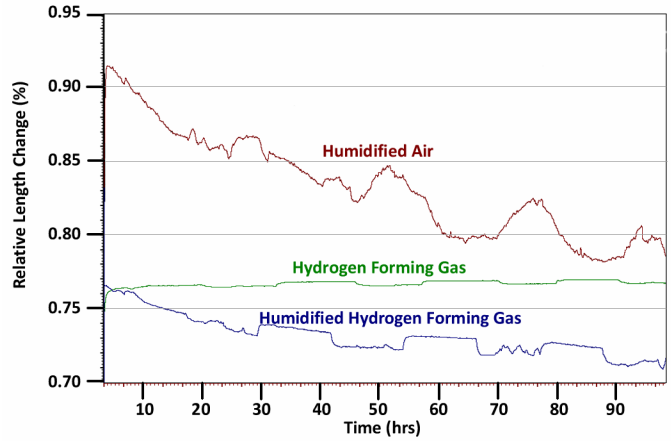

Figure 9: Dilatometer analysis of MSU1 (Al_2O_3 96.31%, $Al_6Si_2O_{13}$ 3.69%) at 1000°C for 100 hours in unconditioned air, humidified air ($x(H_2O)$=0.023 atm), hydrogen forming gas (5.2% H_2, 94.8% N_2) and humidified forming gas (5.1% H_2, 92.7% N_2, 2.3% H_2O).

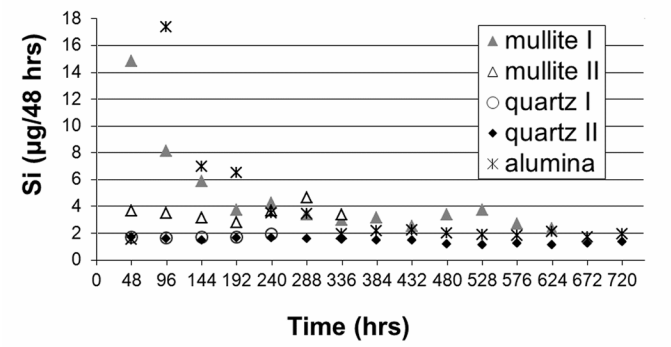

Figure 10: RBS data from transpiration experiments showing Si volatility rates versus total heating time for 3:2 mullite, low purity alumina and quartz tubes at 800°C in humidified air. $x(H_2O)$=0.60 atm

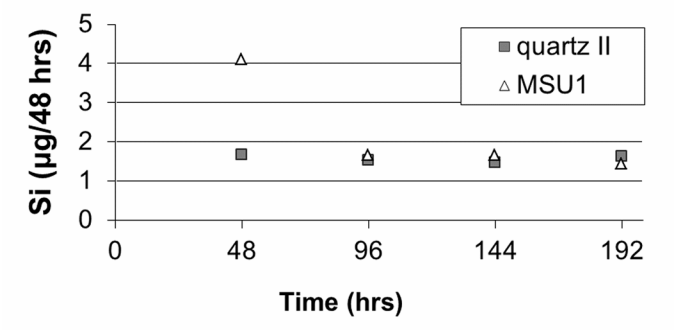

Figure 11: RBS comparison of volatility rates for an empty quartz tube and the identical quartz tube containing MSU1 (Al_2O_3 96.31%, $Al_6Si_2O_{13}$ 3.69%) samples at 800°C, exposed to the same humidified air. $x(H_2O)$=0.60 atm

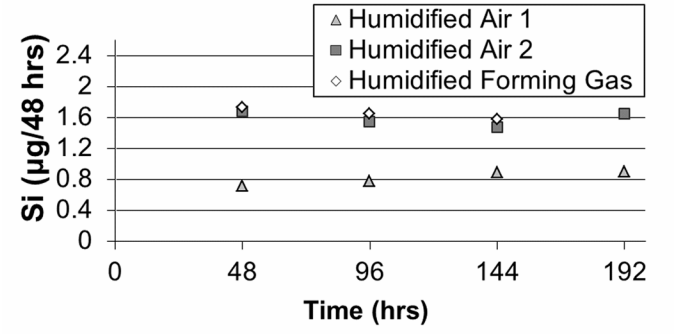

Figure 12: RBS volatility rates of quartz tubes at 800°C in humidified air 1 ($x(H_2O)$=0.023 atm), humidified air 2 ($x(H_2O)$=0.60 atm) and humidified forming gas (5% H_2, balance N_2 [$x(H_2O)$=0.58 atm]).

Tables

Table 1: TGA-MS summary of compounds released at 850°C in argon + 20 wt% H_2O.

Composition	Time (hrs)	Volatile Compound	Ion Current (A)
3:2 Mullite	25	Al_2O_3	1.70E-11
	50	Al_2O_3	1.70E-11
	50	2SiO	1.86E-11
Low Purity Alumina	25	Al_2O_3	1.73E-11
	25	$Si_2O(OH)_6$	1.67E-11
High Purity Alumina	50	Below Detection Limits	

Table 2: Change in MSU1 aluminosilicate (Al_2O_3 96.31%, $Al_6Si_2O_{13}$ 3.69%) thermal expansion coefficient (TEC) from hours 0 to 100 at 1000°C.

Environment	TEC ($*10^{-6}$ K^{-1})
Humidified Air	9.3 → 8.0
H_2 Forming Gas	7.79 → 7.83
Humidified H_2 Forming Gas	7.8 → 7.3

INVESTIGATION OF ALUMINOSILICATE AS A SOLID OXIDE FUEL CELL REFRACTORY

Contribution of Authors and Co-Authors

Lead corresponding author: Paul S. Gentile
Contributions: Collaborated on the conception and design of the study. Collected, assembled, analyzed and interpreted experimental data. Conducted literature review, led writing efforts, preparing manuscript, tables and figures for publication. Provided final approval of the manuscript and submitted it to Journal of Power Sources for review.

Co-author: Stephen W. Sofie
Contributions: Collaborated on the conception and design of the study. Assisted with the interpretation of assembled data. Provided critical revisions of the article regarding important intellectual content. Provided final approval of the article content and journal source.

Manuscript Information Page

- INVESTIGATION OF ALUMINOSILICATE AS A SOLID OXIDE FUEL CELL REFRACTORY
- Authors: Paul S. Gentile, Stephen W. Sofie
- Journal Name: Journal of Power Sources
- Status of manuscript (check one)

  ☐ Prepared for submission to a peer-reviewed journal

  ☒ Officially submitted to a peer-reviewed journal

  ☐ Accepted by a peer-reviewed journal

  ☐ Published in a peer-reviewed journal

- Publisher: Elsevier
- Submitted October 25, 2010

INVESTIGATION OF ALUMINOSILICATE AS A SOLID OXIDE FUEL CELL REFRACTORY

Paul S. Gentile[a], Stephen W. Sofie[a]

[a] Montana State University, Mechanical Engineering Dept., P.O. Box 173800, Bozeman, MT, 59717

Research Highlights

- Enriched mullite surface concentrations indicate the bulk is a long term Si source.
- Si diffusion at the aluminosilicate surface is accelerated in the presence of H_2O.
- Vapors from aluminosilicate preferentially deposit on YSZ rather than Ni.
- Amorphous siliceous deposits diffused into the YSZ along grain boundaries.
- Aluminosilicate vapors in the SOFC anode fuel stream caused rapid degradation.

Abstract

Aluminosilicate represents a potential low cost alternative to alumina for solid oxide fuel cell (SOFC) refractory applications. The objectives of this investigation are to study: (1) changes of aluminosilicate chemistry and morphology under SOFC conditions, (2) deposition of aluminosilicate vapors on yttria stabilized zirconia (YSZ) and nickel, and (3) effects of aluminosilicate vapors on SOFC electrochemical performance. Thermal treatment of aluminosilicate under high temperature SOFC conditions is shown to result in increased mullite concentrations at the surface due to diffusion of silicon from the bulk. Water vapor accelerates the rate of surface diffusion resulting in a more uniform distribution of silicon. The high temperature condensation of volatile gases released from aluminosilicate preferentially deposit on YSZ rather than nickel. Silicon vapor deposited on YSZ consists primarily of aluminum rich clusters enclosed in an amorphous siliceous layer. Increased concentrations of silicon are observed in enlarged grain boundaries indicating separation of YSZ grains by insulating glassy phase. The presence of aluminosilicate powder in the hot zone of a fuel line supplying humidified hydrogen to an SOFC anode impeded peak performance and accelerated degradation. Energy dispersive x-ray spectroscopy detected concentrations of silicon at the interface between the electrolyte and anode interlayer above impurity levels.

1.0 Introduction

Aluminosilicate is a potential alternate material for refractory and gas delivery tubing throughout solid oxide fuel cells (SOFCs) due to its high tolerance to thermal shock [**1**], low thermal conductivity, and relatively low cost. Stationary tubular SOFCs utilizing high purity alumina refractory have been operated at 1000°C for over 69,000 hours with

less than 0.1% degradation per 1,000 hours [**2**], however the industry standard alumina requires expensive processing of the raw material to remove naturally occurring silicon impurities. The studied aluminosilicate containing silica chemically bonded as mullite (96.3% Al_2O_3, 3.7% $Al_6Si_2O_{13}$) can be freeze cast to a wide variety of shapes for which density can be readily manipulated, minimizing manufacturing wastes and further reducing cost. The introduction of Si is of concern due to the potential for silicon diffusion from the aluminosilicate bulk to the surface where a chemical reaction can occur, volatizing the silicon and transporting it in a gaseous form to the fuel cell. Aluminosilicate components can be exposed to air and fuel streams supplied to the fuel cell; therefore silicon poisoning issues are relevant in both reducing and oxidizing atmospheres. It has been shown that silicon accumulates at the triple phase boundary (TPB) where it creates a glassy silicon oxide phase. [**3-5**] This glassy phase represents an electronic and ionic insulator [**6**], retards water [**7**] and may block active nickel catalytic sites resulting in increased activation polarization and thus degradation. The presence of silicon at the TPB may be due to vapor deposition but also can be due to solid state diffusion of silicon impurities in the SOFC electrolyte or silica based glass seals. [**8-10**] Regardless of the mechanism of transport, the long duration operational requirements of SOFCs exceeding 40,000 hours will likely provide sufficient time for transport related degradation.

Chemical reactions at the gas-solid interface can result in the volatility of harmful silicon vapors from aluminosilicate refractory. It is therefore important to understand the change in the aluminosilicate surface chemistry due to bulk diffusion. Silicon diffusion is very sluggish in silica and aluminosilicates due to the strong covalent bonding within the

SiO_4 tetrahedra [**11**,**12**]. After reacting aluminosilicate (79.8 % SiO_2, 20.2% Al_2O_3) with H_2 gas at temperatures from 1300-1500°C, Tso and Pask [**13**] observed the formation of an outer surface layer of α-Al_2O_3 void of SiO_2 and an intermediate transition layer with SiO_2 content similar to that of mullite. After reacting 3:2 mullite with H_2 the alumina outer layer void of SiO_2 was again observed. The depletion of SiO_2 may be due to the release of SiO gases (Eqn. 1) in a reducing atmosphere. Mullite was also reported to decompose into corundum (Al_2O_3) and volatile silicon monoxide (SiO) gas in a carbon monoxide (CO) environment (Eqn. 2), where the rate is governed by diffusion rather than the reaction at the phase boundary. [**14-15**]

1 $\mathbf{Al_6Si_2O_{13}}$ (s) + $\mathbf{2H_2}$(g) → $\mathbf{3Al_2O_3}$(s) + $\mathbf{2SiO}$(g) +$\mathbf{2H_2O}$(g)

2 $\mathbf{Al_6Si_2O_{13}}$ (s) + $\mathbf{2CO}$(g) → $\mathbf{3Al_2O_3}$(s) + $\mathbf{2SiO}$(g) + $\mathbf{2CO_2}$(g)

The volatility of silicon vapors from silica at high temperatures has been studied extensively. [**16-25**] Recently, thermodynamic equilibrium modeling, thermal gravimetric coupled with evolved gas analysis and Rutherford Backscattering transpiration studies were reported to explore the volatility of silicon vapors from silica, 3:2 mullite and aluminosilicate under SOFC operating conditions. [**26,27**] It was found that an initial rapid release of silicon vapors was followed by a diffusion limited slower release, indicating that surface residues from manufacturing processes or changes in surface chemistry and morphology are contributing to a decrease in chemical reactivity at the gas-solid interface. The mullite bond ($3Al_2O_3 \cdot 2SiO_2$) was shown to offer only a slight improvement in silicon stability over SiO_2 in the presence of water vapor where volatile silicon hydroxide ($Si(OH)_4$) (Eqns. 3 & 4) and oxy hydroxide (SiO(OH)) (Eqns.

5 & 6) gases dominate. [**22,23,25**] In addition to silicon hydroxide, oxy hydroxide and monoxide, volatile silane gases may form in a reducing atmosphere. [**27**]

3 $\mathbf{SiO_2}(s) + \mathbf{2H_2O}(g) \rightarrow \mathbf{Si(OH)_4}(g)$

4 $\mathbf{Al_6Si_2O_{13}}(s) + \mathbf{4H_2O}(g) \rightarrow \mathbf{3Al_2O_3} + \mathbf{2Si(OH)_4}(g)$

5 $\mathbf{2SiO_2}(s) + \mathbf{H_2O}(g) \rightarrow \mathbf{2SiO(OH)}(g) + \mathbf{½O_2}(g)$

6 $\mathbf{Al_6Si_2O_{13}}(s) + \mathbf{H_2O}(g) \rightarrow \mathbf{3Al_2O_3} + \mathbf{2SiO(OH)}(g) + \mathbf{½O_2}(g)$

Some species in vapor form could have little to no effect on SOFC performance if they never condense and deposit which may be likely under 700 – 1000°C operation, although it could become an emissions concern if harmful vapors are vented. Singh and Vora [**28**]showed that silicon can deposit on nickel anode SOFC fibers at 1000°C in the presence of methane reformation. However, the chemical reformation of methane on the nickel surface may yield an additional mechanism (i.e. low partial pressure of water vapor (Eqn. 7)) to promote silicon deposition (Eqn. 8) that may not be present in pre-reformed or hydrocarbon free streams. Silicon monoxide gas has been shown to form an amorphous monoxide when condensing on a cooler surface, followed by a phase transformation to a more stable mixture (Eqn. 9). [**15**] Silane gases may also deposit at the TPB when exposed to oxygen ions transported across the electrolyte.

7 $\mathbf{CH_4} + \mathbf{H_2O} \rightarrow \mathbf{CO} + \mathbf{3H_2}$

8 $\mathbf{Si(OH)_4}(g) \rightarrow \mathbf{SiO_2}(s) + \mathbf{2H_2O}(g)$

9 $\mathbf{2SiO}(s) \rightarrow \mathbf{SiO_2}(s) + \mathbf{Si}(s)$

The objectives of this investigation are to: (1) study the changes in bulk and surface chemistries of aluminosilicate refractory due to diffusion and gas-solid interface reactions, (2) identify the chemistry and bonding mechanisms of aluminosilicate vapors

deposited on yttria stabilized zirconia (YSZ) or nickel, and (3) determine the effects of volatile gases released from aluminosilicate on solid oxide fuel cell performance. While extensive efforts have been made to investigate silica and aluminosilicates for a wide variety of high temperature applications this study is specifically focused on SOFC environments at temperatures between 800 – 1000°C. For IT-SOFC operating temperatures (600-800°C) solid state diffusion and volatility of silicon are limited by thermodynamics and kinetics [**27**], making their observation difficult in experiments truncated to last several orders of magnitude less than 40,000 hours. SOFC silicon poisoning experiments were conducted at 800°C to minimize causes of degradation observed at 1000°C such as nickel agglomeration [**29**], degradation of 8 YSZ (8 mole % yttria) electrolyte to 9.5 YSZ [**30**] and delamination due to variations in thermal expansion coefficient.

2.0 Experimental Material and Methods

Three separate experiments were conducted: (1) examination of the changes in aluminosilicate surface morphology and chemistry, (2) evaluation of aluminum and silicon deposition on YSZ and nickel, and (3) silicon poisoning in electrolyte supported SOFCs. A low cost aluminosilicate composition (96.3% Al_2O_3, 3.7% $Al_6Si_2O_{13}$) was utilized for this study and freeze cast prior to sintering to achieve approximately 70% theoretical density. Samples were cut into 14 mm squares, 2 mm thick, from a sintered refractory block utilizing a slow speed diamond saw and air dried for 24 hours. Additionally, aluminosilicate powder was crushed from the sintered refractory into a powder utilizing a mortar and pestle (Diamonite^{TM}) manufactured from finely powdered

synthetic sapphire. Samples were thermally treated in a 6 cm diameter alumina (99% Al_2O_3) tube (McDanel AP35) furnace under controlled flow atmospheres. Gases were fed to a gas control box (Linseis L40/2054) where flow rates were regulated at 1.5 liters per hour and 0.7 MPa. The series of gases utilized included humidified ultra-high purity (UHP) air, hydrogen forming gas (5% H_2 Balance N_2), and humidified hydrogen forming gas. A compressed gas cylinder provided the hydrogen forming gas while the UHP hydrocarbon free compressed air was provided with a zero air generator (Packard 2500). The specified gases were humidified utilizing a bubbler containing deionized water at ambient temperature. Complete saturation is assumed based on the gas path length through the water resulting in the partial pressure of water vapor during humidified experiments of $x(H_2O)=0.027$ atm in air and $x(H_2O)=0.023$ atm in the reducing hydrogen forming gas. Aluminosilicate square samples under the controlled flow atmospheres were heated from ambient to 1000°C at a ramp rate of 5°C per minute, held at temperature for 100 hours, cooled to ambient conditions at 5°C per minute and stored in polyethylene airtight bags at room temperature until analysis. The untreated samples were analyzed as the freeze cast and sintered block prior to any long duration thermal treatment.

The morphology and chemistry of silicon species deposited on nickel oxide and YSZ pucks was studied utilizing nickel oxide (Alfa Aesar Lot #C01R001) and 8 mol % yttria stabilized zirconia (TZ-8YS, Tosoh Corporation) powder separately pressed into pellets (1.27 cm diameter) in a uniaxial press at 35 MPa and 70 MPa, respectively. NiO and YSZ pellets were pressure-less sintered in air at 5 °C per minute from ambient to 1400 °C (NiO) and 1500 °C (YSZ), dwelled at the maximum temperature for 2 hours,

and cooled back to ambient temperature at 5 °C per minute. Four pellets at a time were then thermally treated in the alumina tube furnace in humidified UHP air, forming gas (5% H_2, balance N_2), or humidified forming gas. Gases were controlled as previously described. One NiO and one YSZ pellet were placed in the furnace in direct physical contact with the aforementioned aluminosilicate powder; two additional pellets (one NiO and one YSZ) were placed 15 cm downstream free of physical contact with the aluminosilicate powder. Both sets of pellets were placed within the hot zone of the furnace, equidistance from the center.

2.1 Characterization

Field emission scanning electron microscopy (FE-SEM), energy dispersive spectroscopy (EDS), x-ray photoelectron spectroscopy (XPS) and x-ray diffraction (XRD) were used to study the change in the bulk (> 20 μm below surface), bulk-surface (penetration depth of < 20 μm) and surface (< 0.01 μm penetration depth) of aluminosilicate under SOFC operating conditions. FE-SEM (Zeiss VP55 Supra) was used to image the microstructure of the aluminosilicate, bonding of the vapor deposited aluminum and silicon on the YSZ and NiO pucks, and cross sections of SOFC unit cells. Sputter coating using an iridium target at 20 mA for 30 seconds, carbon tape and graphite paste were used to permit the imaging of the electronically insulating samples. EDS elemental mapping was used to evaluate the dispersion of Si in the sputter coated aluminosilicate, YSZ and NiO samples. Bulk-surface scans show the atomic concentrations with a penetration depth of less than 20 μm, and cross section scans study the bulk. EDS is not a quantitative method but does effectively detect small variations in

trace Si concentration as a function of position and can be used for relative comparison. EDS maps, point scans and line scans were conducted with a 20 kV energy beam. XRD (X1-Advanced Diffraction System, Scintag Inc., USA) was utilized to detect the presence of new phases in the aluminosilicate powder after thermal treatment for 100 hours at 1000°C under humidified air, forming gas or humidified forming gas. The XRD tube introduced the x-rays at 45 kV and 40 mA, while the detector was operated at 1kV. Scans were collected from 2θ angle of 20° to 95° at step increments of 0.05°. Phases were compared against the database of JCPDS powder diffraction files.

XPS, also known as electron spectroscopy for chemical analysis (ESCA), was used to study the changes in surface molecular chemistry of the aluminosilicate, YSZ and NiO samples due to thermal treatments as previously described. All XPS spectra were obtained using a PHI MultiTechnique system (Model 5600). The Electron Energy Analyzer (Model 10-360) incorporated into the 5600 is an SCA, and the input lens to the analyzer is an Omni Focus III lens. All spectra were obtained with the x-ray source operating at 300 watts (15 kV). The excitation x-ray source used was a MgKα monochromator (Model 10-610) located at 54.7° relative to the analyzer axis. The Omni Focus III lens was used to scan the spectrum while the SCA was operated at constant pass energy, resulting in constant resolution across the entire spectrum. All of the spectra were obtained using an 800 μm diameter analysis area and samples were mechanically fastened to the specimen mount. A broad scan survey spectrum was first obtained to identify the elements present and the elemental composition. All XPS spectra recorded and stored using the software system (AugerScan Version 3.22) were taken at a pass energy of 46.95 eV with a step size of 0.400 eV. Since the samples studied were

insulating charge compensation was applied. To ensure proper charge correction on the insulating samples the position of the C 1s line from adventitious hydrocarbon was measured. Any shift from 284.8 eV [**31**], indicative of static charging, was compensated with adjustment of emission control (mA) and electron energy (%). Once the survey scan was completed detailed multiplex scans of the peaks of interest were obtained for a more comprehensive picture of the chemical composition. The narrow scans were adjusted to encompass the peaks and were obtained with pass energy of 23.5 eV and a step size of 0.025 eV. Each scan was swept and cycled repeatedly for averaging. XPS peak intensities of the Al(2p) and Si(2p) spectrums were measured for the aluminosilicate after background signals were subtracted using the Shirley integration method. The background level upon which the peak is superimposed is a characteristic of the specimen, the excitation source and the transmission characteristics of the instrument. Surface Si/Al ratio was calculated using the equation below [**32**];

10 (Conc. of Si)/(Conc. of Al) = (I_{Si}/I_{Al}) x (ASF_{Al}/ASF_{Si})

where I and ASF are the intensity of the spectrum and the atomic sensitivity factor of an individual element, respectively. The ASF of each element for the monochromatic x-ray source utilized at 54.7° are Al(2p) = 0.234 and Si(2p) = 0.339. [**31**]

2.2 Electrochemical Performance Test

The electrochemical performance test apparatus utilized has been described in detail elsewhere. [**26,33**] Commercial grade electrolyte supported button cells (NextCell) with an electrolyte diameter of 25 mm and active area of 1.2 cm^2 were operated at constant voltage (0.7 V) and temperature (800 °C) for over 225 hours. The cells were

brought from ambient to 800 °C at a rate of 2.5 °C per minute in a clamshell furnace, with N_2 supplied to the anode (50 mL/min) and UHP air to the cathode (50 mL/min). During operation H_2 (99.999%) humidified via a room temperature bubbler to saturation was supplied to the anode (73 mL/min) and UHP air was supplied to the cathode (218 mL/min). The cell was sandwiched between two 6 cm diameter Inconel metal platens which delivered the fuel to the anode (top) and air to the cathode (bottom) through a 0.635 cm hole bored through their center axis. Stacked from the bottom to top platen was silver paste enhancing the electrical connection, silver mesh disc, button cell and nickel foam without contact paste. The sample cell (100610) had 10.5 grams of the aforementioned aluminosilicate powder in the hot zone of the fuel feed line while the reference cell (100625) did not have any aluminosilicate present. Post mortem cross sectional analysis was conducted on fractured cells via FE-SEM and EDS.

3.0 Results & Discussion

3.1 Aluminosilicate Surface Morphology and Chemistry

FE-SEM micrographs with EDS maps overlaid are presented in Figure 1 for the aluminosilicate samples untreated or after heat treatment for 100 hours at 1000°C in dry reducing gas, humidified reducing gas or humidified air. Micrograph EDS maps of the aluminosilicate show silicon dispersion across the bulk-surface. The aluminosilicate material after treatment in humidified hydrogen or humidified air indicates Si migration is accelerated in the presence of water vapor, yielding a more uniform distribution of Si at the bulk-surface. Surface diffusion occurs along defects and is typically faster than bulk chemical diffusion in silicon systems. [**34**] EDS maps of the cross section of all the

aluminosilicate samples after thermal treatment show the dispersion of Si in the bulk is mainly between alumina clusters. Solid state diffusion of silicon within the aluminosilicate bulk is likely occurring along these grain boundaries. The EDS cross section map of the forming gas sample (Figure 1 top center) includes the bulk-surface, demonstrating a higher concentration of Si in the bulk-surface compared to the bulk. Uncertainty for EDS concentration analysis is generally ±5% [**35**] and can only be used for relative comparison rather than to obtain quantitative data. Figure 2 shows relative Si concentration calculated using EDS is significantly higher at the bulk-surface compared to the bulk for all thermally treated samples, but not the untreated sample. The enrichment of silicon concentrations at the surface is likely due to silicon diffusion rather than alumina volatility since alumina has been demonstrated to be stable in the presence of water vapor up to 1300°C [**36**]. Higher relative silicon concentrations at the bulk-surface indicate the rate of silicon solid-state diffusion in the bulk is faster than the rate for which silicon at the bulk-surface is depleted via chemical volatility. The formation of a surface chemistry rich in silicon supplied from the bulk may yield long term steady state silicon volatility rates governed by chemical reactions at the gas-solid interface until the bulk and bulk-surface regions are depleted or a hermetic barrier is formed.

The increase in Si/Al relative concentration ratio from XPS data of the thermally treated samples, Figure 3, indicates the migration of silicon to the surface from the bulk during thermal treatments. This surface XPS trend is found to be similar to the EDS bulk-surface scans. The Al(2p) and Si(2p) peaks for each sample are normalized and superimposed in Figure 4 to show peak shifts associated with changes in bonding characteristics of Al-Si-O. Variations in the ratio of alumina to aluminosilicate can be

correlated with shifts in the Al(2p) and Si(2p) spectrum maxima. [**32**] Since the dynamics involved in variations of bindings energies are imperfectly understood, we rely on experimental data from standard materials. The range of reported binding energies for several directly comparable aluminum [**37-40**] and silicon [**31,39,41-45**] spectra, Table 1, that were carefully evaluated to instrumental calibration and static charge reference values are shown with vertical gray bars in Figure 4. The Si(2p) peaks show considerably more noise than the Al(2p) due to the low relative concentration of silicon in the refractory utilized in this study. The Al(2p) peak binding energy of the untreated aluminosilicate sample indicates it is composed mainly of alumina near the surface. Thermal treatment resulted in an increase in binding energy of the Al(2p) peak corresponding to increases in the quantity of mullite, in agreement with the EDS results and Si/Al ratio previously discussed. The Si(2p) peaks for the reducing samples indicate a binding energy corresponding to SiO; whereas the untreated and oxidizing heat treated samples show a distribution associated more closely with aluminosilicates. SiO is stable in a reducing atmosphere at 1000°C, and would remain stable after cool down in the reducing atmosphere to ambient temperatures when the aluminosilicate is exposed to air. The shoulder at the right edge (99.5 eV) of the Si(2p) spectrum is due to the presence of crystalline silicon (Si) [**42**]. This shoulder was previously identified in another aluminosilicate XPS study [**32**] as the second satellite peak of the Al(2s) spectrum indicating the presence of extra aluminum oxide. However, the use of a monochromatized x-ray source in this study eliminates these satellite spectra. [**46**] This is confirmed by the absence of the entire family of minor satellite peaks from the Al(2s) main spectrum peak located at lower energies (Mg displacement, eV: α_3 – 8.4, α_4 – 10.1,

α_5 – 17.6) [**31**] in all XPS spectrum. Crystalline silicon on the surface of the sample will react with oxygen or hydrogen to form more stable compounds. [**27**] The depletion of crystalline Si at the surface may be one of several contributing factors leading to the previously reported [**27**] initial break-in period of rapid silicon release which is followed by slower diffusion limited silicon volatility.

All XRD scans of the aluminosilicate powder untreated or thermally treated include the presence of diffraction peaks at the same 2θ angles, demonstrating no new phases are detected within the limits of XRD. All diffraction peaks were identified and correlated with 3:2 mullite [**47**] (PDF 15-0776) and alumina [**48**] (PDF 43-1484) reference diffraction patterns, demonstrating impurity levels are below detection limits. Variations in compound peak intensities related to enrichment of discrete SiO_x phases are indistinguishable or convoluted due to preferred orientation.

3.2 Aluminum and Silicon Deposition on YSZ and Nickel

FE-SEM images with corresponding EDS elemental maps of the YSZ pellets are shown in Figure 5 to illustrate the interactions of YSZ, Si and Al in the different atmospheres studied. Strong interaction of the aluminum/silicon adsorbate with the YSZ substrate downstream of the aluminosilicate source, as indicated by wetting of the adsorbate, is shown in both fuel and air atmospheres. Conversely, YSZ specimens in direct physical contact with the aluminosilicate powder in the fuel atmospheres were void of glassy deposits suggesting a stronger affinity towards silicon vapor species (Figure 6 left). The FE-SEM micrographs and EDS maps in Figure 5 clearly indicate aluminum rich clusters are enclosed in an amorphous siliceous layer, but also establishes that

aluminosilicate is volatizing to the downstream pellet. The YSZ downstream sample treated in humidified forming gas (Figure 5 bottom row) includes significantly smaller and more evenly dispersed aluminum containing clusters throughout the amorphous siliceous layer in comparison to both YSZ samples treated in humidified air. Tubular silicon deposits are also observed in the top right hand corner of the humidified forming gas EDS/FE-SEM image indicating preferential growth. Figure 5 and Figure 6 (right) reveal extensive grain and grain boundary enlargement around the edge of the clusters due to the amorphous siliceous layer. Furthermore, the EDS line scan in Figure 6 confirms increases in the Si concentration (marked a, b, c, d or e) correlate with the grain boundaries locations marked correspondingly along the EDS scan arrow, clearly indicating silicon diffusion into the YSZ along grain boundaries, potentially isolating YSZ grains with a glassy phase.

XPS scans of the same samples were conducted using an 800 μm diameter spot size to ensure maximum averaging. Although FE-SEM and EDS maps show migration into the YSZ, Figure 7 shows that no changes in peak shape or binding energies are apparent in the Zr(3d) and Y(3d) spectra, implying no new compounds are being formed with the YSZ and deposited silicon within detection limits. This confirms that the mechanism of silicon transport occurs through grain boundaries, and while the silicon may not affect the individual grains from a chemical perspective, an insulating grain boundary region can effectively nullify oxygen ion transport. Under a reducing atmosphere Al(2p) peaks from the YSZ samples in direct contact with aluminosilicate are greater in intensity than the downstream samples, suggesting higher concentrations of aluminum. This correlates with the EDS results that show samples in direct contact with

the aluminosilicate, which is predominately alumina (96.3% Al_2O_3, 3.7% $Al_6Si_2O_{13}$), have unperturbed chunks physically adsorbed to the surface; where the downstream samples include regions rich in alumina that are encapsulated in an amorphous siliceous based layer adsorbed onto the YSZ and penetrating the grain boundaries. The amorphous layer is likely thick enough to inhibit the escape of photoelectrons from the alumina rich under layer, resulting in what appears to be a lower concentration of aluminum. Substantial noise to signal ratio in the Al(2p) spectra from the humidified air samples suggests the siliceous amorphous layer is coherent.

The nickel pellets were all carefully inspected via FE-SEM and EDS for aluminum or silicon bonded to the surface. While small chucks of the aluminosilicate refractory are apparent on the nickel surface no wetting or diffusion of silicon into the nickel grain structure is visually apparent on either the nickel samples in direct physical contact with the aluminosilicate or downstream of the aluminosilicate (Figure 8 and Figure 9). The nickel sample downstream of the aluminosilicate in flowing humidified forming gas (Figure 8) had tubular aluminosilicate rods (similar to the YSZ sample thermally treated in the same atmosphere) that appeared physically deposited on the nickel, but were absent of a wetted amorphous siliceous layer. SiO is suggested via thermodynamic equilibrium modeling as a significant volatile silicon gas released from aluminosilicate under a reducing atmospheres at 1000°C [**27**]; the observation of aluminosilicate rod shaped deposits only under a humidified reducing atmosphere suggests water vapor encourages preferential growth. Clusters (~20 μm in diameter) on the surface of the nickel pellets after thermal treatment in humidified air include large amounts of refractory impurities (Na, Cl, K, Rh, S, Ca and P) and silicon. Refractory

impurities may decrease the activation energy of aluminosilicates, in turn increasing the volatility of silicon containing gases. These impurities appear to have a stronger affinity for the nickel substrate as they were not detected on YSZ pellets.

The surface of the nickel is visibly different in Figure 8 compared with Figure 9 due to the reduction of the nickel oxide pellet to form metallic nickel. EDS line scans (Figure 8) demonstrate the presence of oxygen correlates with aluminum and silicon yet is absent where nickel is present, indicating the reduction of nickel oxide to metallic nickel during the thermal treatments in the reducing atmospheres is the cause of change in morphology. The change in chemical composition from nickel oxide to nickel metal can result in significantly different interactions and wetting of adsorbate with aluminum and silicon vapor deposits. However, despite the weaker metallic bonding in the reduced nickel samples the formation of an amorphous siliceous phase or silicon adsorption/diffusion into the nickel bulk is not apparent, indicating that silicon poisoning may be more strongly associated with degradation of oxygen ion transport in YSZ electrolytes and anode cermets.

3.3 SOFC Silicon Poisoning

Results of electrochemical performance testing presented in Figure 10 on two identical commercial SOFC button cells under duplicate experimental conditions, with the only exception the presence of aluminosilicate in the hot zone of the anode fuel delivery tube, indicate silicon poisoning can occur in relatively short time scales at lower temperatures than the studies above. The reference cell (100625) performed as expected based on the manufacturer's specifications. [**49**] However, the sample cell (100610) with

aluminosilicate present reached 71% of the reference cell peak performance and degraded 15% in 150 hours. The reference cell and sample cell followed an identical rate of performance increase during the first 15 hours. The initial SOFC break-in period showing substantial performance improvement during startup may be attributed to changes in the electrode microstructural and cathode/electrolyte interface chemistry [**50**], or activation of the anode through reduction of the nickel oxide to nickel metal and increase of the triple-phase boundary [**51**]. The reference cell continues to increase current output during cell activation to 0.14 A at 0.7 V until it stabilizes at 150 hours. However, the sample cell current output begins to steadily decline at 100 hours after reaching a maximum of only 0.10 A at 0.7 V. A previously conducted experiment in our research facility on commercial electrolyte supported SOFCs from an alternate supplier where the aluminosilicate was introduced in-situ into the hot zone of the fuel delivery tube demonstrated immediate performance degradation followed by a steady state decline in power output further supporting the silicon induced degradation of these cells is due to the refractory material. [**26**] The aluminosilicate powder represents a high surface area flow field designed to reduce kinetic limitations and accelerate the volatility of silicon species. Although the high surface area flow field may not be a direct representation of commercial applications for aluminosilicate refractory, the long operating times of stationary SOFCs and extensive use of refractory material provide an ample opportunity for silicon poisoning by vapor species.

Post-mortem cell analysis via FE-SEM and EDS (Figure 11) on the sample cell revealed silicon within the YSZ electrolyte. A clear distinction in silicon concentration was identified in the anode interlayer compared with the electrolyte suggesting silicon

impurities in the YSZ are a significant source. Furthermore, small regions of relatively high concentrations of silicon are observed at the anode/electrolyte interface in the sample cell as seen in the EDS line scan (Figure 11). At this time we are not able to determine whether the silicon has migrated via solid state diffusion from the anode interlayer and electrolyte, or if it was vapor deposited as condensed volatile gases released from the aluminosilicate. However, the absence of high silicon concentrations at the TPB of the reference cell, poor sample cell performance and rapid degradation in the sample cell compared to the reference cell suggest silicon is indeed being transported from the aluminosilicate powder and deposited in the hot regions of the fuel cell. Additionally, delamination at the TPB was prevalent across the sample cell but not the reference cell. The presence of a siliceous glass between the anode interlayer and electrolyte generates the potential for mechanical stresses due to the mismatch of thermal expansion coefficients that can lead to delamination.

The replacement of high purity alumina with aluminosilicate to reduce SOFC costs where the insulation is not isolated from the cells (tubular more so than planar) is shown to substantially increase degradation. This study suggests that aluminosilicates do release SOFC degrading vapors such that, in parallel with stainless steel interconnect studies and chromium volatility, the development of environmental barrier coatings or infusion of different compounds into the aluminosilicate are necessary to lock up the silicon. Further, planar SOFCs commonly employ glass seals which can introduce a significant source of silicon. Due to the required physical contact between the glass seal and electrolyte to separate oxidant and fuel gas streams, and the observed rapid diffusion of silicon into the YSZ microstructure along the grain boundaries, solid state diffusion of

silicon from the glass seal to the TPB seems very plausible. Lower temperatures below 800°C will facilitate kinetic limitations of silicon transport and volatilization, however, the deviation from reference cell performance after only 15 hours at 800°C suggests that transport of silicon to active cell regions will be degrading. Furthermore, silicon's affinity for YSZ observed in the deposition study suggests volatile silicon gases from glass seals may also represent a significant source of long term degradation.

4.0 Conclusion

It was shown that silicon can diffuse through aluminosilicate refractory bulk to the gas interface, enriching surface mullite concentrations. Surface diffusion is accelerated by water vapor, creating a more uniform distribution of silicon on the aluminosilicate surface. In the absence of hydrocarbon reformation and electrochemical activity, vapors from aluminosilicate were preferentially deposited on yttria stabilized zirconia rather than nickel in both fuel and air atmospheres. Surface adsorption and grain boundary diffusion of siliceous species was detected on the YSZ samples, potentially isolating YSZ grains with a glassy phase; whereas the aluminosilicate was scarcely perturbed upon adsorption to the nickel samples. The presence of aluminosilicate powder within the hot zone of the fuel line supplying the anode caused cell performance to deviate from the reference cell free of aluminosilicate after 15 hours at 800°C, reaching 71% of the maximum power density achieved by the reference cell and degrading 0.1% per hour. Post fuel cell testing identified anode/electrolyte interface delamination and concentrations of silicon above impurity levels in the interface region.

5.0 Glossary

EDS – Energy dispersive x-ray spectroscopy

FE-SEM – Field emission scanning electron microscopy

SOFC – Solid oxide fuel cell

TPB – Triple phase boundary

XPS – X-ray photoelectron spectroscopy

XRD – X-ray diffraction

YSZ – Yttria stabilized zirconia

Acknowledgements

The authors gratefully acknowledge Montana State University's Imaging and Chemical Analysis Laboratory; as well as the financial support by the United States Department of Energy, National Energy Technology Laboratory, under SECA Cooperative Agreement No. DE-FC26-05NT42613. Any opinions, findings, conclusions, or recommendations expressed herein are those of the authors and do not necessarily reflect the views of the DOE.

References

[1] K. S. Mazdiyasni and L. M. Brown, "Synthesis and Mechanical Properties of Stoichiometric Aluminum Silicate (Mullite)," *J. Am. Ceram. Soc.*, 55 548-552 (Jun 2006).

[2] Siemens AG. (2010, October) Siemens.com Global Website. [Online]. http://www.energy.siemens.com/co/en/power-generation/fuel-cells/benefits-

features.htm

[3] M. Aoki et al., "Solute segregation and grain-boundary impedance in high-purity stabilized," *J. Am. Ceram. Soc.*, 79 1169-1180 (1996).

[4] S.P. S. Badwal, J. Drennan, A. E. Hughes and B.A. A. Sexton, "A study of impurity phase segragation in fully stabilized yttria-zirconia," *Mater. Sci. Forum*, 34-36 195-199 (1988).

[5] G. M. Ingo and G. Padeletti, *Surf. Interface Anal.* p. 21 (1994).

[6] Joshua L. Hertz, Avner Rothschild and Harry L. Tuller, "Highly enhanced electrochemical performance of silicon-free platinum–yttria stabilized zirconia interfaces," *J. Electroceram.* (September 2007).

[7] M. Mogensen, K. V. Jensen, M. J. Jorgensen and S. Primdahl, "Progress in understanding SOFC electrodes," *Solid State Ionics*, 150 123-129 (2002).

[8] M. S. Schmidt, K. V. Hansen, K. Norman and M. Mogensen, "Effects of trace elements at the Ni/ScYSZ interface in a model solid oxide fuel cell anode," *Solid State Ionics*, 179 1436-1441 (2008).

[9] M. Backhaus-Ricoult and M. F. Tichet, "Interfacial chemistry at metal electrode–oxide electrolyte contacts," *Solid State Ionics*, 150 143-156 (2002).

[10] A. Bernasik, K. Kowalski and A. Sadowski, "Surface segregation in yttria-stabilized zirconia by means of angle resolved X-ray photoelectron spectroscopy," *J. Phys. Chem. Solids*, 63 [2] 233-239 (2002).

[11] P. , Borchardt, G., Schmuckerb, M. and Schneider, H. Fielitz, "Silicon tracer

diffusion in single crystalline 2/1-mullite measured by SIMS depth profiling," *Physical Chemistry Chemical Physics* 2279–2282 (2003).

[12] Frederic Bejina and Olivier Jaoul, "Silicon diffusion in silicate materials," *Earth Planet. Sci. Lett.*, 153 229-238 (October 1997).

[13] Stephen T. Tso and Joseph A. Pask, "Reaction of Silicate Glasses and Mullite with Hydrogen Gas," *J. Am. Ceram. Soc.*, 65 [8] 383-387 (1982).

[14] V. E. Roshin, A. V. Roshin, A. A. Berdnikov and Yu N. Goikhenberg, "Formation and Sublimation of the Intermediate Products of the Reduction of Silicon from its Dioxide," *Russ. Metall. (Engl. Transl.)*, 4 281-285 (2008).

[15] W. Kronert and H. Buhl, "The influence of various gaseous atmospheres on refractories of the system Al2O3-SiO2 (Part II)," *Interceram*, 2 140-146 (1978).

[16] C. J. van Nieuwenburg and P. M. van Zon, "Semi-quantitative measurements of the solubility of quartz in supercritical steam," *Recl. Trav. Chim. Pays-Bas*, 54 p. 129 (1935).

[17] G. W. Morey and J. M. Hesslegesser, "Solubility of quartz and some other substances in superheated steam at high pressures," *Trans. ASME*, 73 865-875 (1951).

[18] G. C. Kennedy, "A portion of the system silica-water," *Econ. Geol.*, 46 p. 821 (1951).

[19] M. D. Allendorf, C. F. Melius, P. Ho and M. R. Zachariah, "Theoretical study of the thermochemistry of molecules in the Si-O-H system," *J. Phys. Chem.*, 99 15284-

15293 (1999).

[20] E. L. Brady, "Chemical Nature of Silica Carried by Steam," *J. Phys. Chem.*, 57 706-710 (1953).

[21] A. Hashimoto, "The effect of H2O gas on volatilities of planet-forming major elements: I. Experimental determination of thermodynamic properties of Ca-, Al-, and Si-hydroxide gas molecules and its application to the solar nebula, Geochim.," *Geochim. Cosmochim. Acta*, 56 511-532 (1992).

[22] D. L. Hildenbrand and K. H. Lau, "Thermochemistry of gaseous SiO(OH), SiO(OH)2, and SiO2," *J. Chem. Phys.*, 101 [7] 6076-6079 (1994).

[23] N. Jacobson, M. Dwight, E. Opila and E. Copland, "Interactions of water vapor with oxides at elevated temperatures," *J. Phys. Chem. Solids*, 66 471-478 (2005).

[24] O. H. Krikorian, "Predictive calculations of volatilities of metals and oxides in steam-containing environments.," *High Temp. - High Pressures*, 14 387-397 (1982).

[25] E. J. Opila, D. S. Fox and N. S. Jacobson, "Mass Spectrometric Identification of Si-O-H(g) Species from the Reaction of Silic with Water Vapor at Atmospheric Pressure," *J. Am. Ceram. Soc.*, 80 1009-1012 (1997).

[26] Paolo R. Zafred, Stephen W. Sofie and Paul S. Gentile, "Progress in understanding silica transport process and effects in solid oxide fuel cell performance," in *Proceedings of the ASME Eight International Fuel Cell Science, Engineering & Technology Conference*, Brooklyn, New York, USA, 2010.

[27] Paul S. Gentile, Stephen W. Sofie, Camas F. Key and Richard J. Smith, "Silicon

Volatility from Alumina and Aluminosilicates under Solid Oxide Fuel Cell Operating Conditions," *J. Am. Ceram. Soc.* (Submitted September 2010).

[28] Prabhakar Singh and Shailesh D. Vora, "Vapor Phase Silica Transport during SOFC Operation at 1000C (Invited)," in *A collection of papers presented at the 29th International Conference on Advanced Ceramics and Composites*, Cocoa Beach, Florida, January 23-28, 2005, pp. 99-110.

[29] D. Simwonis, F. Tietz and D. Stover, "Nickel coarsening in annealed Ni/8YSZ anode substrates for solid oxide fuel cells," *Solid State Ionics*, 132 241-251 (2000).

[30] Manohar S. Sohal, "Degradation in Solid Oxide Cells During High Temperature Electrolysis," Idaho National Laboratory, Idaho Falls, Idaho, INL/EXT-09-15617, 2009.

[31] John F. Moudler, William F. Stickle, Peter E. Sobol and Kenneth D. Bomben, *Handbook of X-ray Photoelectron Spectroscopy*. Eden Prairie, Minnesota: Perkin-Elmer Corporation - Physical Electronics Division, 1995

[32] Surasak Wannaparhun and Sudipta Seal, "Surface chemical reactions of aluminosilicate composites at extreme atmospheres using electron spectroscopy for chemical analysis," *Journal of Materials Chemistry*, 13 323-327 (January 2003).

[33] A. Lussier, S. W. Sofie, J. Dvorak and Y. U. Idzerda, "Mechanism for SOFC Anode Degradation from Hydrogen Sulfide Exposure," *Int. J. Hydrogen Energy*, 33 p. 945 (2008).

[34] Per Kofstad and Truls Norby, "Defects and Transport in Crystalline Solids,"

University of Oslo, Norway, Compendium for the advanced level course Defect Chemistry and Reactions in Solids (KJM 4120) 2004.

[35] A., Jensen, S.H., Bilde-Sørensen, J.B., and Mogensen, M. Hauch, "Silica Segregation in the Ni/YSZ Electrode," *Journal of the Electrochemical Society* A619-A626 (2007).

[36] E. J. Opila, N. S. Jacobson, D. L. Myers and E. H. Copland, "Predicting Oxide Stability in High-Temperature Water Vapor," Glenn Research Center, NASA, Cleveland, OH, Research Summary 2006.

[37] L. Ley, F. R. McFeely, S. P. Kowalczyk, J. G. Jenkin and D. A. Shirley, "Many-body effects in x-ray photoemission from magnesium," *Phys. Rev.*, 11 p. 600 (1975).

[38] J. Ashley Taylor, "An XPS study of the oxidation of AlAs thin films grown by MBE," *J. Vac. Sci. Technol.*, 20 751-756 (1982).

[39] C. D. Wagner et al., "Auger and photoelectron line energy relationships in aluminum–oxygen and silicon–oxygen compounds," *J. Vac. Sci. Technol.*, 21 933-945 (1982).

[40] Joseph C. Klein and David M. Hercules, "Surface characterization of model Urushibara catalysts," *J. Catal.*, 82 424-441 (1983).

[41] P. R. Anderson and W. E. Jr. Swartz, "X-Ray Photoelectron Spectroscopy of Some Aluminosilicates," *Inorg. Chem.*, 13 2293-2294 (1974).

[42] T. P. Nguyen and S. Lefrant, "XPS study of Si0 thin films and SiO-metal interfaces," *J. Phys.: Condens. Matter*, 1 5197-5204 (1989).

[43] V. Atzrodt, T. Wirth and H. Lange, "Investigation of NiSi and Pd3Si thin films by AES and XPS," *Phys. Status Solidi A*, 62 [2] 531-537 (1980).

[44] A. F. Povey, R. O. Ansell, T. Dickinson and P.M. A. Sherwood, "An X-ray photoelectron spectroscopic study of stainless steel electrodes after polarisation in the regions of transpassivity and secondary passivity ," *J. Electroanal. Chem.*, 87 189-201 (1978).

[45] M. Klasson et al., "Electron escape depth in silicon," *J. Electron Spectrosc. Relat. Phenom.*, 3 427-434 (1974).

[46] C. J. Corcoran, H. Tavassol, M. A. Rigsby, P. S. Bagus and A. Weickowski, "Application of XPS to study electrocatalysts for fuel cells," *J. Power Sources*, 195 7856-7879 (2010).

[47] A. N. Winchell and H. Winchell, *The microscopical characters of artificial inorganic solid substances.* New York: Academic Press Inc., 1964

[48] D. Grier and G. McCarthy, ICDD Granat-in-Aid, 1991, North Dakota State University.

[49] NexTech Materials. (2010, October) AZoM - The A to Z of Materials. [Online]. http://www.azom.com/details.asp?ArticleID=2894#_Long_Term_Performance

[50] Ellen Ivers-Tiffee, Andre Weber, Klaus Schmid and Volker Krebs, "Macroscale modeling of cathode formation in SOFC," *Solid State Ionics*, 174 223-232 (2004).

[51] Guo-Bin Jung, Kai-Fan Lo and Shih-Hung Chan, "Effect of pretreatments on the anode structure of solid oxide fuel cells ," *J. Solid State Electrochem.*, 11 1435-1440

(2007).

Figures

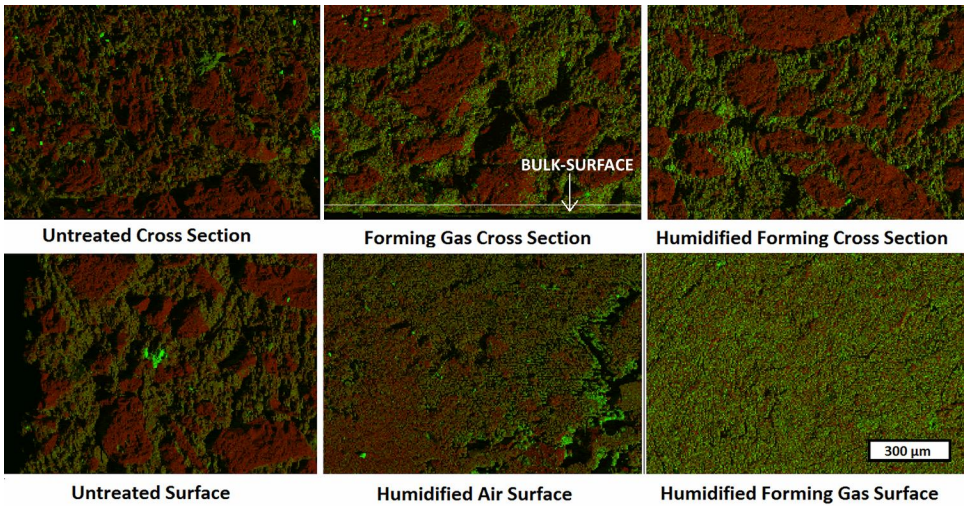

Figure 1: FE-SEM micrographs with overlaid EDS maps of the cross sections (top row) or bulk-surface (bottom row) of aluminosilicate material untreated or thermally treated at 1000°C for 100 hours in the stated gas. Si is displayed in green (light gray tone) and Al is displayed as red (dark gray tone).

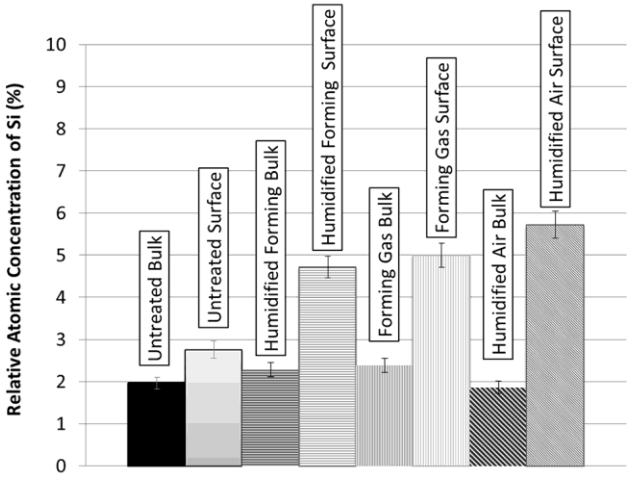

Figure 2: Qualitative EDS analysis of relative silicon concentration (with error bars) on the cross section or bulk-surface of aluminosilicate specimens treated for 100 hours at 1000°C. All scans were taken at 100 x magnification; scan areas are approximately 0.88 mm^2 (1.1 mm x 0.8 mm).

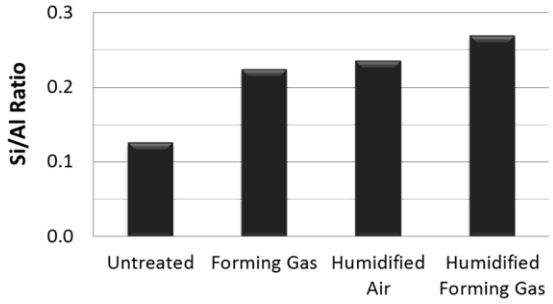

Figure 3: Relative surface Si/Al concentration ratio calculated via XPS utilizing the Al(2p) and Si(2p) spectrum from aluminosilicate samples untreated or after thermal treatment in the stated gases for 100 hours at 1000°C.

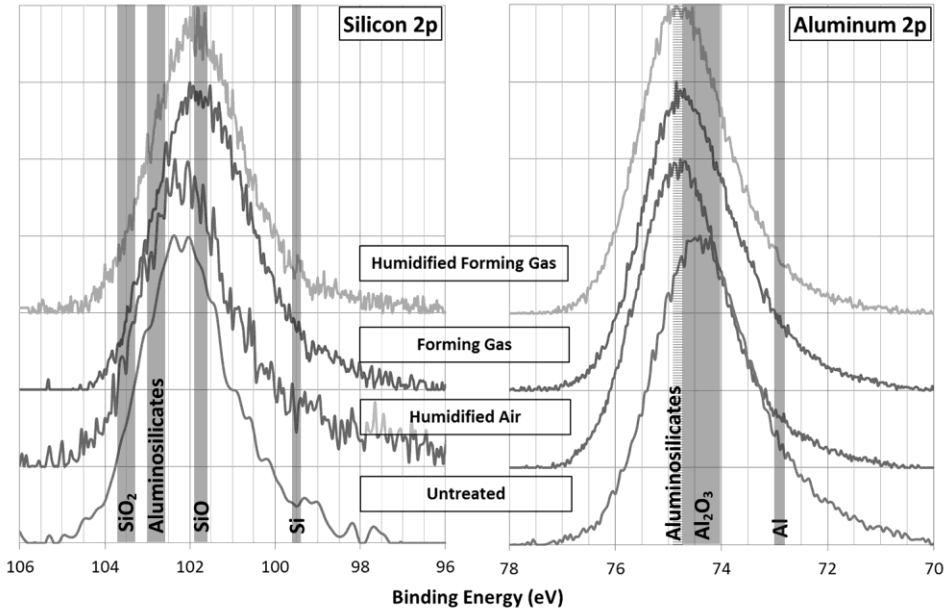

Figure 4: XPS surface scans of the Si(2p) and Al(2p) spectra from an aluminosilicate samples untreated or after thermal treatment for 100 hours at 1000°C in the stated gases. Gray bars indicate ranges of reported peak maxima (Table 1).

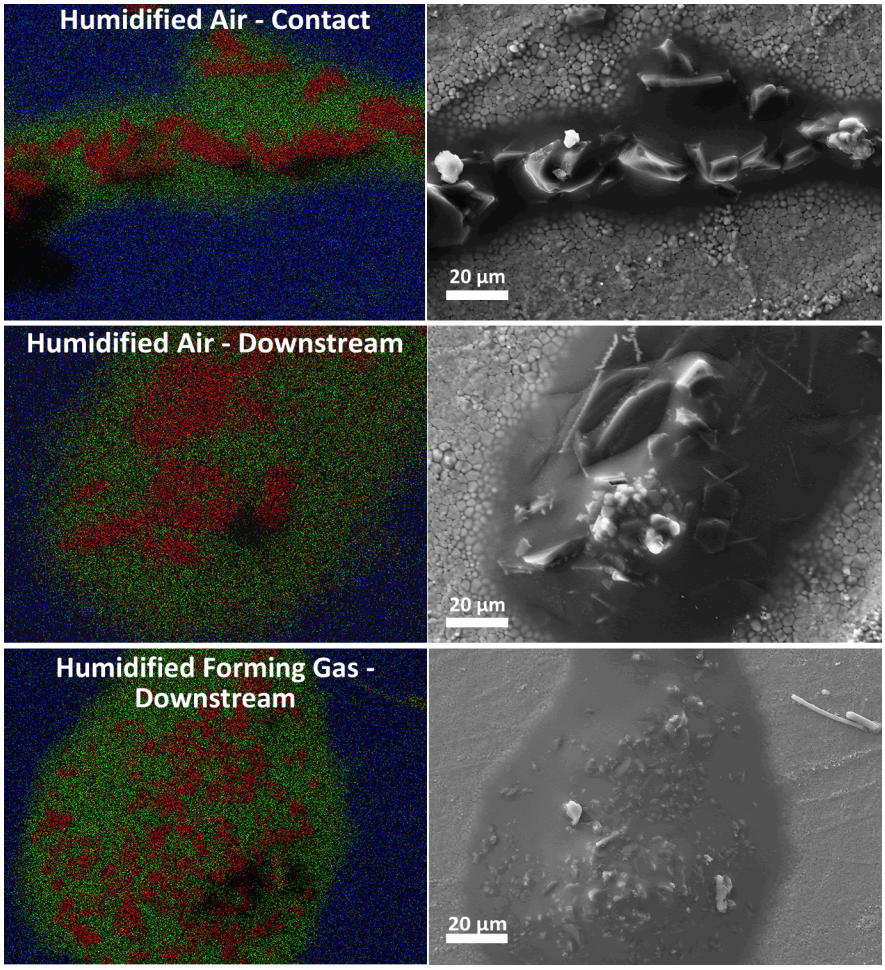

Figure 5: EDS elemental maps (left) (Si-green (light gray tone), Al –red (mid gray tone), Zr-blue (dark gray tone)) and corresponding FE-SEM micrographs (right) of YSZ pellets in direct physical contact or downstream of the aluminosilicate source at 1000°C for 100 hours in flowing humidified air or humidified forming gas.

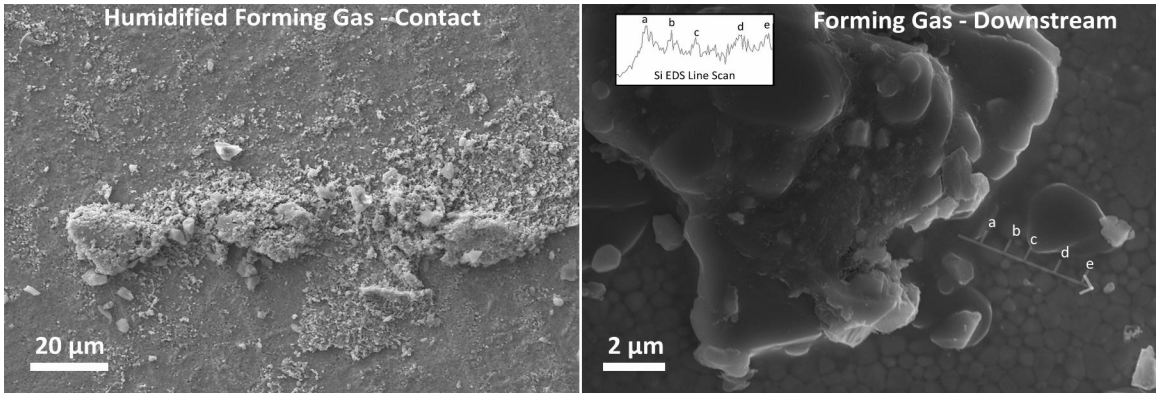

Figure 6: FE-SEM micrograph and EDS line scan of YSZ pellets in direct physical contact (left) or downstream (right) of aluminosilicate source for 100 hours at 1000°C in the stated gases.

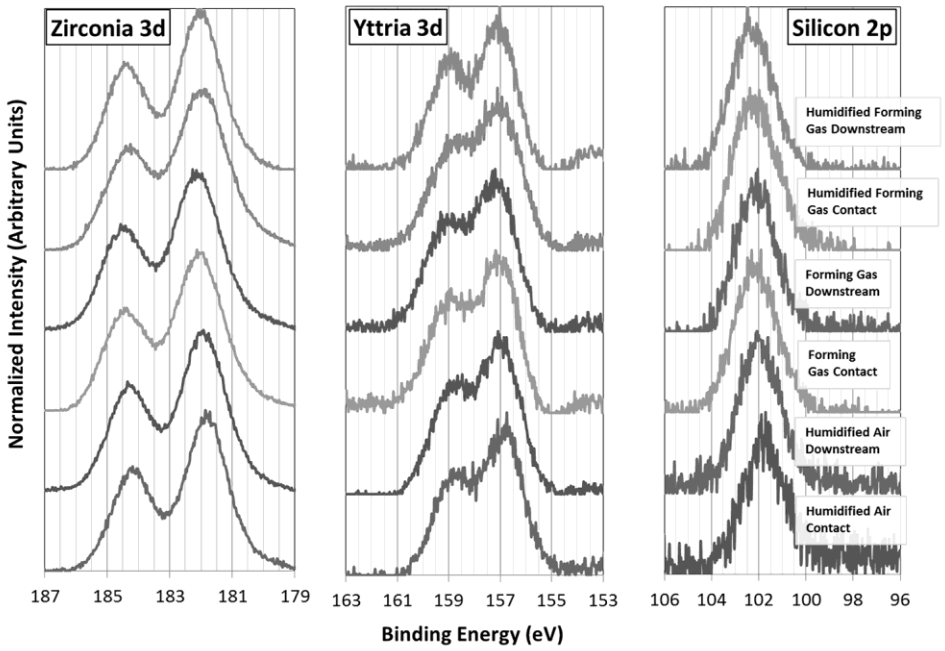

Figure 7: XPS surface scans of the Zr(3d), Y(3d) and Si(2p) peaks from on YSZ samples in direct physical contact or downstream after thermal treatment for 100 hours at 1000°C in oxidizing and reducing atmospheres.

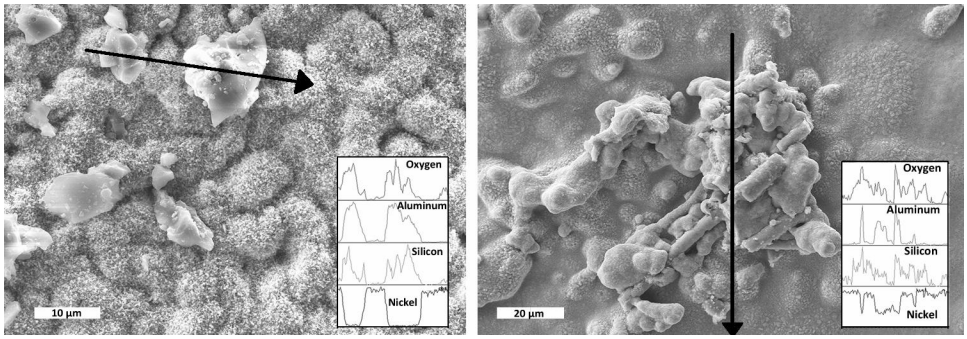

Figure 8: FE-SEM micrographs and EDS line scans of a nickel pellet in direct physical contact (left) or downstream (right) from aluminosilicate (MSU1) powder for 100 hours at 1000 C in flowing humidified forming gas .

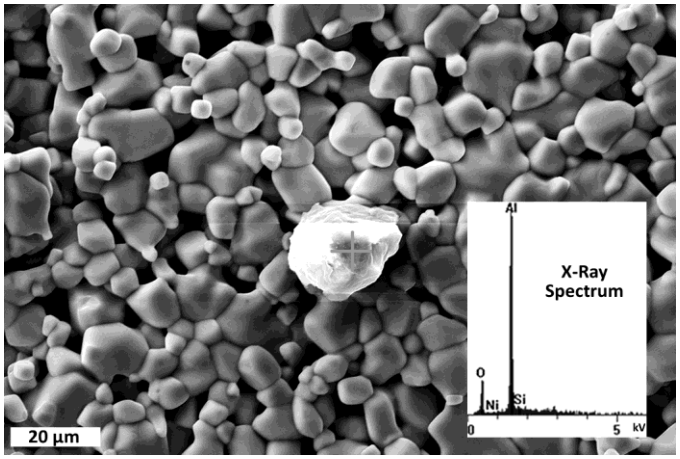

Figure 9: FE-SEM micrograph and x-ray spectrum (20kV) of a nickel pellet in direct physical contact with the aluminosilicate source at 1000°C for 100 hours in flowing humidified air.

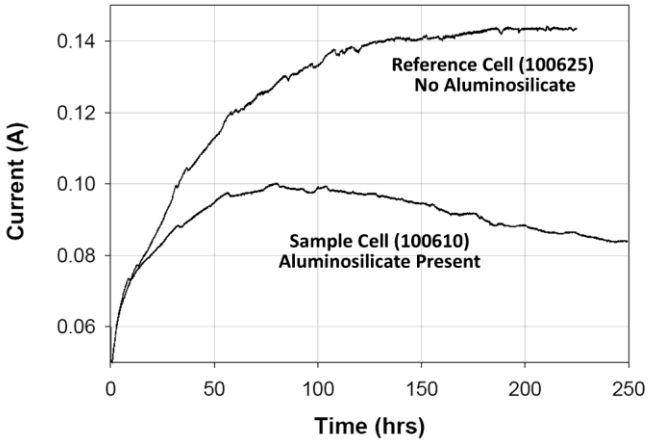

Figure 10: Electrochemical performance test on two identical electrolyte supported SOFC unit cells (1.23 cm^2 active area) at 800°C, constant voltage (0.7 V) and flow rates (H_2 – 73 mL/min, UHP air – 218 mL/min). Sample cell (100610) included 10.5 grams of aluminosilicate powder in the hot zone of the fuel feed line.

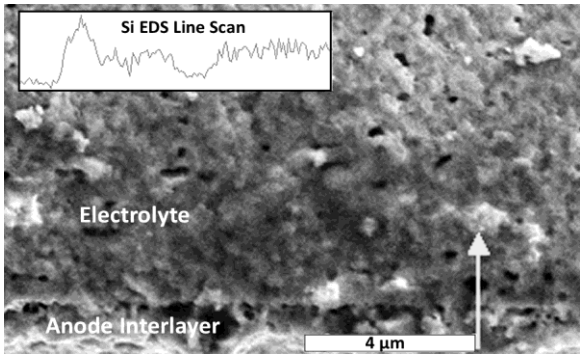

Figure 11: FE-SEM micrograph and Si EDS line scan of the cross section of the planar SOFC sample cell (100610) after being run for 250 hours at 800°C and constant voltage (0.7 V) with aluminosilicate present in the hot zone of the fuel delivery system. A Si peak is detected at the triple phase boundary; the constant detection level in the electrolyte is presumably YSZ impurity.

Tables

Table 1

Compound [Citation]	**Binding Energy (eV)**	
	Si 2p	**Al 2p**
Si [**43**] [**44**] [**31**]	99.5	
SiO [**42**]	101.7	
Al [**37**] [**38**]		72.8
Al_2O_3 [**38**] [**39**] [**40**]		73.7-74.7
Al_2SiO_5, sillimanite [**39**] [**41**]	102.6	74.6
Al_2SiO_5, kyanite [**41**]	102.8	74.7
Al_2SiO_5, mullite [**41**]	103.0	74.8
SiO_2 [**45**] [**39**]	103.3-103.7	

SUPPLEMENTAL RESULTS & DISCUSSION

Alternative Refractory Material Microstructures

Microstructures of the alumina powder, dense alumina refractory board and aluminosilicate refractory blanket are presented in Figure 11. The high purity alumina powder microstructure remained unchanged after thermal treatment in unconditioned air at 900°C for 72 hours. Sintering as indicated by necking between powder agglomerations and grain development were not observed. Alumina is well known to remain stable in air at 900°C for extended periods. The untreated low density alumina refractory board (ZAL-15AA) contained small agglomerations (1-2 μm) of inorganic alumina binder attached to the surface of ceramic fibers. After thermal treatment the presence of the agglomerations is significantly reduced suggesting solid state diffusion or gas phase volatility. High surface area inorganic binders may represent a significant source of silicon vapors in SOFC refractory materials if a silicon based binder is used. The microstructure of the refractory blanket processed without inorganic binders consisted of aluminosilicate ceramic fibers absent of any small agglomerations.

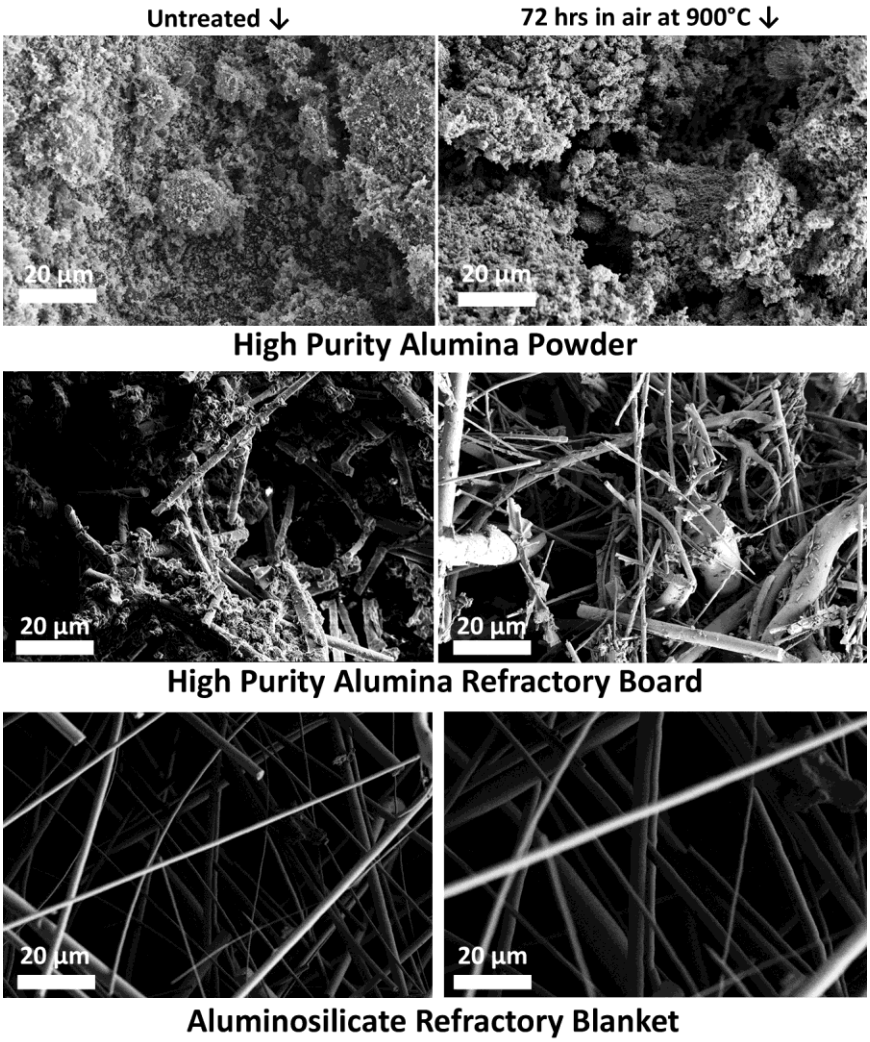

Figure 11: Micrographs of alternative SOFC refractory materials.

Aluminosilicate Morphology and Chemistry

XPS Curve Decomposition

XPS spectra can be deconvoluted and curve fit with multiple components to identify molecular compositions at the surface. For comparison with results presented in the third manuscript [8], curve fitting of the Si(2p) peak from the aluminosilicate surface was completed (Figure 12). The background of the XPS spectra was first

subtracted utilizing the Shirley integration method. Gaussian, Lorentzian and mixed functions can be used for curve fitting. Due to similarity in results and arbitrary nature of the choice, curves were fit with 100% Gaussian functions. The full width at half maximum (FWHM) for the fitting curves were set in accordance with values reported in the literature. [14] [15] The resultant curve shown in maroon (Figure 12) is the summation of all decomposed curves. The maxima of decomposed peaks (Table 4: XPS curve fit summaryTable 4) do not correlate with reported maxima values for pure compound reference curves from the literature (Table 5). Significant shoulders due to the emergence of additional peaks were not recorded. Deconvolution produces sharper peaks and aids in identifying the exact energy of peaks; however, deconvolution of the spectra also did not establish the presence of multiple peaks. Therefore it was concluded XPS curve fitting is not applicable to this data set.

Table 4: XPS curve fit summary

Atmosphere	Curve #	Area	Area %	Position	Intensity	FWHM
Dry Forming Gas	1	3335	85%	101.9	1362	2.3
	2	597	15%	99.2	244	2.3
Humidified Air	1	3315	87%	102.0	1354	2.3
	2	490	13%	98.9	200	2.3
Humidified Forming Gas	1	3651	100%	101.8	1429	2.4
Untreated	1	977	85%	102.2	421	2.2
	2	169	15%	100.1	69	2.3

Table 5: Published Si(2p) binding energies

Compound	Si(2p) Binding Energy (eV)	Reference
Si	99.5	[14] [16][17]
SiO	101.7	[18]
Al_2SiO_5	102.6-103	[15] [19]
SiO_2	103.3-103.7	[19][20]

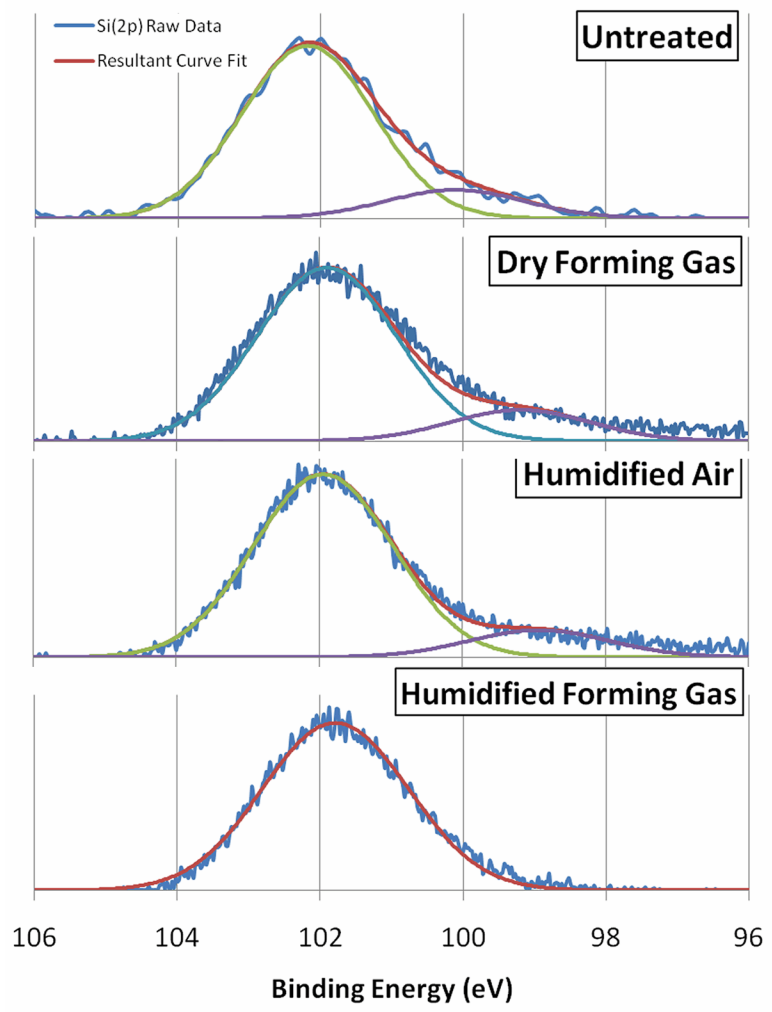

Figure 12: XPS curve fits

X-ray Diffraction

All XRD scans of the aluminosilicate powder untreated or thermally treated at 1000°C for 100 hours include the presence of diffraction peaks at the same 2θ angles (Figure 13), demonstrating no new phases are detected within the limits of XRD. There are noteworthy fluctuations in relative peak intensities suggesting the chemical composition varies between untreated and thermally treated samples. However, due to

the potential of preferential ordering of the crystals XRD cannot be used to draw any conclusions regarding changes in the chemical composition.

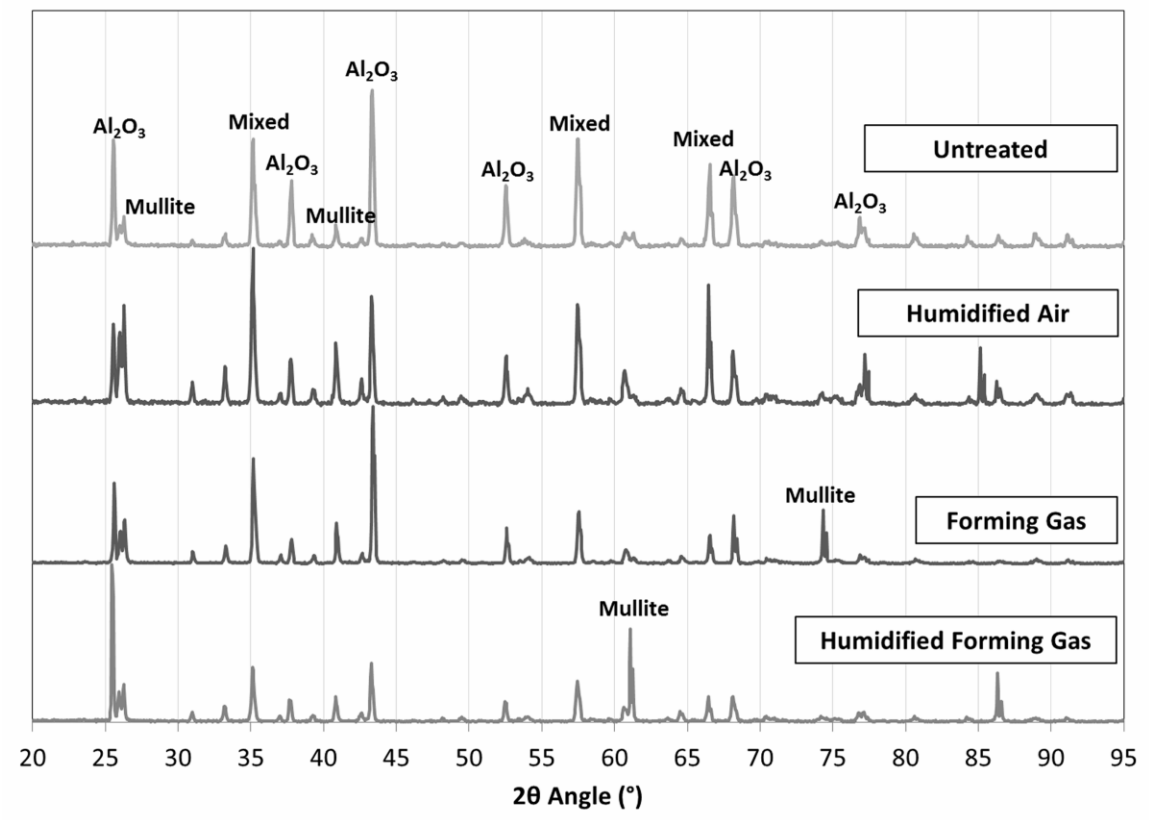

Figure 13: X-ray diffraction pattern of aluminosilicate powder

Deposition of Aluminosilicate Vapors on SOFC Materials

Formation of a zirconium silicide ($ZrSi_xO_y$) has been reported [21] in ultrathin ZrO_2 films prepared by chemical vapor deposition on Si(100) above 900°C in a vacuum. The silicide was identified via XPS based on the introduction of a silicide peak in the Zr(3d) spectra. The silicide peak remained absent from Zr(3d) spectra reported [8] after exposing YSZ to aluminosilicate at 1000°C for 100 hours under SOFC gases, reaffirming no chemical reactions appear to be occurring between the zirconia and aluminosilicate

adsorbent. Hughes and Sexton [22] identified intergranular phases in YSZ as a silicate thin film which did not form new phases with zirconia or yttria in specimens when sintered below1400°C. In addition to yttrium orthosilicate ($Y_2O_3 \cdot SiO_2$), other stable yttrium silicates are known where the ratio of yttria to silica is less than 1. [23] Chemical shifts in spectra maxima of Y(3d), consistent with shifts reported in thin films containing a significant fraction of silicate (Y-O-Si) bonding units [24], are attributed to the donation of electrons from yttrium to neighboring Si-O bonds in agreement with the electronegativities of Y, Si and O. These chemical shifts in the Y(3d) spectra were not observed in the YSZ samples exposed to aluminosilicate at 1000°C for 100 hours under SOFC gases (Manuscript 3, Figure 7). While secondary silica based phases are favorable at SOFC sintering and fabrication temperatures, no secondary phases are evident in vapor deposited silicon species at SOFC operation temperatures.

The formation of nickel-silicon alloys during the high temperature deposition of aluminosilicate vapors on nickel substrates was not observed in this study [8] despite the existence of several known stable compounds (NiSi, $NiSi_2$, Ni_2Si, Ni_3Si, Ni_3Si_2 and Ni_5Si_2). [25] A thin film of SiO_2 oxide on Ni films was reported to inhibit the Ni-Si reaction below 800°C, but in the absence of the oxide $NiSi_2$ was found to exist at 800 and 900°C. [26] Therefore it is reasonable to conclude that deposited silicon phases on the nickel were the more stable oxides, inhibiting reaction between the nickel substrate and siliceous adsorbent. Furthermore, these results suggest nickel introduced during the sintering process of the refractory may aid in the lockup of the silicon.

Further investigation was conducted to determine if the cluster found on the sample treated in humidified air and in direct contact with the aluminosilicate powder [8] is an anomaly or indicative of pockets where vapor species could deposit. This sample was the only specimen in direct contact with the aluminosilicate powder showing agglomerations that formed a siliceous layer which wet the surface and diffused into the YSZ along enlarged grain boundaries. Furthermore, this aluminosilicate agglomerate was a linear ridge, in contrast to the deposits reported on downstream samples that appeared circular. An additional cluster which wet the YSZ surface was observed on this humidified air sample in direct contact with the aluminosilicate (Figure 14). This cluster is circular, similar to the other clusters reported. Further analysis of the other YSZ samples in direct contact with the aluminosilicate powder did not lead to the discovery of clusters which wet the surface. These results suggest the aluminosilicate has a higher tendency to form vapor species in a dry or humidified reducing atmosphere, but not in humidified air.

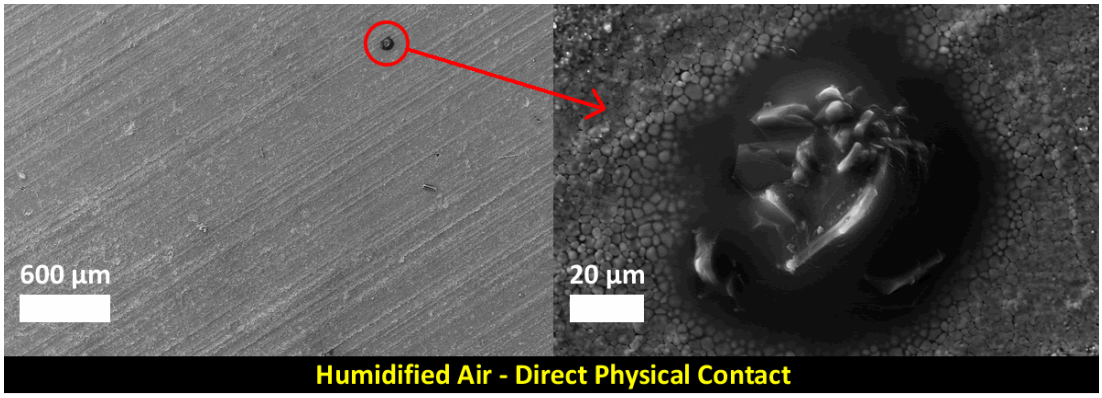

Figure 14: Aluminosilicate cluster on YSZ in direct contact with powder after heat treatment in humidified air at 1000°C for 100 hours.

Silicon Volatility

Thermodynamic Equilibrium & Kinetics

Chemical equilibrium is reached when a reaction occurs at the same rate in both directions. Kinetics determines the time required to reach equilibrium. In consecutive reactions the rate-determining step (diffusion, chemical reactions at the surface, etc.) often determines the kinetics. Kinetics is mainly influenced by the physical state of the reactants, concentrations of the reactants, temperature, pressure and the presence of catalysts. In a closed system isolated from its surroundings equilibrium will eventually be reached despite kinetic limitations. However, in an open system the flow rates of gases must be chosen to eliminate any diffusion effects or kinetic limitations and permit equilibrium pressure to be established. Based on the stabilization of volatility rates measured via TGA and RBS [7] it appears thermodynamic equilibrium is reached after an initial instability period extending 100-200 hours. This initial instability period is due to changes in the aluminosilicate interface where gas-solid chemical reactions are occurring. The burn-off of manufacturing residues and surface impurities may contribute to initial rapid releases. In addition, the formation of an aluminosilicate surface chemistry rich in silicon supplied from the bulk may yield long term steady state silicon volatility rates governed by chemical reactions at the gas-solid interface until the bulk and bulk-surface regions are depleted or a hermetic barrier is formed.

Thermodynamic Equilibrium Dopant Studies

Additional thermodynamic simulations were performed to estimate the ability of liquid dopants to react and, consequently, lock up the free silica in less volatile phases. The calcium nitrate decomposition begins at low temperatures (<200°C), reacting with silicon to form $CaSiO_3$. The $CaSiO_3$ remained stable until 1200°C, the temperature limit of the simulation. Volatile silicon hydroxides, oxy hydroxides and dioxides continued to develop at SOFC operating temperatures indicating that even with additional $CaSiO_3$ present the formation of volatile species continues under equilibrium conditions. Higher dopant concentrations, kinetic transport limitations or surface effects may limit this behavior in experimental testing.

Magnesium nitrate decomposed immediately to form the more chemically stable $MgSiO_3$ which remained stable until 860°C under the modeled humidified air, H_2 forming gas, humidified H_2 forming gas, and simulated reformate environments. In the simulated reformate environment the magnesium nitrate first decomposed into $MgCO_3$ and then began forming $MgSiO_3$ at only 60°C. The $MgSiO_3$ was then converted into $MgSiO_4$ at 860°C until 1020°C when it decomposed into $MgAl_2O_4$. The presence of multiple magnesium silicate phases indicates significant potential of forming intermediate phases that may disrupt the volatilization process. The silicon oxy hydroxides and dioxides continue to form despite the addition of the magnesium nitrate; however, the benefit of magnesium would be the ability to form secondary phases over a broader stoichiometry between magnesium and silicon. Magnesium oxide is well understood to form surface hydrates when exposed to moisture indicating stability of the

mixed phases, but the volatilization of magnesium for which the affects in the anode are uncertain.

Titanium is not available in the form of a nitrate as are many of the transition metals. To facilitate penetration of the porous refractory a titanium solution, titanium isopropoxide, is available. Nevertheless, the reaction with the aluminosilicate was modeled with titanium oxide, which is the decomposition product of the isopropoxide. The titanium dioxide remained stable when modeled in humidified air, humidified H_2forming gas, simulated reformate, and syngas. In the H_2 forming gas model, the titanium dioxide decomposed from titanium propoxide to form the more stable TiN at 350°C and Ti_4O_7 at 700°C. The Ti_4O_7 is a unique metastable oxide of titanium. In an oxygen rich environment this phase will readily transition to TiO, Ti_2O_3, and TiO_2 in a progressive manner. The TERRA database includes the following titanium silicon compounds: TiSi, $TiSi_2$ and Ti_5Si_3. From the basis of the simulation, the titanium oxides did not react with silicon under the modeled conditions.

Silicon Poisoning in SOFCs

Voltage-current (VI) and power density curves (Figure 15) were collected at 1000°C throughout the in-situ aluminosilicate poisoning electrochemical performance test previously reported [6]. A slight increase in power due to initial cell activation was observed between the scans taken at 2.5 and 13 hours. Cell performance degraded rapidly after in-situ introduction of the aluminosilicate powder into the hot zone of the fuel gas stream at 24 hours. The change in activation polarization attributed to formation of siliceous phases in the anode and deactivation of the nickel catalyst is negligible.

Furthermore, the absence of a significant drop in power output at high current densities eliminates concerns the fuel stream is restricted from reaching the anode due to the collapse of the aluminosilicate flow field. The significant increase in ohmic polarization is plausibly due to the poor ionic conducting siliceous phases that were shown to deposit on YSZ electrolyte material and isolate individual grains. [8] Extended operating periods common to stationary SOFC (>40,000 hours) will likely provide ample time to shut off ionic transport across the electrolyte.

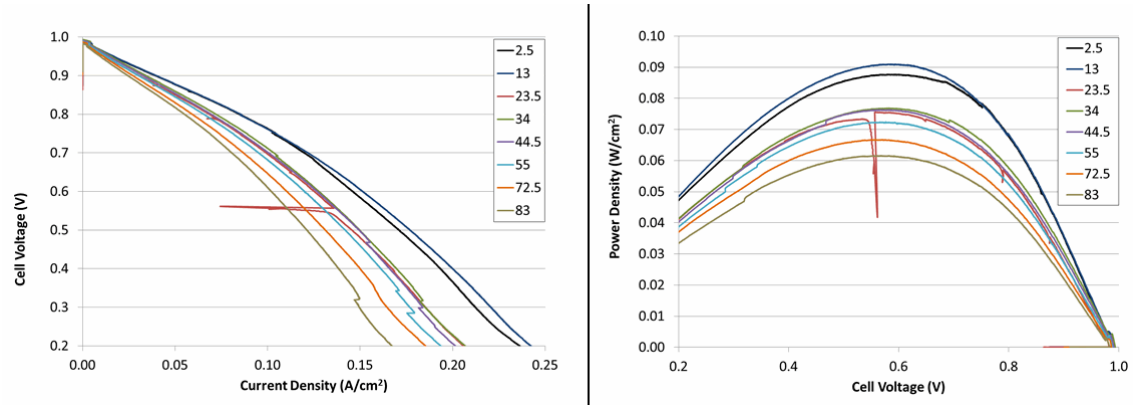

Figure 15: Electrochemical performance (1000°C) testing of ESC after in-situ introduction of aluminosilicate powder into the fuel stream at 24 hours.

Siemens' tubular cells distribute the mechanical stresses, eliminate the use of glass seals, utilize a unique nickel anchoring technique to avoid solid state migration and are cathode supported which minimizes the electrolyte thickness; these modifications allow continuous operation at 1000°C. The commercial cell results reported [8] using the permanent aluminosilicate flow field in the hot zone of the anode fuel feed line were conducted at 800°C for comparison with the aforementioned in-situ study conducted at 1000°C. The commercial electrolyte supported planar cell with the permanent flow field was operated at 800°C to avoid nickel agglomeration[27], degradation of 8 mole % YSZ

electrolyte to 9 mole % YSZ[28], failure of contact pastes and increased delamination due to thermal stresses. The reference cell reached a stable power output in accordance with manufacturer's specifications; in contrast the sample cell was rapidly poisoned by aluminosilicate vapors deposited at the TPB. At 800°C the volatility of silicon gases from the aluminosilicate is slowed due to thermodynamic and kinetic limitations. In the humidified H_2 gas silicon volatility is predominately $Si(OH)_4$ at 800°C, whereas at 1000°C the release of SiO becomes significant. The increased presence of SiO will result in vapor deposition at the anode/electrolyte interface due to the following reaction with oxygen ions transported across the membrane:

$$\mathbf{2 \cdot SiO}(g) + \mathbf{O_2^-} \rightarrow \mathbf{2 \cdot SiO_2}(s) + \mathbf{2e^-}$$

Furthermore, the lower operating temperature increases the likelihood of vapor deposition due to the decreased stability of volatile gases.

CONCLUSION

Aluminosilicate (96.3% Al_2O_3, 3.7% $Al_6Si_2O_{13}$) was investigated as a low cost alternative to high purity alumina for SOFC refractory insulation and fuel/oxidant gas delivery tubes. Extensive research findings have been previously reported regarding the stability of aluminosilicate, mullite, alumina and silica. However, this dissertation addresses lower temperatures and water vapor partial pressures associated specifically with SOFC conditions not previously explored. Changes in aluminosilicate chemistry and bulk, volatility of silicon vapors, deposition of aluminosilicate vapors on SOFC materials and effects on SOFC electrochemical performance were studied to assess the suitability as a high purity alumina replacement. It is shown thermodynamically and empirically that low cost aluminosilicate refractory remains chemically and thermally unstable under SOFC operating conditions between 800°C and 1000°C.

Silicon was shown to diffuse along grain boundaries in the aluminosilicate bulk, enriching surface concentrations. Accelerated diffusion in the presence of water vapor created a more uniform layer of silicon at the surface. Chemical reactions at the dense aluminosilicate surface and SOFC gas stream interface releasing silicon vapors that can be transported to the fuel cell were thermodynamically modeled. Thermodynamic equilibrium predicts aluminosilicate remains stable in dry air throughout SOFC operating temperatures; however in a dry reducing atmosphere aluminosilicate volatilizes into silicon monoxide (SiO) and hydrides (SiH_x). The introduction of water vapor replicate of actual SOFC gas streams significantly increases thermodynamic equilibrium partial pressures of volatile silicon hydroxide and oxy-hydroxide. Despite the increase of silicon

hydroxide and oxy-hydroxide partial pressures, the total silicon vapor partial pressure remains higher in a dry reducing atmosphere than a humidified reducing atmosphere due to the low partial pressure of oxygen.

Thermal gravimetric analysis demonstrated aluminosilicate powder was stable in humidified H_2. A discrete change in slope (Δ mass/Δ time) suggests decomposition of aluminosilicate at 1000°C is slowed after 85 hours due to solid state diffusion limitations and the burn-off of low stability crystalline silicon residues at the surface. Steady state conditions maintained throughout the remainder of the 250 hour TGA experiment and after 100 hours in RBS transpirations studies suggest thermodynamic equilibrium is reached despite kinetic limitations.

Aluminosilicate vapors were shown to preferentially deposit at 1000°C on YSZ rather than nickel. Aluminosilicate vapors deposited on YSZ as alumina rich agglomerates enclosed in an amorphous siliceous layer. The absence of peak broadening or shifting in Si(2p), Zr(3d) and Y(3d) XPS spectra reveal no new phases are being formed within XPS detection limits. High concentrations of silicon were identified in enlarged YSZ grain boundaries, indicating diffusion along grain boundaries. Separation of YSZ grains by an insulating siliceous glassy phase which increase ionic resistance in the SOFC electrolyte appears to be an important mechanism of silicon poisoning. A high surface area aluminosilicate powder within the hot zone of the anode fuel stream rapidly accelerated cell degradation. VI scans denote degradation primarily to increases in ohmic polarization. Silicon concentrations above impurity levels were detected at the electrolyte/active anode interface.

REFERENCES CITED

[1] EG&G Technical Services, Inc., *Fuel Cell Hanbook*. West Virginia, USA: U.S. Department of Energy - Office of Fossil Energy, November 2004

[2] V. L. Stolyarova and G. A. Semenov, *Mass Spectrometric Study of the Vaporization of Oxide Systems*. Chichester: John Wiley & Sons, 1994

[3] M. S. Schmidt, K. V. Hansen, K. Norman and M. Mogensen, "Effects of trace elements at the Ni/ScYSZ interface in a model solid oxide fuel cell anode," *Solid State Ionics*, 179 1436-1441 (2008).

[4] M. Backhaus-Ricoult and M. F. Tichet, "Interfacial chemistry at metal electrode–oxide electrolyte contacts," *Solid State Ionics*, 150 143-156 (2002).

[5] A. Bernasik, K. Kowalski and A. Sadowski, "Surface segregation in yttria-stabilized zirconia by means of angle resolved X-ray photoelectron spectroscopy," *J. Phys. Chem. Solids*, 63 [2] 233-239 (2002).

[6] Paolo R. Zafred, Stephen W. Sofie and Paul S. Gentile, "Progress in understanding silica transport process and effects in solid oxide fuel cell performance," in *Proceedings of the ASME Eight International Fuel Cell Science, Engineering & Technology Conference*, Brooklyn, New York, USA, 2010.

[7] Paul S. Gentile, Stephen W. Sofie, Camas F. Key and Richard J. Smith, "Silicon Volatility from Alumina and Aluminosilicates under Solid Oxide Fuel Cell Operating Conditions," *Int. J. Appl. Ceram. Technol.* (Submitted September 2010).

[8] Paul S. Gentile and Stephen W. Sofie, "Investigation of Aluminosilicate as a Solid Oxide Fuel Cell Refractory," *J. Power Sources* (Submitted October 2010).

[9] Siemens Energy Inc., Material Properties BP95/12-MA Castings, 2008.

[10] V. Gorokhovsky et al., "Tribological performance of hybrid filtered arc-magnetron coatings Part I: Coating deposition process and basic coating properties characterization," *Surf. Coat. Technol.*, 206 [6] 3732-3747 (December 2006).

[11] D. A. and Easterling, K. E. Porter, *Phase Transformations in Metals and Alloys*. New York: Van Nostrand Reinhold Company, 1981

[12] C. Collins et al., "Chromium volatility of coated and uncoated steel interconnects for SOFCs," *Surf. Coat. Technol.*, 201 4467-4470 (2006).

[13] A. Lussier, S. W. Sofie, J. Dvorak and Y. U. Idzerda, "Mechanism for SOFC Anode Degradation from Hydrogen Sulfide Exposure," *Int. J. Hydrogen Energy*, 33 p. 945 (2008).

[14] John F. Moudler, William F. Stickle, Peter E. Sobol and Kenneth D. Bomben, *Handbook of X-ray Photoelectron Spectroscopy*. Eden Prairie, Minnesota: Perkin-Elmer Corporation - Physical Electronics Division, 1995

[15] P. R. Anderson and W. E. Jr. Swartz, "X-Ray Photoelectron Spectroscopy of Some Aluminosilicates," *Inorg. Chem.*, 13 2293-2294 (1974).

[16] V. Atzrodt, T. Wirth and H. Lange, "Investigation of NiSi and Pd3Si thin films by AES and XPS," *Phys. Status Solidi A*, 62 [2] 531-537 (1980).

[17] A. F. Povey, R. O. Ansell, T. Dickinson and P.M. A. Sherwood, "An X-ray photoelectron spectroscopic study of stainless steel electrodes after polarisation in the regions of transpassivity and secondary passivity ," *J. Electroanal. Chem.*, 87 189-201 (1978).

[18] T. P. Nguyen and S. Lefrant, "XPS study of Si0 thin films and SiO-metal interfaces," *J. Phys.: Condens. Matter*, 1 5197-5204 (1989).

[19] C. D. Wagner et al., "Auger and photoelectron line energy relationships in aluminum–oxygen and silicon–oxygen compounds," *J. Vac. Sci. Technol.*, 21 933-945 (1982).

[20] M. Klasson et al., "Electron escape depth in silicon," *J. Electron Spectrosc. Relat. Phenom.*, 3 427-434 (1974).

[21] T. S. Jeon, J. M. White and D. L. Kwong, "Thermal stability of ultrathin ZrO2 films prepared by chemical vapor deposition on Si(100)," *Appl. Phys. Lett.*, 78 368-370 (November 2000).

[22] A. E. Hughes and B. A. Sexton, "XPS study of an intergranular phase in yttria-zirconia," *J. Mater. Sci.*, 24 1057-1061 (1989).

[23] Ernest M. Levin, *Phase diagrams for ceramists*, M. K. Reser, Ed. Columbus, Ohio, USA: American Ceramic Society, 1964

[24] J. J. Chambers and G. N. Parsons, "Yttrium silicate formation on silicon: Effect of silicon preoxidation and nitridatoin on interface reaction kinetics," *Appl. Phys. Lett.*, 77 2385-2387 (October 2000).

[25] L. Kaufman, "Coupled phase diagrams and thermochemical data for transition metal binary systems. VI," *Calphad*, 3 p. 45 (1979).

[26] P. S. Lee et al., "On the Ni–Si phase transformation with/without native oxide ," *Microelectron. Eng.*, 51-52 583-594 (May 2000).

[27] D. Simwonis, F. Tietz and D. Stover, "Nickel coarsening in annealed Ni/8YSZ anode substrates for solid oxide fuel cells," *Solid State Ionics*, 132 241-251 (2000).

[28] Manohar S. Sohal, "Degradation in Solid Oxide Cells During High Temperature Electrolysis," Idaho National Laboratory, Idaho Falls, Idaho, INL/EXT-09-15617, 2009.